Silica-supported PdGa Nanoparticles: Metal Synergy for Highly Active and Selective CO_2-to-CH_3OH Hydrogenation

Scott R. Docherty,[a] Nat Phongprueksathat,[b] Erwin Lam,[a] Gina Noh,[a] Olga V. Safonova,[c] Atsushi Urakawa,[b] Christophe Copéret*[a]

a. Department of Chemistry and Applied Biosciences, ETH Zürich, Vladimir Prelog Weg 1-5, CH-8093 Zurich, Switzerland

b. Catalysis Engineering, Department of Chemical Engineering, Delft University of Technology, Van der Maasweg 9, 2629 HZ Delft, The Netherlands

c. Paul Scherrer Institute, CH-5232 Villigen, Switzerland.

Supporting Information

Table of Contents

S1. General considerations

Materials: Unless otherwise indicated, all manipulations were undertaken using conventional air-free techniques (glove box (Argon) and Schlenk techniques (Argon)). Pentane, heptane, dichloromethane, diethyl ether and toluene were purified using double MBraun SPS alumina columns, and stored over activated Molecular Sieves (4 Å, Merck) in an argon atmosphere. Benzene (C_6H_6) was distilled from purple Na^0/benzophenone under Ar and stored over activated molecular sieves (4 Å, Merck). d_2-dichloromethane was vacuum distilled from activated molecular sieves (4 Å, Merck) and stored under argon. C_6D_6 was vacuum transferred from purple Na^0/benzophenone and degassed by three consecutive freeze-pump-thaw cycles, prior to being stored in an argon filled glovebox. CD_2Cl_2 was dried over molecular sieves (4 Å, Merck), vacuum transferred and degassed by three consecutive freeze-pump-thaw cycles, prior to being stored in an argon filled glovebox. 1,5-Cyclooctadiene (98%, Tokyo Chemical Industry (TCI)) and *tert*-butyl alcohol (reagent grade, Sigma-Aldrich) were distilled from CaH_2 onto activated molecular sieves (4 Å, Merck), under argon. $SiCl_4$ was distilled under argon prior to use. Imidazole was recrystallized from dichloromethane under air prior to use. Methanol was dried over activated molecular sieves (3Å, Merck), and freeze-pump-thaw-degassed for 3 consecutive cycles prior to use. Tetramethyltin ($SnMe_4$) (Sigma-Aldrich, 98% purity), $Ga(acac)_3$ (acac- = acetylacetonate) (abcr, 98%), $Ga(NO_3)_3(H_2O)_9$ (abcr, 99.99% Ga) were used as received. Ferrocene ($FeCp_2$) was purchased from Sigma-Aldrich and sublimed under reduced pressure prior to use. $[Mg(CH_2Ph)_2(THF)_2]$, $Pd(COD)Cl_2$ and $Ga(OSi(O\textit{t}Bu)_3)_3(THF)$, were synthesized as described in earlier literature.[1–3] $HOSi(O\textit{t}Bu)_3$ was prepared according to literature procedure and sublimed under reduced pressure prior to use.[4] *Celite*® and Molecular Sieves (4 Å, Merck) were activated under high vacuum (10^{-5} mbar) overnight at 350 °C. Deionized water was collected from Merck Millipore Synergy® Water Purification System. $PdCl_2$, CaH_2 and NaH were used as received (Sigma-Aldrich). SiC (carborundum powder, 24 grit, Fisher Scientific) was calcined at 700 °C prior to being stored in an argon filled glovebox.

Silica (Aerosil Degussa, 200 $m^2 g^{-1}$) was compacted with deionized water, dried at 100 °C for 7 days, crushed and sieved (250−400 μm) for easier handling. Sieved silica-700 ($SiO_{2\text{-}700}$) was calcined at 500°C in air for 12 h, allowed to return to room

temperature and treated under high vacuum (10^{-5} mbar) at 500°C for 12 h (ramp: 5 °C min^{-1}) and then at 700 °C for 24 h (ramp: 1.7 °C min^{-1}). Quantification of the -OH density of $SiO_{2\text{-}700}$ using $[Mg(CH_2Ph)_2(THF)_2]$ yielded 0.26 mmol -OH g^{-1}, corresponding to 0.8 accessible -OH groups nm^{-2}.

Note that, henceforth, pristine refers to the as-synthesized material, while spent refers to the catalyst after >36 hours of reaction.

Infrared (IR) Spectroscopy: ATR-IR (infrared) spectra were recorded inside an Ar-filled glovebox on a Bruker FT-IR Alpha spectrometer with ATR-IR attachment and are reported as absorption maxima in cm^{-1}. Peak intensities are described using the convention strong (s), medium (m) and weak (w). A typical experiment consisted of the measurement of transmission in 16 scans in the range 4000 to 400 cm^{-1}, unless otherwise declared. Transmission-IR were recorded on Bruker FT-IR Alpha spectrometer equipped with RockSolid interferometer, DTGS (deuterated triglycine sulfate) detector, SiC globar source; solid samples were mounted on a magnetic pellet holder. A typical experiment consisted of the measurement of transmission in 32 scans in the region from 4000 to 400 cm^{-1}. For adsorption experiments, spectra were recorded in a transmission mode on a Nicolet 6700 FTIR spectrophotometer, an uncooled deuterated tryglycine sulfate (DTGS)KBr detector, using 32 scans at a resolution of 2 cm^{-1}. For adsorption experiments, a wafer of catalyst material (0.01-0.02 g cm^{-1}) was pressed into an aluminium ring, which was placed into a glass IR cell with CaF_2 windows. For IR spectra with adsorbed CO, the evacuated cell was exposed to ~10 mbar CO at 298 K for 5 min, a spectrum was measured, and the cell was then evacuated (10^{-5} mbar) for 15 min at 298 K, before a second measurement was undertaken. For methanol adsorption, the evacuated cell was exposed to ~200 mbar dry, degassed methanol at 298 K for 5 min, a spectrum was measured, and the cell was then evacuated (10^{-5} mbar) for 15 min at 298 K, before a second measurement was undertaken. Spectra were analyzed using ThermoScientific™ OMNIC™ 8 Software. Spectra are normalized to the Si-O-Si overtone peak maximum at 1868 cm^{-1} for all materials.

Nuclear magnetic resonance spectroscopy (NMR): Solution ^{1}H-NMR, ^{13}C-NMR and DEPT-90 spectra were obtained on BrukerR DRX 300 spectrometer (7.05 T, Larmor Frequency: 300 MHz (1H), 75.5 MHz (^{13}C)), in deuterated methylene chloride

(CD_2Cl_2) or deuterated benzene (C_6D_6) at room temperature. The ^{1}H and ^{13}C chemical shifts are referenced relative to residual solvent peaks.[5] Chemical shifts are reported in parts per million (ppm) and coupling constants ($^{N}J_{X\text{-}X}$) are given in Hertz (Hz). Where appropriate, signal multiplicity has been condensed to a single letter format, i.e.: s=singlet, d=doublet, t=triplet, q=quartet, m=multiplet. Solvent peaks are denoted with an asterisk. Unless noted, ^{13}C spectra were recorded using 1024 scans.
For quantification of graftings or -OH densities, ferrocene ($FeCp_2$) was used as internal standard, and extended recycle delay (58 s) was used to ensure accurate quantification.

Solid-state NMR spectra of grafted samples were recorded on a Bruker 400 MHz NMR spectrometer using a double resonance 3.2 mm CP-MAS probe. Samples were packed in 3.2 mm zirconia rotors, spectra were recorded at 278 K. Samples exposed to $^{13}CO_2$ were recorded on a Bruker 400 MHz spectrometer using double resonance 4mm CP-MAS probe. Samples were packed in 4 mm zirconia rotors inside an Ar-filled glovebox, and recorded at 298 K using otherwise identical parameters, unless otherwise declared. In all cases, the downfield ^{13}C resonance of adamantane (38.4 ppm) was used as an external secondary reference to calibrate chemical shifts.

Chemisorption: Chemisorption experiments were carried out on a BELSORP-max apparatus (Bel-Japan). Approximately 100 mg of reduced catalyst was loaded in an airtight cell inside a glovebox which was then mounted on the apparatus. The sample was pre-treated at 300°C for 1 h at 10^{-5} mbar. The chemisorption measurements were performed at 40 °C, the pressures at equilibrium were recorded when the pressure variation was below 0.6% for 1200 seconds. In the case of H_2, the uptake was calculated by fitting the isotherm with a dissociative Langmuir isotherm model (equation S1). In the case of CO, the uptake was calculated by fitting the isotherm using a retentive Langmuir model (equation S2).

$$Q_{H2} = \frac{\sqrt{K_{H2}\left(\frac{P_{H2,eq}}{P^{\theta}}\right)}}{1+\sqrt{K_{H2}\left(\frac{P_{H2,eq}}{P^{\theta}}\right)}} \cdot Q_{H2,max} \qquad \text{(S1)}$$

$$Q_{CO} = \frac{K_{CO}\left(\frac{P_{CO,eq}}{P^{\theta}}\right)}{1 + K_{CO}\left(\frac{P_{CO,eq}}{P^{\theta}}\right)} \cdot Q_{CO,max} \quad \text{(S2)}$$

Where $P_{X,eq}$ the equilibrium adsorbed gas pressure, Q_x the adsorbate (x = H_2 or CO) uptake (μmol g_{cat}^{-1}), $Q_{X,max}$ the saturation uptake of adsorbing gas and K_X the thermodynamic constant for the chemisorption process. For CO chemisorption, a stoichiometry of 1:1 ($CO:Pd_{surface}$) is assumed when considering metal dispersion. To obtain comparable estimates of metal distribution, dispersion is normalized to Pd content for the samples described.[6]

Electron Microscopy: Particle size estimations were obtained by transmission electron microscopy (TEM) JEOL JEM-1400 Plus microscope. For the determination of the particle size distribution, >200 individual particles were considered, and the mean particle size and standard deviation are given according to a normal distribution function. Powdered samples were mixed in solid form with a Lacey-C 300 mesh Cu grid (Ted Pella). Comparison of exposed surface w.r.t. chemisorption was estimated using a truncated square octahedron model (see Figure S42).

Energy dispersive X-ray (EDX) mapping was measured on a Talos F200 X microscope without exposing the samples to air prior to measurement. Powdered samples were mixed in solid form with a Lacey-C 300 mesh Cu grid inside of a glovebox under an atmosphere of Ar before being mounted on a vacuum transfer tomography holder from Fischione Instruments (model #2560) inside a glove box, from which the sample was subsequently transferred to the chamber of the microscope in the absence of air. Signals attributed to Cu and C are assigned to background scattering from the grid used.

Evaluation of Catalytic Performance: CO_2 hydrogenation rates were measured at 230 °C at differential conversions (<10%) on all samples (~0.20 g_{cat}), diluted with 5 g SiC (Fisher Scientific) and held against a sintered metal frit axially centered within a tubular reactor (316 S.S., 9.1mm i.d.) with plug-flow hydrodynamics. Samples were loaded in an argon filled glovebox, to a reactor equipped with a bypass, enabling air-

free handling of catalyst throughout reaction. Temperatures were measured with a K-type thermocouple held at the mid-point of the packed bed and maintained using a resistively heated furnace with electronic controllers. Samples were treated at 300 °C in 5:1 H_2/N_2 (60 sccm; PanGas 99.999% H_2; PanGas 99.999% N_2; 1 bar(g)) for 1 h before cooling to reaction temperature (230 °C in N_2 flow (50 sccm, 1 bar(g)). After which, CO_2 (CarbaGas), H_2 (CarbaGas), and Ar (CarbaGas) (1:3:1)) were introduced using electronic mass flow controllers (BronkhorstEL-FLOW), and the reactor was pressurized (25 bar(g)). Reactor pressure was maintained at 25 bar(g) by a back--pressure regulator (BronkhorstEL-PRESS). Different contact times were probed by screening gas flow rates ranging from 100 sccm to 6 sccm, with a fixed flowrate of 50 sccm used as a reference for quantifying deactivation at fixed intervals. Where appropriate, catalyst deactivation was accounted for using a 2nd order polynomial for correction. Transfer lines were heated (120 ^{o}C) to prevent product condensation. Reactant and product concentrations in the reactant and effluent streams were measured by on-line gas chromatography (Agilent 7890N GC) equipped with Restek Rt-U-BOND (30 m x 0.53 mm x 20 μm) and Rt-Msieve 5A (30 m x 0.53 mm x 50 μm) columns and flame ionization (CH_3OH, dimethyl ether) and thermal conductivity detection (Ar, CO_2, CO and CH_4). Products measured were primarily CO, CH_3OH, and small amounts of dimethyl ether (<5% selectivity). Argon is used as an internal standard for GC quantification. The carbon balance is greater than 97% for all reactions performed. In the case of Pd@SiO_2, small amounts of CH_4 were also observed. Dimethyl ether, the bimolecular dehydration product of CH_3OH, was detected for PdGa@SiO_2 and is accounted for in CH_3OH rates and selectivities (2:1 CH_3OH:dimethyl ether). Rates are normalized by the number of moles of transition metal in each catalyst, to enable direct comparison. Product selectivity is defined on a per-carbon basis.

Reaction rates, conversions and selectivities were calculated using the following equations:

$$r_x(\mathrm{mmol}_X\ \mathrm{s}^{-1}\ \mathrm{mol}_{\mathrm{TM}}^{-1}) = \frac{F_{out} \cdot c_{X,out}}{m_{cat} \cdot n_{\mathrm{TM}}} \quad \text{(S3)}$$

$$S_X = \frac{F_{X,out}}{\sum_{i=1}^{n} F_{i,out}} \quad \text{(S4)}$$

$$\chi_{CO2} = \frac{\sum_{i=1}^{n} F_{i,out}}{F_{CO2,in}} \quad \text{(S5)}$$

Where F_{out} is the total outlet flowrate (mmol s^{-1}), $c_{X,out}$ is the fraction of feed composed component X, m_{cat} is the mass of catalyst used, and n_{TM} is the number of moles of transition metal per gram of catalyst. Selectivity is defined as the outlet flow of the component in question, $F_{X,out}$, divided by the sum of outlet flows for all carbon containing products, $\sum_{i=1}^{n} F_{i,out}$, while conversion is defined as the sum of outlet flows for all carbon containing products, $\sum_{i=1}^{n} F_{i,out}$, divided by the inlet flow of CO_2, $F_{CO2,in}$. Note that all concentrations are normalised per carbon to enable accurate comparison.

Intrinsic formation rates (i.e. rate at zero contact time) are obtained by using a second order polynomial fit on the experimental data, and extrapolating to zero residence time. For post reaction analysis, the reactor was cooled, depressurized, and purged with N_2 (50 sccm, 30 minutes). Using a custom Hi-vacuum line adaptor, the reactor was then evacuated (10^{-5} mbar) prior to being introduced into an argon-filled glovebox. Samples were then analysed without exposure to air (IR, XAS, TEM).

S2. Synthesis of Molecular Precursors

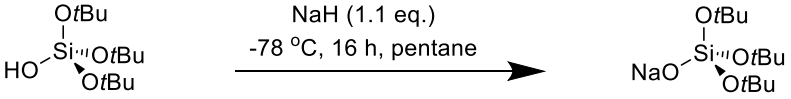

$HOSi(OtBu)_3$ **$NaOSi(OtBu)_3$**

Synthesis of $NaOSi(OtBu)_3$: In an adaptation of a reported procedure,[7] to a cooled (-78 °C) slurry of NaH (200 mg, 8.34 mmol, 1.1 eq.) in pentane (50 mL) was added dropwise a solution of $HOSi(OtBu)_3$ (2.00g, 7.56 mmol) in pentane (50 mL). The resulting mixture was allowed to reach room temperature over the course of 16 hours, after which, the reaction mixture was filtered, and the filtrate collected. Solvent was removed under reduced pressure to yield a white, analytically-pure solid.

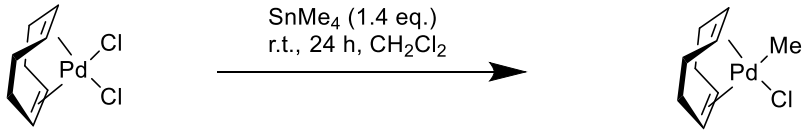

$Pd(COD)Cl_2$ **$Pd(COD)MeCl$**

Synthesis of Pd(COD)MeCl: Using an adaptation of a reported procedure,[8] $Pd(COD)Cl_2$ (1.21 g, 4.24 mmol) was dissolved in CH_2Cl_2 (50 mL). To this was added $SnMe_4$ (0.95 mL, 6.85 mmol), the resulting mixture was stirred, at room temperature, for 24 h. The reaction mixture was filtered and the solvent was removed under reduced pressure, whilst maintaining a temperature of 0 °C. The resulting white solid was washed with diethyl ether (3 x 7 mL), and dried in vacuo to yield 730 mg of product (65% yield). The resulting solid was stored at -40 °C in darkness. All manipulations were completed in the absence of light using amber glassware. **^{1}H NMR (300 MHz, C_6D_6):** 5.79 (m, 2H, *sp*^{2}-COD *trans*-Me), 4.30 (m, 2H, *sp*^{2}-COD *trans*-Cl), 1.73-1.48 (m, b, 8H (*sp*^{3}-COD)), 1.33 (s, 3H, Pd-C*H*$_3$)

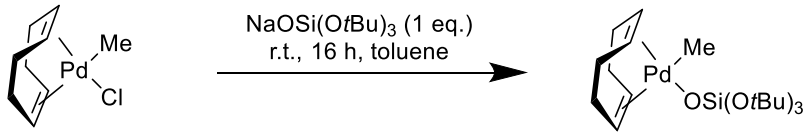

Pd(COD)MeCl **Pd(COD)Me(OSi(O*t*Bu)$_3$)**

Synthesis of Pd(COD)Me(OSi(O*t*Bu)$_3$): Pd(COD)MeCl (1.00 g, 3.77 mmol) was dissolved in toluene (80 mL). To this was added a solution of $NaOSi(OtBu)_3$ (1.08 g, 3.77 mmol) in toluene (20 mL), followed by successive washings of the reaction vessel (2 x 10 mL). The reaction mixture was stirred, at room temperature, for 16 h. Solvent was removed under reduced pressure to yield a dark solid. Remaining solid was washed with Et_2O (3 x 10 mL) and combined washings were concentrated under reduced pressure to yield a white crystalline solid. The solid was dissolved in CH_2Cl_2 (10 mL) and cooled to -40 °C to yield a small amount of white crystals. The reaction mixture was filtered over celite, and the supernatant collected and concentrated under reduced pressure to yield a yellow solid. The solid was dissolved in pentane (3 mL) and cooled to -40 °C overnight, to yield colourless rhombohedral crystals. Successive recrystallizations yielded 1.16 g of product (62% yield). The resulting solid was stored at -40 °C in darkness. All manipulations were completed in the absence of light using amber glassware. The product was characterized by ^{1}H-NMR, ^{13}C-NMR, ^{1}H,^{13}C-HMBC, elemental analysis (EA; C and H), and ATR-IR and single crystal X-ray diffraction. **^{1}H NMR (300 MHz, CD_2Cl_2):** 6.08 (t, 2H, *sp*^{2}-COD *trans*-Me), 4.69 (t, 2H, *sp*^{2}-COD *trans*-OSi(O*t*Bu)$_3$), 2.72-2.28 (m, b, 8H (*sp*^{3}-COD)), 1.30 (s, 27H, OC(C*H*$_3$)$_3$), 0.99 (s, 3H, Pd-C*H*$_3$) **^{13}C NMR (75.5 MHz, C_6D_6):** 123.7 (*sp*^{2}-COD *trans*-Me), 92.2

(*sp*^{2}-COD *trans*-OSi(O*t*Bu)$_3$), 70.9 (O*C*(CH$_3$)$_3$), 32.1 (OC(*C*H$_3$)$_3$), 30.6 (*sp*^{3}-COD), 27.0 (*sp*^{3}-COD), 12.9 (Pd-*C*H$_3$) **IR (ATR, cm^{-1}):** 2964 (s), 2925 (m), 2897 (m), 1383 (w), 1361 (m), 1236 (m), aa93 (m), 1038 (m), 1012 (s), 820 (m), 694 (m), 486 (w)

S3. Characterization of Molecular Precursors

NMR of [(1,5-cyclooctadiene)methyl(tris-*tert*-butoxysiloxy)Palladium(II)]

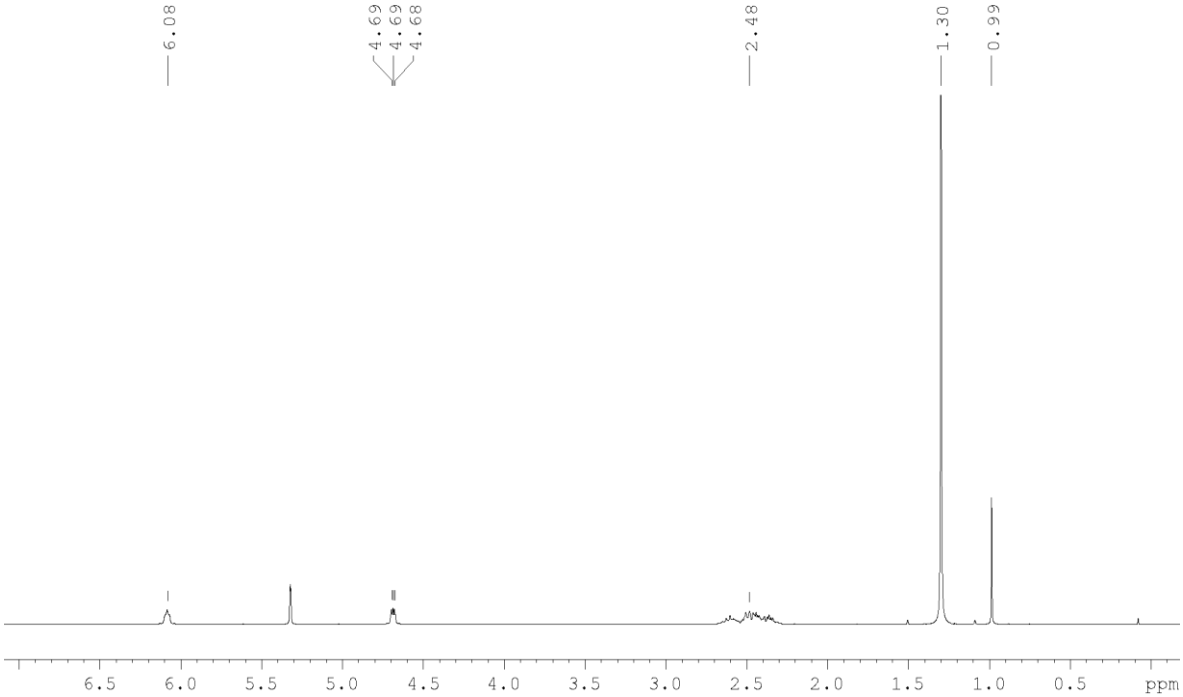

Figure S 1. Pd(COD)Me(OSi(O*t*Bu)$_3$) ^{1}H NMR (300 MHz, CD_2Cl_2, 298 K)

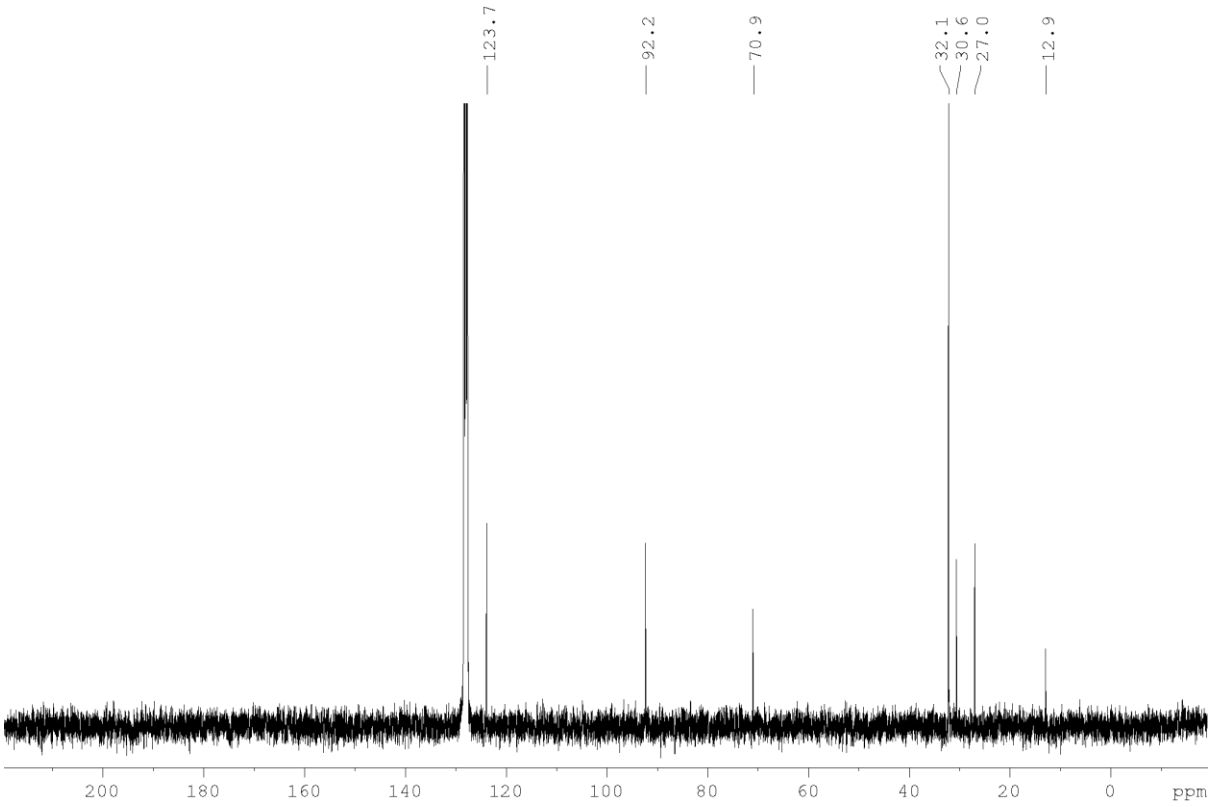

Figure S 2. Pd(COD)Me(OSi(O*t*Bu)$_3$) ^{13}C NMR (75.5 MHz, C_6D_6, 298 K)

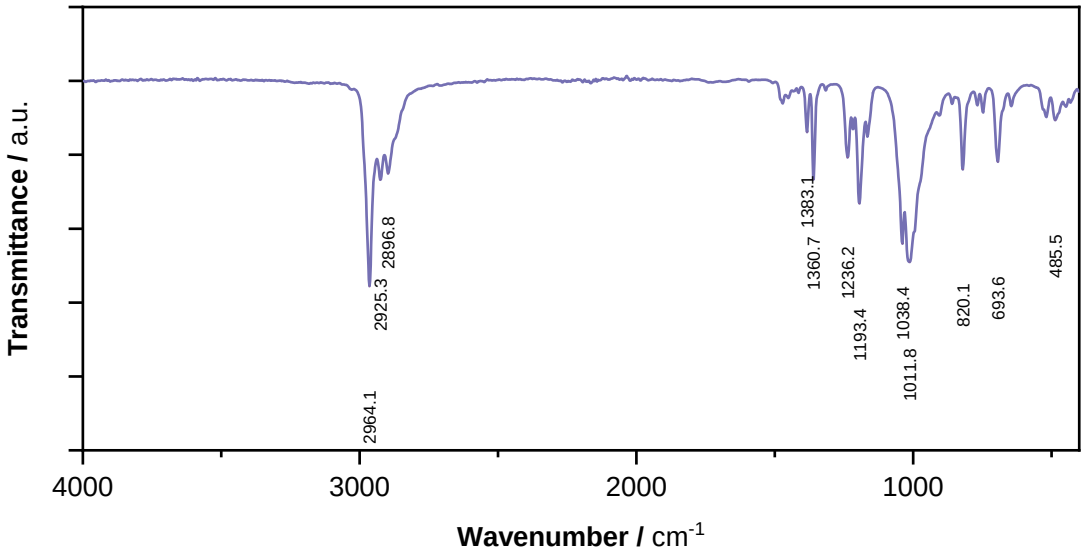

Figure S 3. Pd(COD)Me(OSi(O*t*Bu)$_3$) ATR-IR, Transmittance, range: 4000-400 cm^{-1}

Crystal structure determination of [(1,5-cyclooctadiene)methyl(tris-tert-butoxysiloxy)Palladium(II)] (CCDC Deposition Number 2007107)

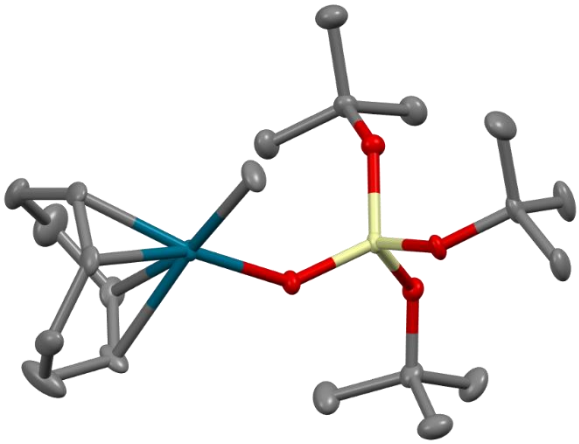

Figure S 4. Crystal structure for Pd(COD)Me(OSi(O*t*Bu)$_3$). Ellipsoids shown at 50% probability, hydrogens omitted for clarity.

Crystals suitable for X-ray diffraction of $C_{21}H_{42}O_4PdSi$ [(1,5-cyclooctadiene)methyl(tris-*tert*-butoxysiloxy)Palladium(II)] were crystallized from a saturated solution of pentane at -40 ºC overnight. A suitable crystal was selected and tip-mounted on a MiTeGen Pin covered with Paratone Oil on a 'Bruker APEX-II CCD' diffractometer. The crystal was kept at 100 K during data collection. Using Olex2,[9] the structure was solved with the olex2.solve structure solution program[10] using Charge Flipping and refined with the ShelXL[11] refinement package using Least Squares minimisation.

Crystal Data for $C_{21}H_{42}O_4PdSi$ (M =493.03 g/mol): monoclinic, space group $P2_1/n$ (no. 14), a = 16.7962(4) Å, b = 17.3969(5) Å, c = 17.0667(5) Å, β = 97.8620(10)°, V = 4940.0(2) Å^3, Z = 8, T = 100 K, μ(MoKα) = 0.821 mm^{-1}, *Dcalc* = 1.326 g/cm^3, 69289 reflections measured (4.682° ≤ 2Θ ≤ 52.892°), 10143 unique (R_{int} = 0.0515, R_{sigma} = 0.0274) which were used in all calculations. The final R_1 was 0.0251 (I > 2σ(I)) and wR_2 was 0.0596 (all data).

S4. Preparation and Synthesis of Supported Materials

Preparation of $SiO_{2\text{-}700}$: Prepared using literature protocol.[12] Titrated hydroxyl density of 0.8 –OH nm^{-2}, consistent with earlier reports.

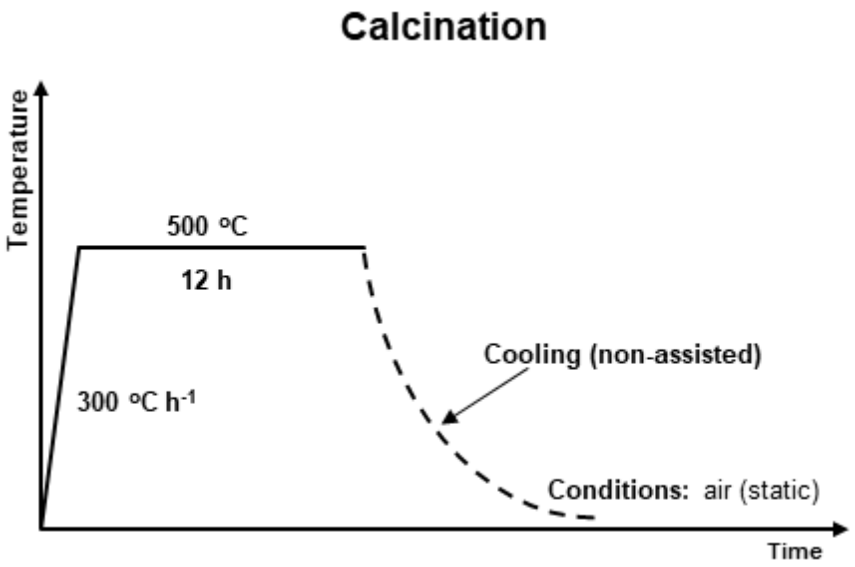

Figure S 5. Schematic for calcination of SiO_2 prior to dehydroxylation under reduced pressure

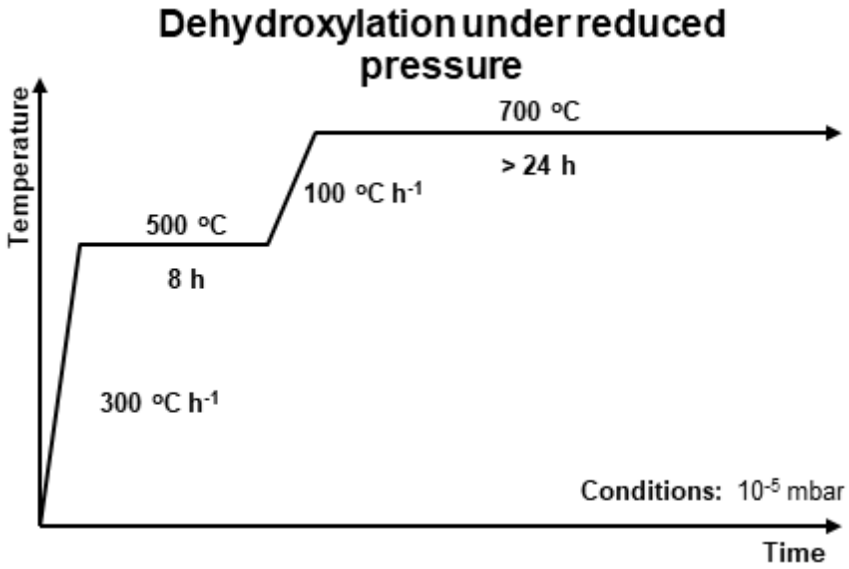

Figure S 6. Schematic for preparation of $SiO_{2\text{-}700}$ temperature programme of dehydroxylation under reduced pressure.

Preparation of Ga@SiO_2: Prepared using literature protocol.[1] Temperature-programme shown in Figure S7

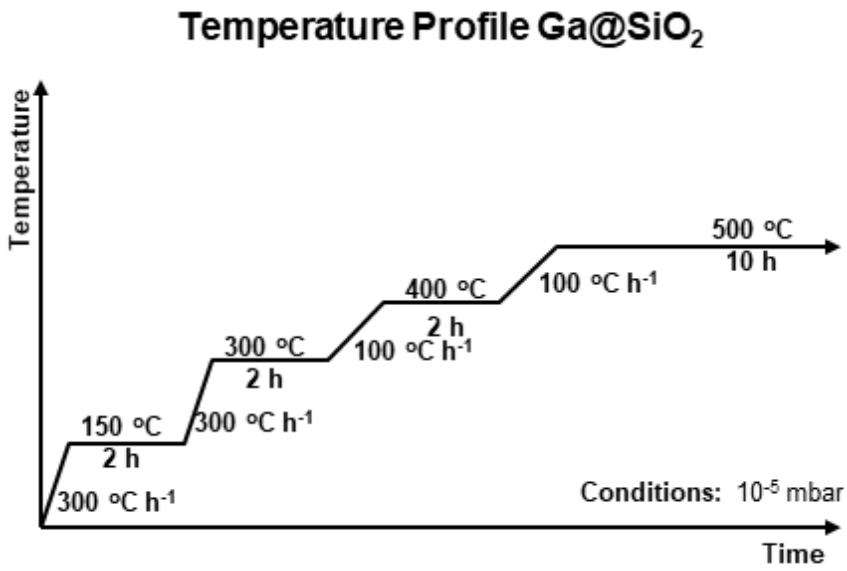

Figure S 7. Schematic for temperature programme employed in preparation of $Ga@SiO_2$ under reduced pressure

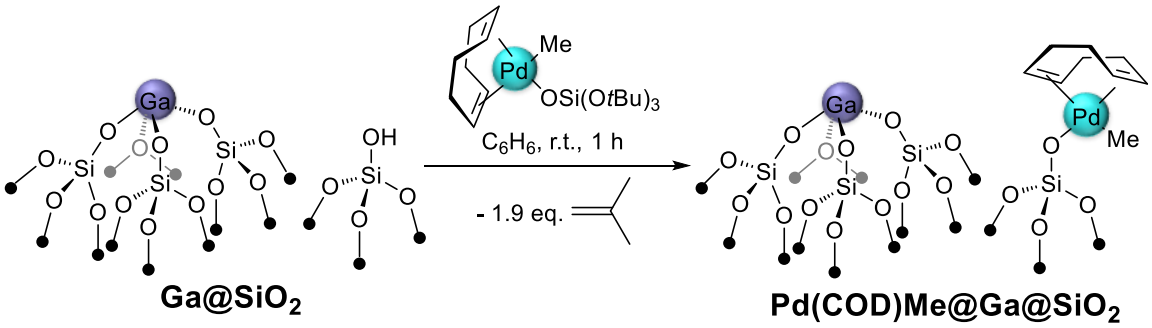

Synthesis of Pd(COD)Me@Ga@SiO$_{2\text{-}700}$: To a suspension of $Ga@SiO_2$ (1.000g) in C_6H_6 (20 mL) was added a clear solution of Pd(COD)Me(OSi(O*t*Bu)$_3$) (78.9 mg, 0.16 mmol) in C_6H_6 (10 mL). The suspension was stirred for 1 hour at 25 °C. After stirring, the material was filtered, rinsed with C_6H_6 (3 x 7 mL) and dried under under high vacuum (10^{-5} mbar). Using ^{1}H NMR spectroscopy (200 MHz, 25 °C, d1 = 58 sec) with ferrocene as an internal standard, Isobutene (1.9 eq.) was identified as the side product of the reaction, no starting material was observed in the washings. Elemental Analysis: Pd 1.66 wt%, Ga, 1.54 wt%; C, 2.12 wt%; H, 0.39 wt%. SSNMR: 126 ppm, 94 ppm, 30 ppm, 27 pmm and 11 ppm

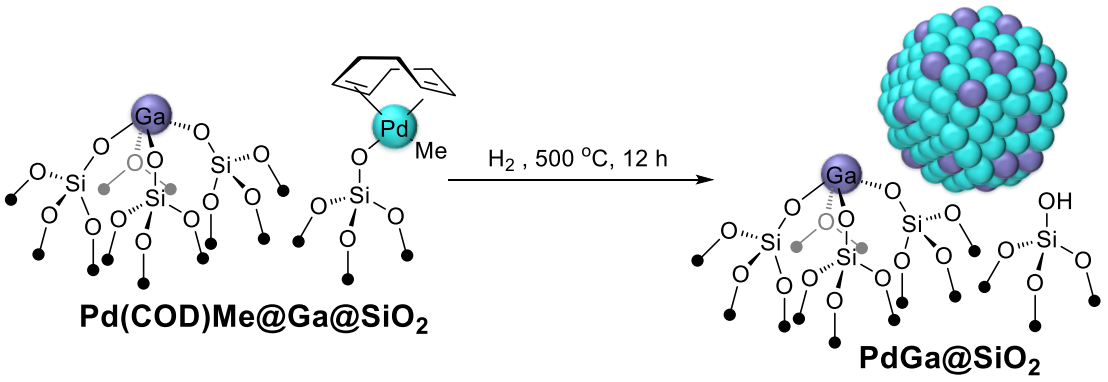

Synthesis of PdGa@SiO$_{2\text{-}700}$: To a glass flow reactor containing a medium porosity glass frit was added Pd(COD)Me@Ga@SiO$_2$ (0.773 g). The flow reactor was evacuated (10^{-5} mbar), and filled with H_2. The reactor was subsequently heated to 500 °C (5 °C min^{-1}) while maintaining a flow of H_2 (960 mbar(a)). After 12 hours of heating, the reactor was evacuated (10^{-5} mbar), while still hot, yielding a dark solid material. Elemental analysis: Pd: 1.08 wt%, Ga 1.66 wt%, H: <0.1 wt%, C: <0.1 wt%

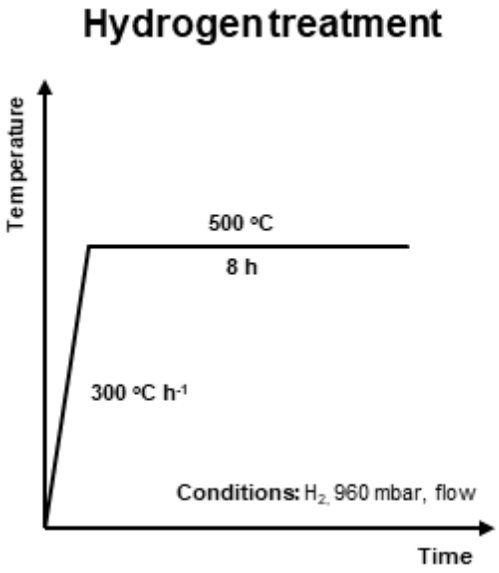

Figure S 8. Schematic for temperature programme employed in hydrogen treatment of PdGa@SiO$_2$

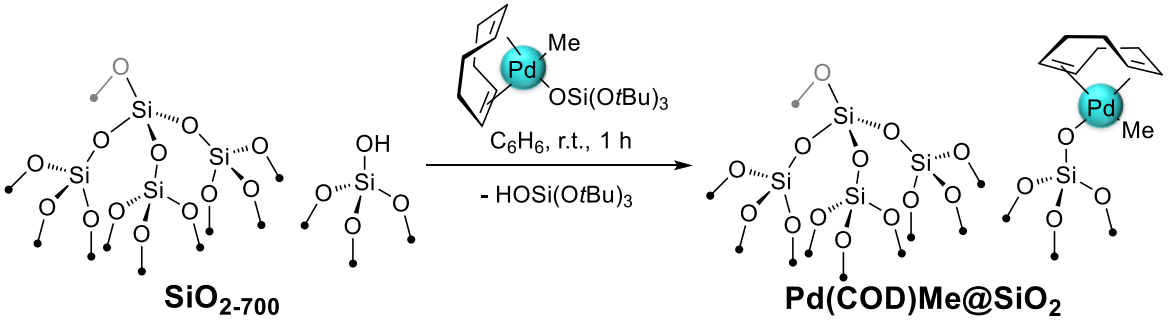

Synthesis of Pd(COD)Me@$SiO_{2\text{-}700}$: To a suspension of $SiO_{2\text{-}700}$ (1.000g, 0.26mmol –OH) in C_6H_6 (20 mL) was added a clear solution of Pd(COD)Me(OSi(O*t*Bu)$_3$) (79.9 mg, 0.16 mmol) in C_6H_6 (10 mL). The suspension was stirred for 1 hour at 25 °C. After stirring, the material was filtered, rinsed with C_6H_6(3 x 7 mL) and dried under under high vacuum (10^{-5} mbar). Using ^{1}H NMR spectroscopy (200 MHz, 25 °C, d1 = 60 sec) with ferrocene as an internal standard, HOSi(O*t*Bu)$_3$ (0.8 eq.) was identified as the side product of the reaction, no starting material was observed in the washings.

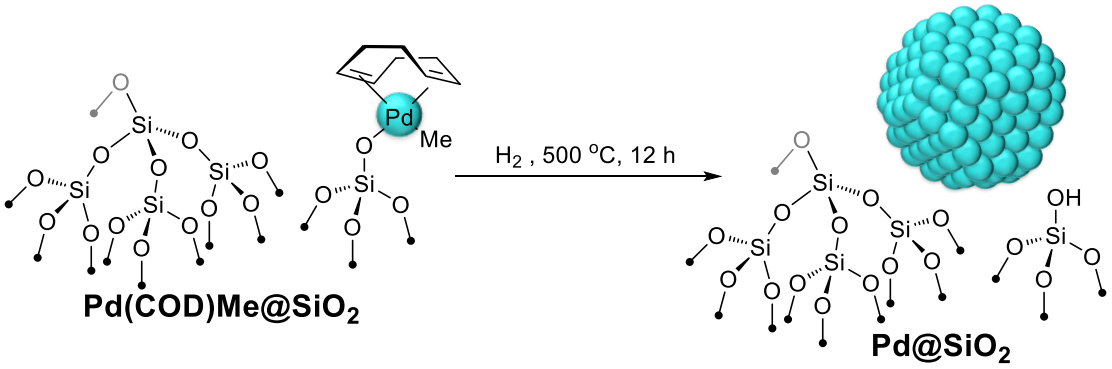

Synthesis of Pd@$SiO_{2\text{-}700}$: To a glass flow reactor containing a medium porosity glass frit was added Pd(COD)Me@SiO_2 (0.773 g). The flow reactor was evacuated (10^{-5} mbar), and filled with H_2. The reactor was subsequently heated to 500 °C (5 °C min^{-1}) while maintaining a flow of H_2 (960 mbar(a)). After 12 hours of heating, the reactor was evacuated (10^{-5} mbar) while still hot, yielding a dark solid material. Temperature programme analogous to that presented in Figure S8. Elemental analysis: Pd: 1.61 wt%, H: <0.1 wt%, C: <0.1 wt%

Synthesis of Pd(COD)Me@$SiO_{2\text{-}700}$ used for analysis by NMR and EA of grafted species: To a suspension of $SiO_{2\text{-}700}$ (0.990g, 0.26mmol –OH) in C_6H_6 (20 mL) was added a clear solution of Pd(COD)Me(OSi(O*t*Bu)$_3$) (106.1 mg, 0.215 mmol) in C_6H_6 (10 mL). The suspension was stirred for 1 hour at 25 °C. After stirring, the material

was filtered, rinsed with C_6H_6 (3 x 7 mL) and dried under under high vacuum (10^{-5} mbar). Using ^{1}H NMR spectroscopy (200 MHz, 25 °C, d1 = 58 sec) with ferrocene as an internal standard, HOSi(O*t*Bu)$_3$ (0.8 eq.) was identified as the side product of the reaction, no starting material was observed in the washings. Elemental analysis: Pd, 1.99 wt%; C, 3.04 wt%; H, 0.58 wt%. SSNMR: 126 ppm, 95 ppm, 29 ppm, 20 ppm, 10 ppm

S5. IR & NMR of Pristine Supported Materials

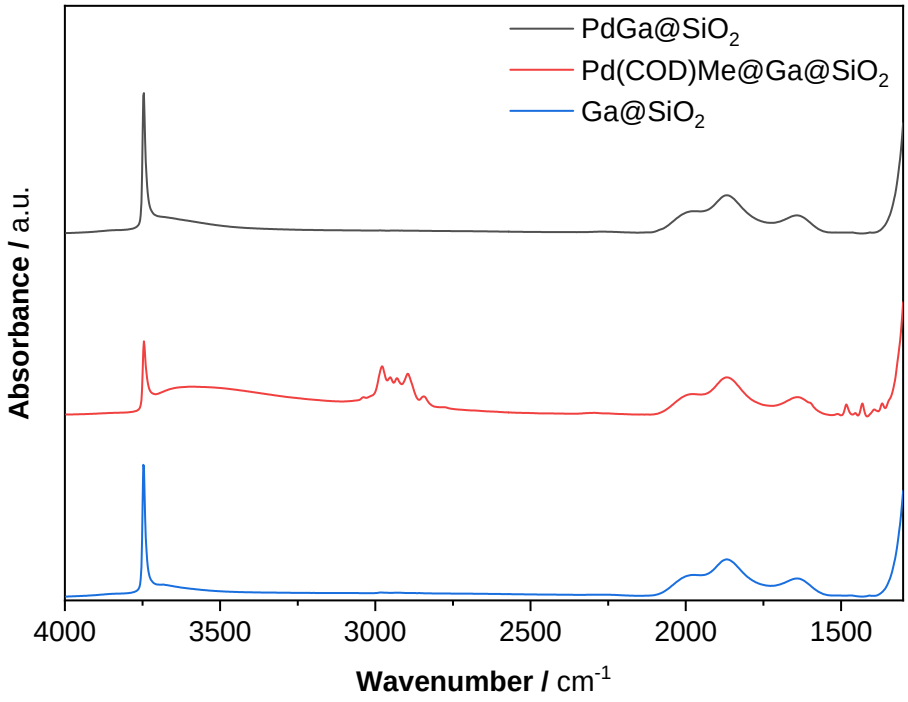

Figure S 9. IR spectra of (a) PdGa@SiO$_2$, (b) Pd(COD)Me@Ga@SiO$_2$ and (c) Ga@SiO$_2$

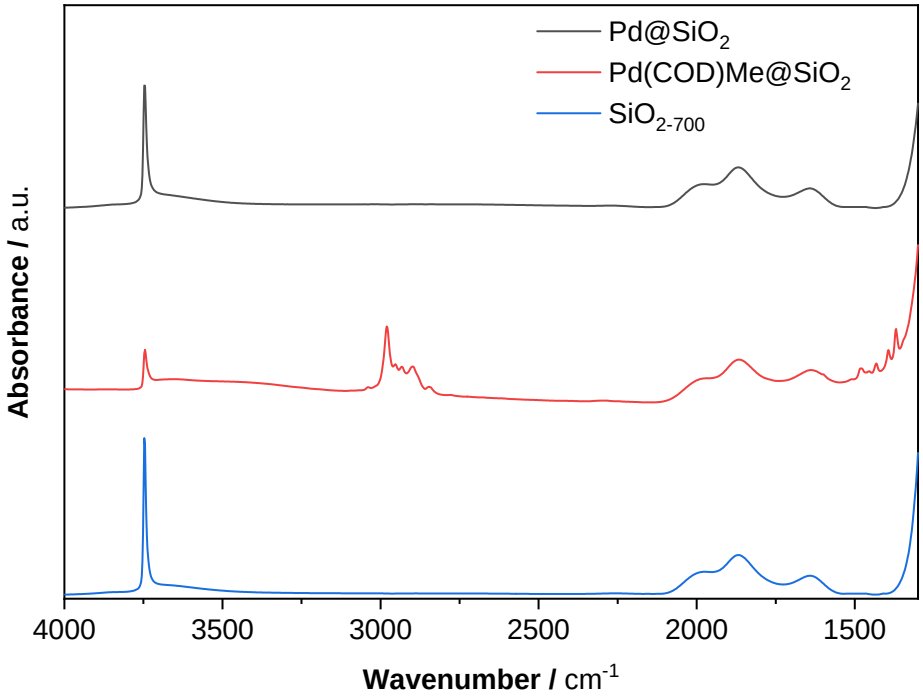

Figure S 10. IR spectra of (a) $Pd@SiO_2$, (b) $Pd(COD)Me@SiO_2$ and (c) $SiO_{2\text{-}700}$

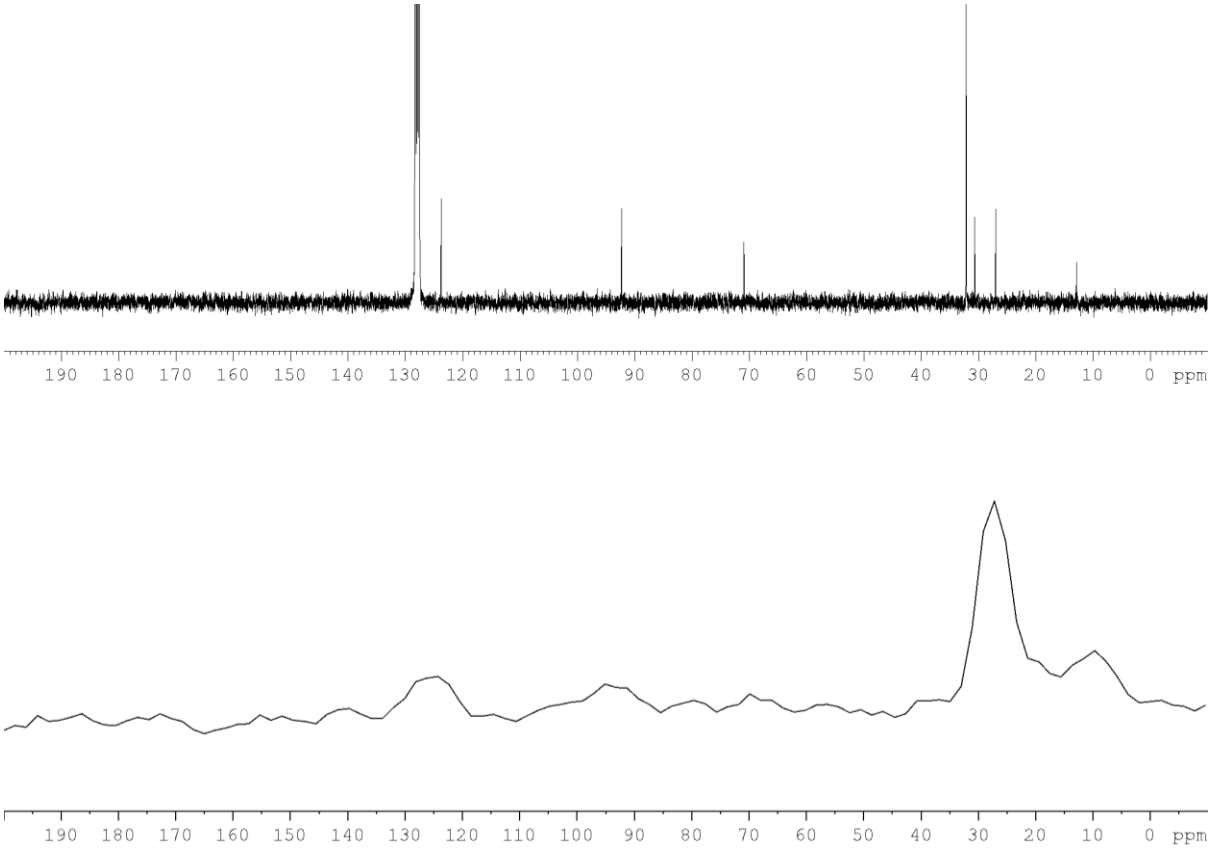

Figure S 11. NMR spectra for (top) $Pd(COD)Me(OSi(O\textit{t}Bu)_3)$ in C_6D_6 (for comparison), and (bottom) ^{13}C CP-MAS for $Pd(COD)Me@Ga@SiO_2$, *NS* = 40680, line broadening 150 Hz

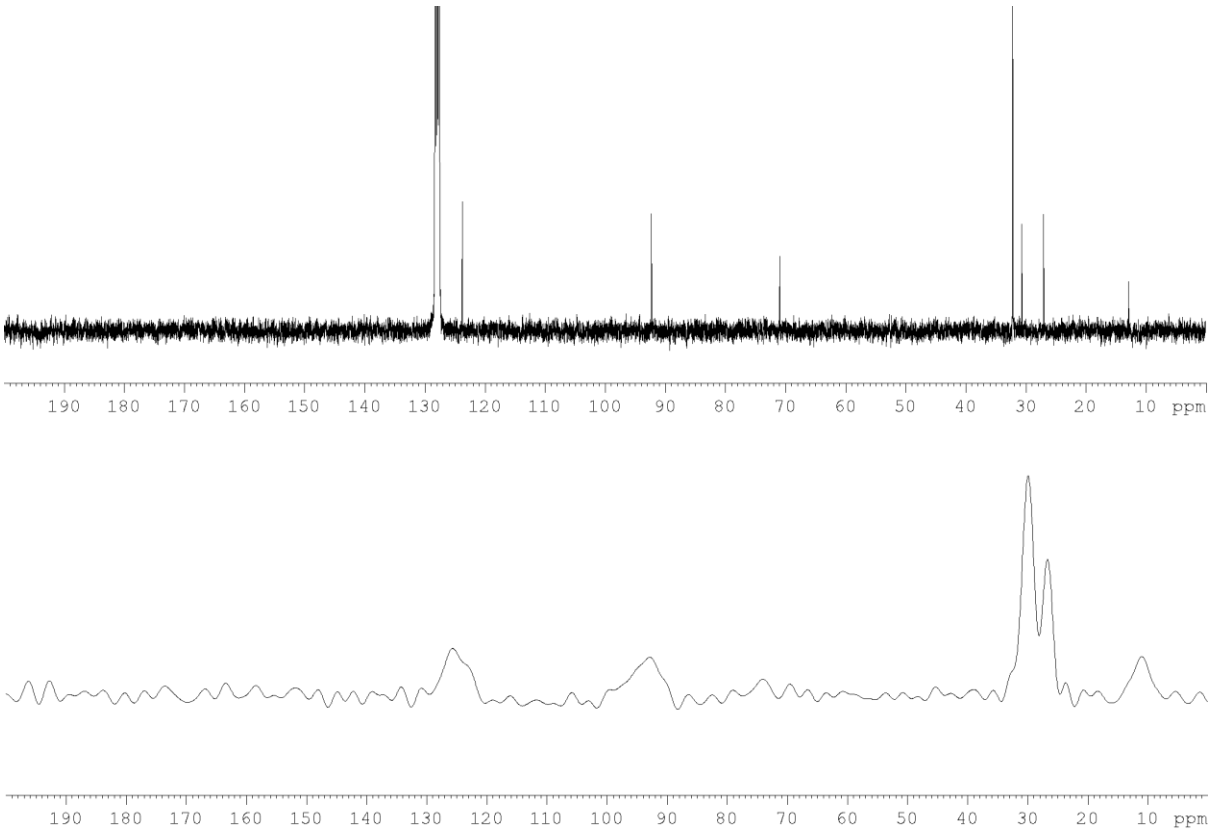

Figure S 12. NMR spectra for (top) Pd(COD)Me(OSi(O*t*Bu)$_3$) in C_6D_6 (for comparison), and (bottom) ^{13}C CP-MAS for Pd(COD)Me@SiO_2, *NS* = 34586

S6. CO and H_2 Chemisorption

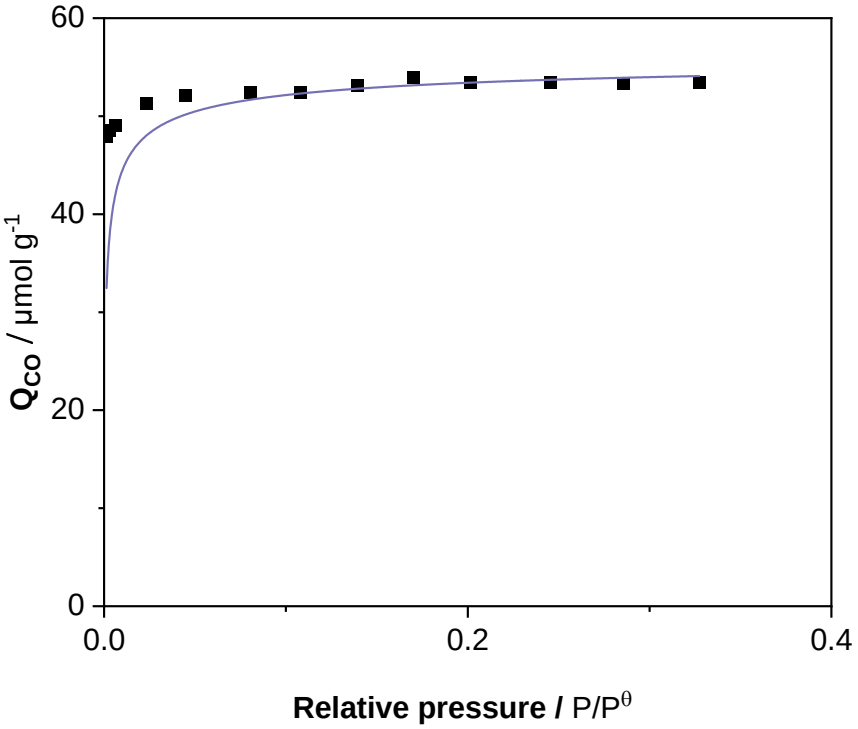

Figure S 13. CO chemisorption isotherm for PdGa@SiO_2, measured at 40 °C (K = 1312 ± 1215, Q_{sat} = 57 ± 1 µmol g^{-1}, r^2 = 1.000, χ^2 = 0.0043)

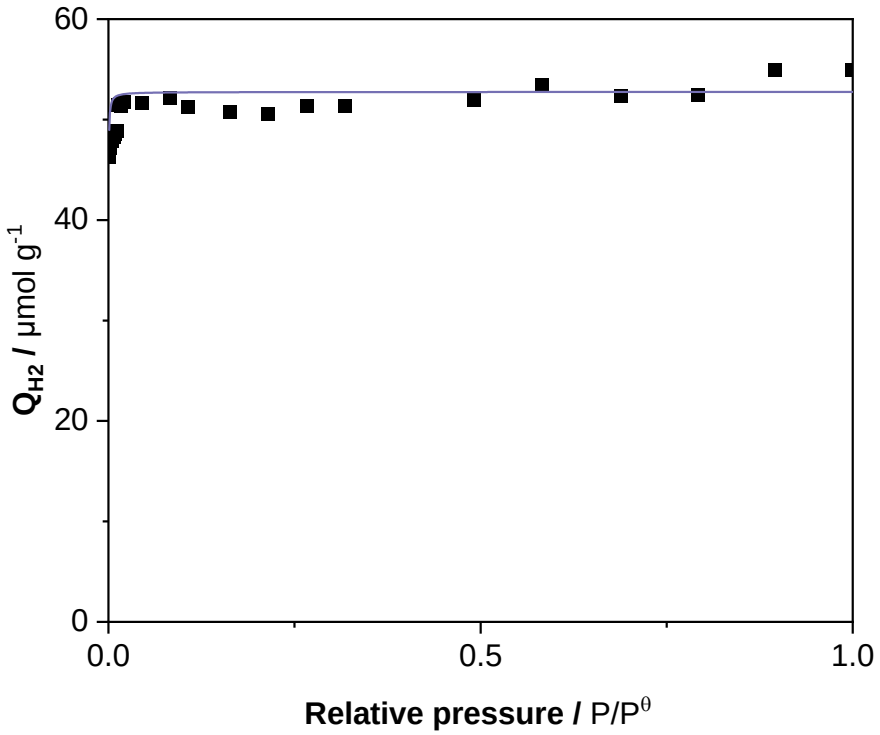

Figure S 14. H_2 chemisorption isotherm for $PdGa@SiO_2$, measured at 40 °C (K = 51 ± 15, Q_{sat} = 56 ± 0.5 µmol g^{-1} r^2 = 1.000, χ^2 = 0.04082)

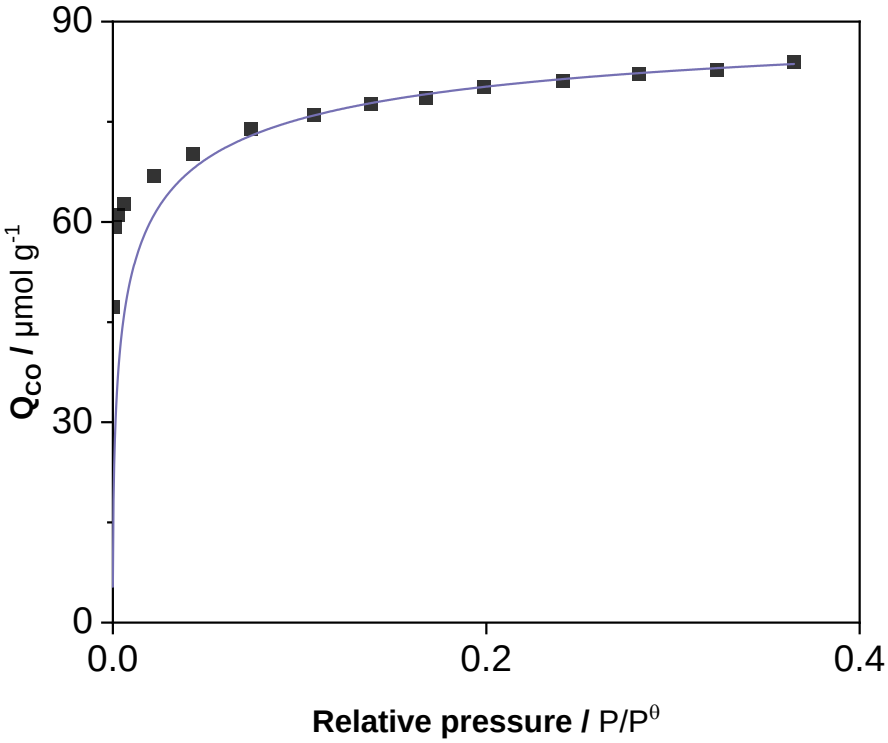

Figure S 15. CO chemisorption isotherm for $Pd@SiO_2$, measured at 40 °C (K = 145 ± 19, Q_{sat} = 95 ± 1 µmol g^{-1}, r^2 = 1.000, χ^2 = 0.0002)

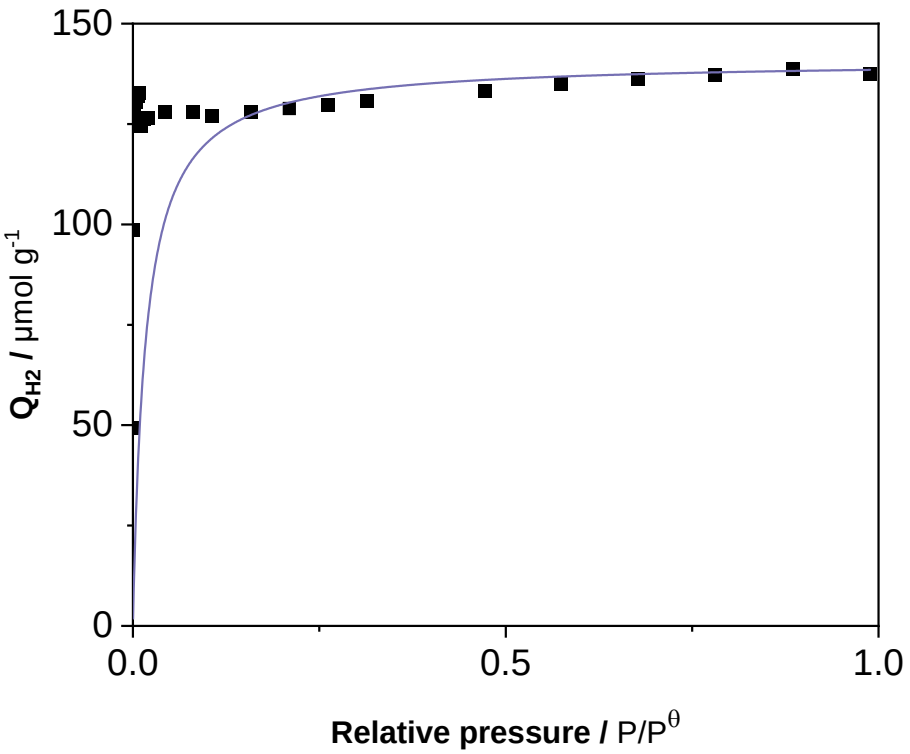

Figure S 16. H2 chemisorption isotherm for Pd@SiO_2, measured at 40 ^{o}C (K = 59 ± 13, Q_{sat} = 141 ± 1 µmol g^{-1}, r^2 = 1.000, χ^2 = 0.02643)

S7. IR Adsorption Studies

General comments for adsorption IR: Experiments were conducted in a glass reactor with IR-transparent CaF_2 windows.

CO Adsorption Studies: CO adsorption studies were performed on a self-supporting pellet of Pd@SiO_2 and were monitored by infrared spectroscopy at 2 cm^{-1} resolution. The mass of each pellet (ca. 2-3 mg) and CO pressures (ca. 8-12 mbar) were used to prevent saturation of the IR spectrum. After placing each sample under high vacuum (10^{-5} mbar), a reference spectrum was recorded. The pellet was then exposed to a known pressure of CO and a spectrum was recorded. Vacuum (10^{-5} mbar) was also applied at room temperature after exposure to CO to probe the reversibility of the adsorption.

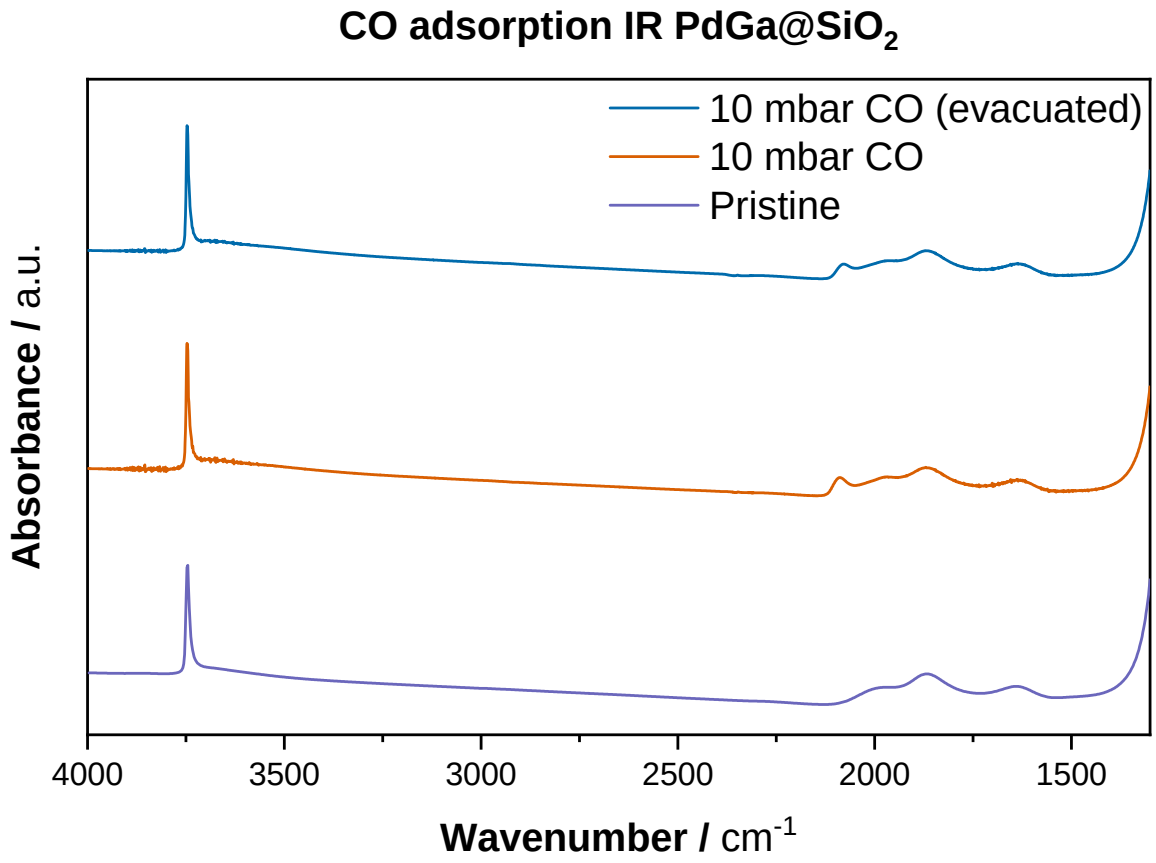

Figure S 17. FTIR spectra of CO adsorbed on (top) PdGa@SiO_2 after evacuating, (middle) PdGa@SiO_2 (10 mbar CO) and (bottom) PdGa@SiO_2 (pristine) at room temperature. Spectra are normalized with respect to the Si-O-Si band of silica at 1868 cm^{-1}

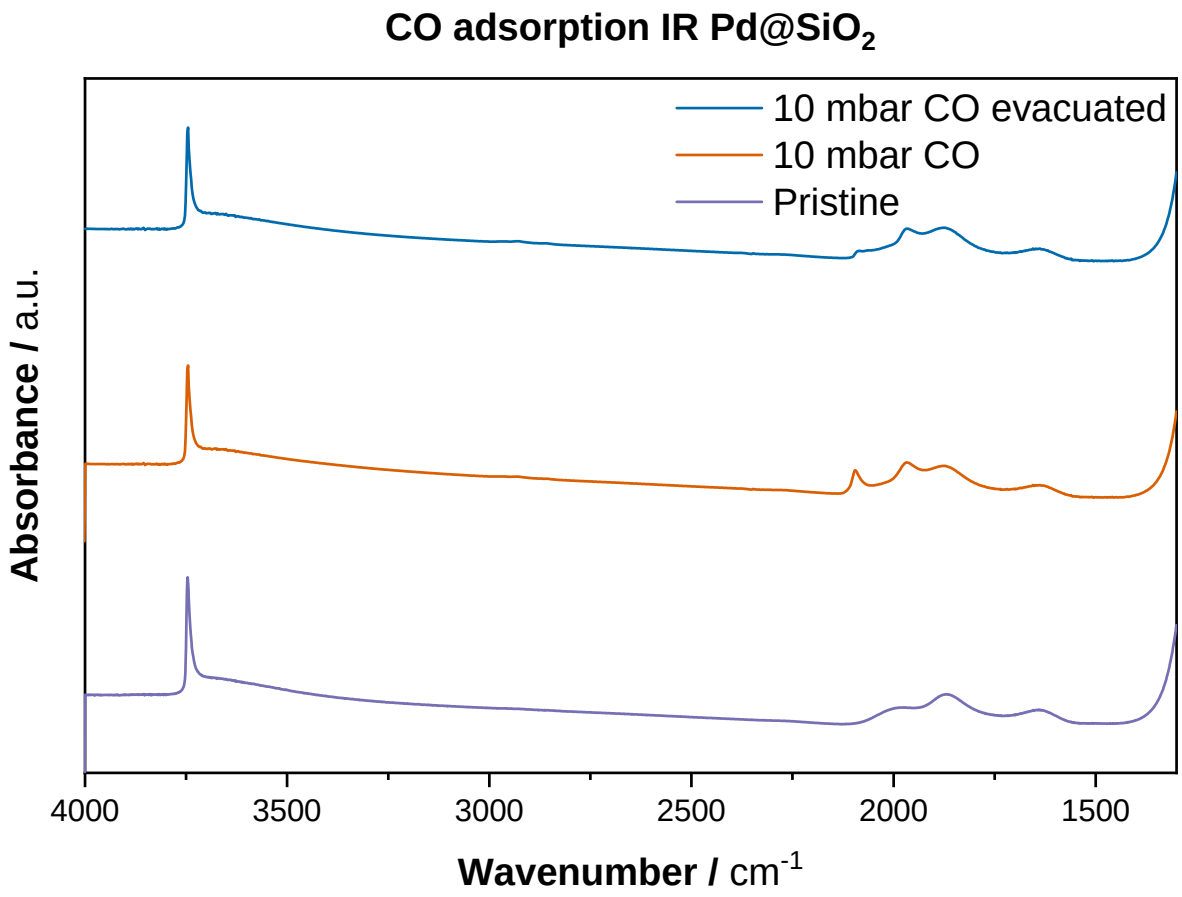

Figure S 18. FTIR spectra of CO adsorbed on (top) $Pd@SiO_2$ after evacuating, (middle) $Pd@SiO_2$ (10 mbar CO) and (bottom) $Pd@SiO_2$ (pristine) at room temperature. Spectra are normalized with respect to the Si-O-Si band of silica at 1868 cm^{-1}

MeOH Adsorption and Desorption Studies: MeOH adsorption studies were performed on a self-supporting pellet of $Pd@SiO_2$ or $PdGa@SiO_2$ and were monitored by infrared spectroscopy at 2 cm^{-1} resolution. The mass of each pellet (ca. 2-3 mg) was used to prevent saturation of the IR spectrum. After placing each sample under high vacuum (10^{-5} mbar), a reference spectrum was recorded. The pellet was then exposed to a known pressure of MeOH (200 mbar) and evacuated (10^{-5} mbar) at room temperature, and a spectrum was recorded.

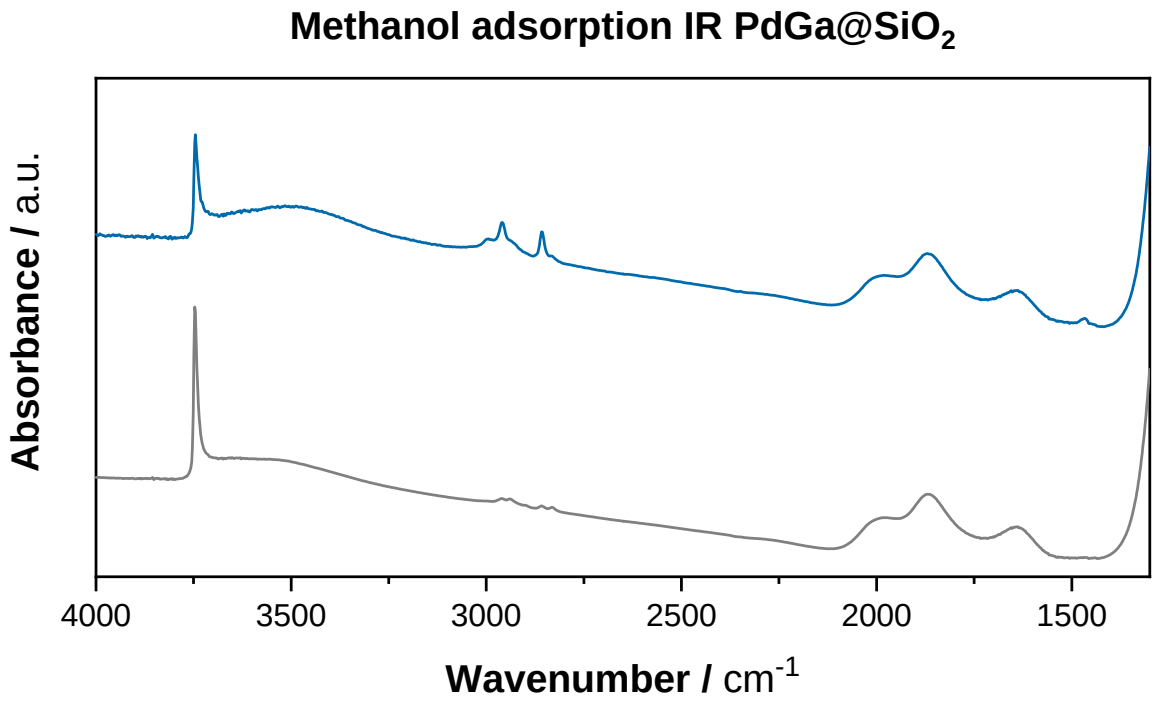

Figure S 19. FTIR spectra of Methanol adsorbed on (top) PdGa@SiO_2 after evacuating, (bottom) PdGa@SiO_2 (pristine) at room temperature. Spectra are normalized with respect to the Si-O-Si band of silica at 1868 cm^{-1}

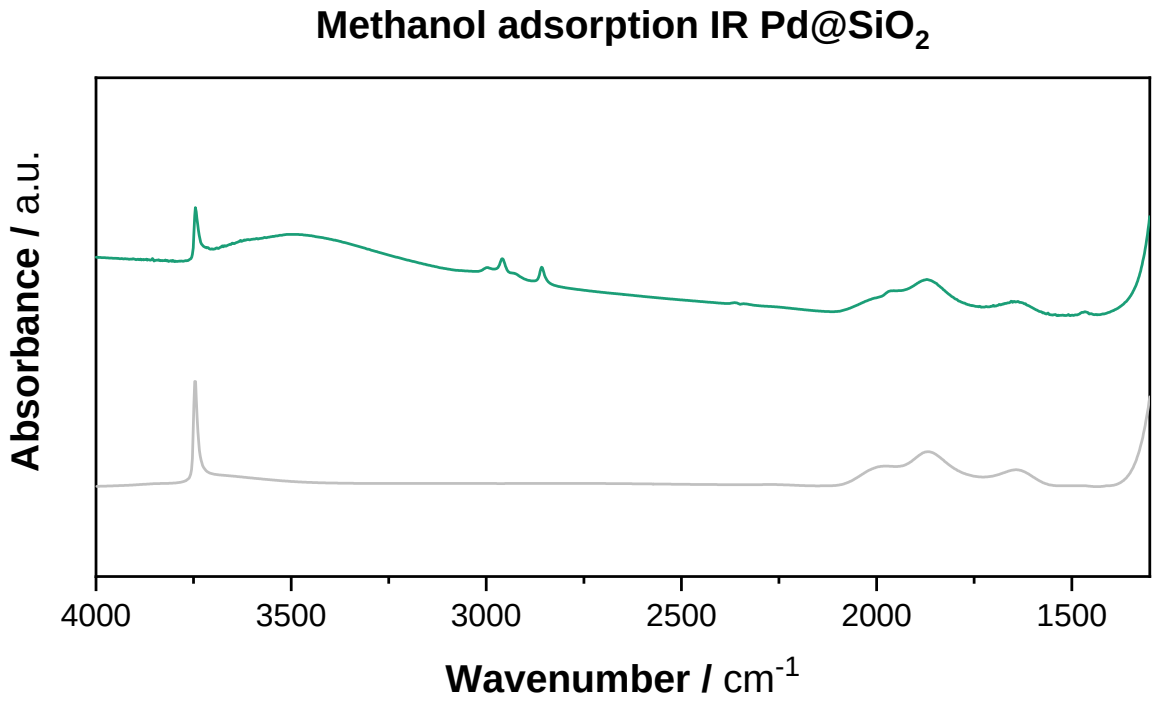

Figure S 20. FTIR spectra of Methanol adsorbed on (top) Pd@SiO_2 after evacuating, (bottom) Pd@SiO_2 (pristine) at room temperature. Spectra are normalized with respect to the Si-O-Si band of silica at 1868 cm^{-1}

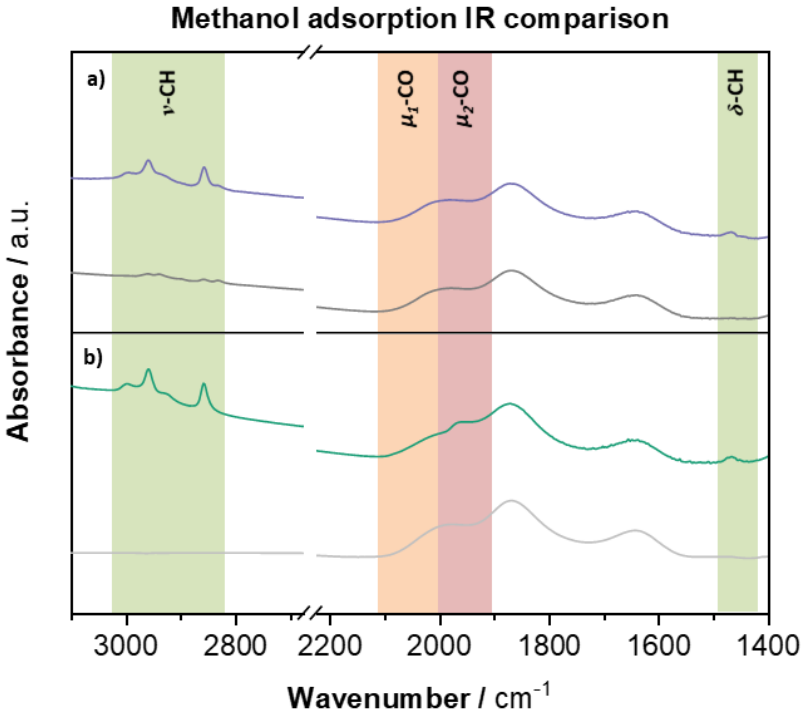

Figure S 21. FTIR spectra of MeOH adsorbed on (a) PdGa@SiO_2 and (b) Pd@SiO_2, after evacuation at room temperature. Spectra are normalized with respect to the Si-O-Si band of silica at 1868 cm^{-1}. Grey traces represent the material prior to adsorption.

S8. X-ray Absorption Spectroscopy

XAS measurements were carried out at the Pd and Ga K edges at the SuperXAS beamline at SLS (PSI, Villigen, Switzerland). The storage ring was operated at 2.4 GeV in top-up mode with a ring current of around 400 mA. The incident photon beam provided by a 2.9 T super bend magnet source was selected by a Si (111) quick-EXAFS monochromator and the rejection of higher harmonics and focusing were achieved by a rhodium-coated collimating mirror for Ga K edge (and platinum-coated mirror for Pd K edge) at 2.5 mrad and a rhodium-coated torroidal mirror for Ga K edge (and platinum-coated mirror for Pd K edge) at 2.5 mrad. The beamsize on the sample was 500 x 100 μm. During measurement, the quick XAS monochromator was rotating with 10 Hz frequency in 2 deg angular range and X-ray absorption spectra were collected in transmission mode using ionization chambers specially developed for quick data collection with 1 MHz frequency. *Ex situ* spectra were collected for 5 min and averaged.

For Pd, the beamline energy was calibrated with Pd reference foil to the Pd K edge position at 24350.0 eV. For Ga, a Zn reference foil was used for energy calibration

(9659.0 eV). To avoid contact with air, all samples were sealed in a glovebox. For *ex situ* samples packed under an inert atmosphere, pressed pellets (with optimized thickness for transmission detection) were placed in two aluminized plastic bags (Polyaniline (15 μm), polyethylene (15 μm), Al (12 μm), polyethylene (75 μm) from Gruber-Folien GmbH & Co. KG, Straubing, Germany) using an impulse sealer inside a glovebox; one sealing layer was removed immediately before the measurements.

In a typical *in situ* experiment, 10-20 mg of the powder sample was packed into a 3 mm quartz capillary (i.d. 2.8 mm), which was connected with a pressurizable gas flow system equipped with 3 mass flow controllers (Bronkhorst) mounted in a parallel configuration, a bypass to enable air-free loading of samples, and a back-pressure regulator (Bronkhorst). H_2, Ar, and mix gas (H_2:CO_2:Ar, 3:1:1) flows were calibrated in the range 0-50 sccm. Samples were heated using a custom-built infrared heater (Elstein-Werk M. Steinmetz GmbH & Co. KG (Germany), 30 mm length, with two heating elements – one above and one below sample capillary). Temperature calibration was performed in the range 25-510 ^oC. In a typical experiment, the sample was first reduced under a flow of H_2 (10 sccm) using a temperature ramp of 5 $^oC\ min^{-1}$, reaching a terminal temperature of 500 ^oC. Spectra were recorded continuously during the hydrogen treatment. The sample was then cooled to room temperature, under a flow of H_2 to enable collection of data for the as-reduced material at lower temperatures, before being heated to 230 ^oC under H_2, pressurized to 5 bar in mixed gas (10 sccm) and measured continuously for 3 h. The sample was then depressurized, and H_2 (10 sccm) was flowed over for 40 minutes. The sample was then re-pressurized to 5 bar in mixed gas (10 sccm) and measured continuously for a further 3 h.

For the analysis of the X-ray Absorption Near Edge Structure (XANES) the edge energy is defined as the first maximum of the derivative of the XANES region. Linear combination fits (LCF) of Ga K edge XANES were fitted using Ga(0) metal and Ga@SiO_2 as reference. For the analysis of Extended X-ray absorption fine structure (EXAFS), data processing was done by standard procedures using the ProXASGui software developed at the SuperXAS beamline, PSI, Villigen. The program package Demeter was used for analysis of EXAFS.[13] S_0^2 value was obtained by fitting Pd foil reference sample for Pd K edge. MCR analysis was performed using the in-built feature of the ProXAS software.

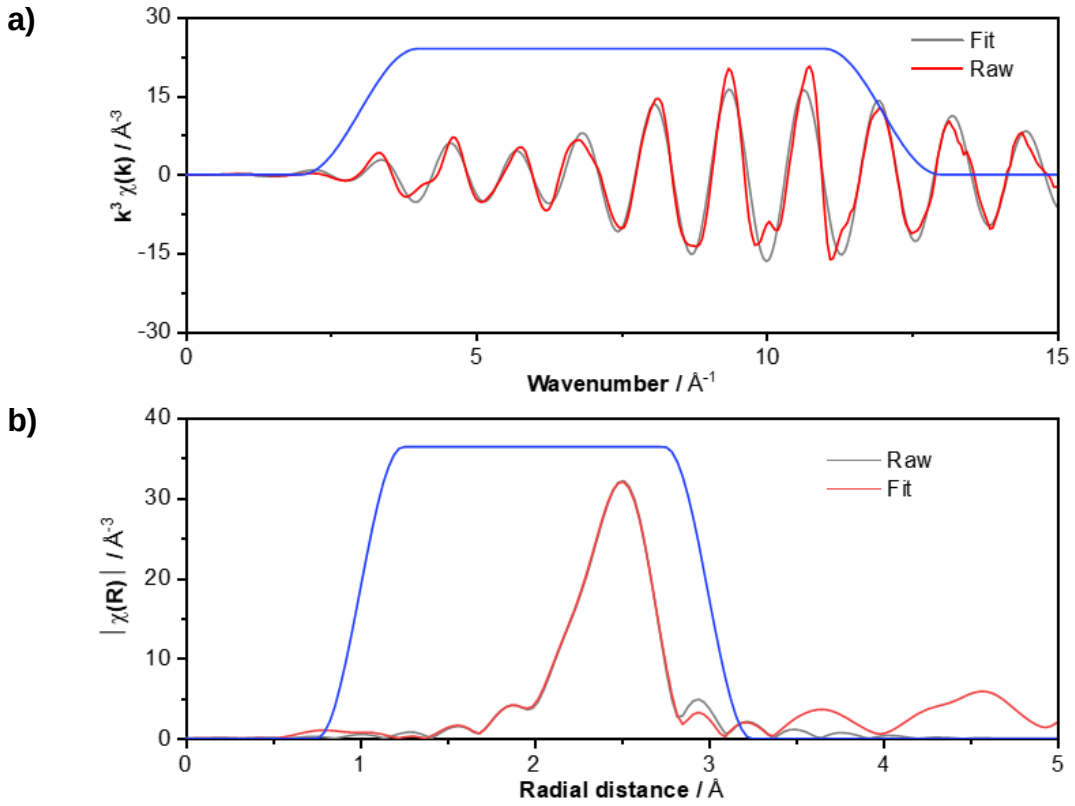

Figure S 22. EXAFS fit for Pd foil (Pd K edge). Used to obtain amplitude reduction factor (S_0^2). (a) K-space with raw (grey) and fitted (red) data. Window (blue) 3.0-12.0 $Å^{-1}$, k-weight = 3, Hanning window, dk = 2; (b) R-space with raw (grey) and fitted (red) data. Window (blue) 1-3. Å, k-weight = 3, Hanning window, dk = 0.5. Fit summarised in table S 1

Table S 1. Summary of fitted parameters for Pd foil (Pd K edge), 3.0-12.0 $Å^{-1}$, k-weight = 3

ΔE0 (eV)	-5.1	+/-	0.3
Pd (1st shell)			
S_0^2	0.817	+/-	0.03
R (Å)	2.742	+/-	0.002
σ^2 ($Å^2$)	0.005	+/-	0.000(1)

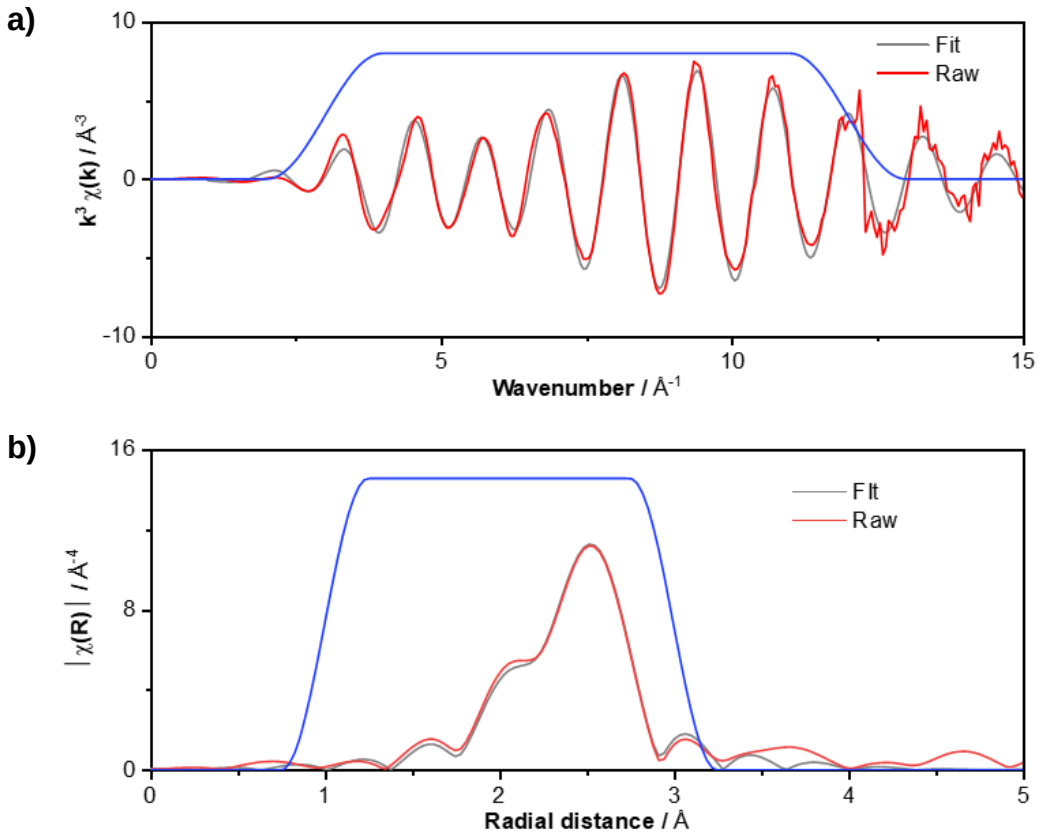

Figure S 23. EXAFS fit for $Pd@SiO_2$ (Pd K edge). (a) K-space with raw (grey) and fitted (red) data. Window (blue) 3.0-12.0 $Å^{-1}$, k-weight = 3, Hanning window, dk = 2; (b) R-space with raw (grey) and fitted (red) data. Window (blue) 1-3. Å, k-weight = 3, Hanning window, dk = 0.5. fit summarised in table S 2

Table S 2. Summary of fitted parameters for $Pd@SiO_2$ (Pd K edge), 3.0-12.0 $Å^{-1}$, k-weight = 3

ΔE^0 (eV)	3.65	+/-	0.4
Pd (1st Shell)			
N	8.1	+/-	0.4
R (Å)	2.73	+/-	0.002
σ^2 ($Å^2$)	0.008	+/-	0.0003

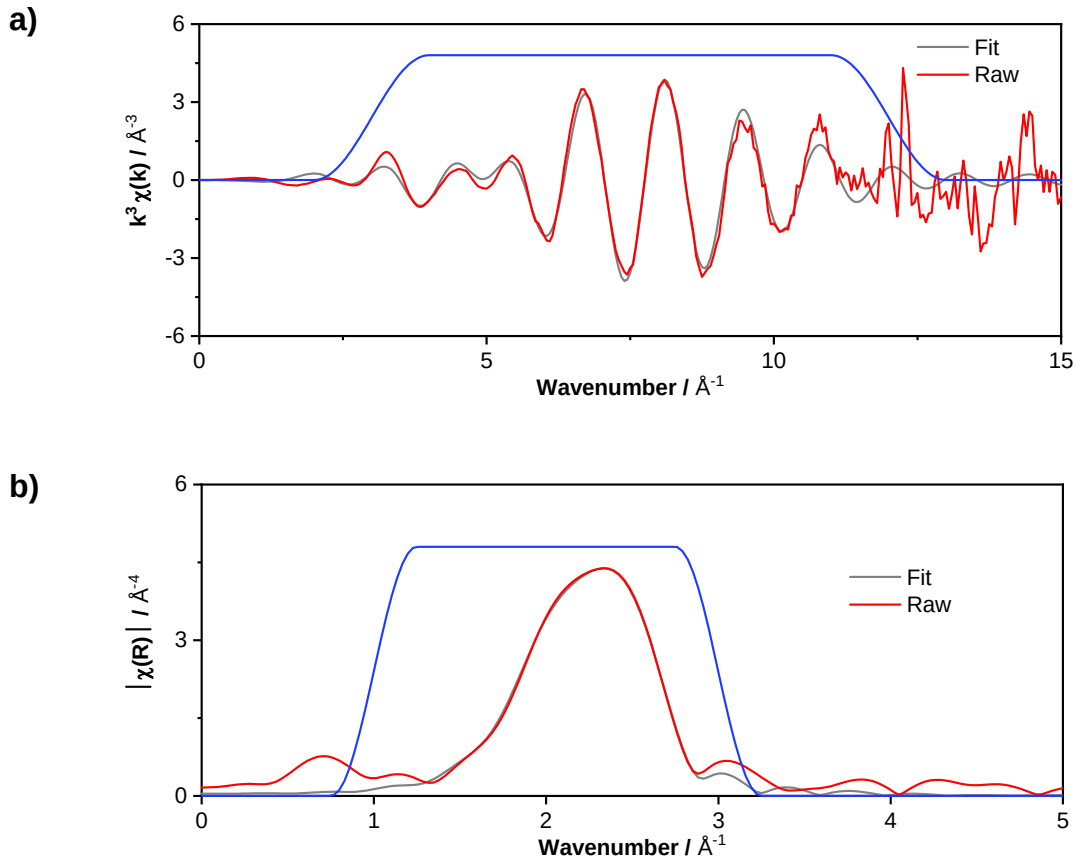

Figure S 24. EXAFS fit for PdGa@SiO_2 (Pd K edge). (a) K-space with raw (grey) and fitted (red) data. Window (blue) 3.0-12.0 $Å^{-1}$, k-weight = 3, Hanning window, dk = 2; (b) R-space with raw (grey) and fitted (red) data. Window (blue) 1-3. Å, k-weight = 3, Hanning window, dk = 0.5. Fit summarised in Table S3

Table S3. Summary of fitted parameters for PdGa@SiO_2 (Pd K edge), 3.0-12.0 $Å^{-1}$, k-weight = 3

ΔE0 (eV)	-0.6	+/-	2.4
Ga (1st Shell)			
No. neighbour	2.9	+/-	0.9
R (Å)	2.48	+/-	0.02
σ^2 ($Å^2$)	0.010	+/-	0.003
Pd (1st Shell)			
No. neighbour	3.1	+/-	0.9
R (Å)	2.73	+/-	0.01
σ^2 ($Å^2$)	0.009	+/-	0.002

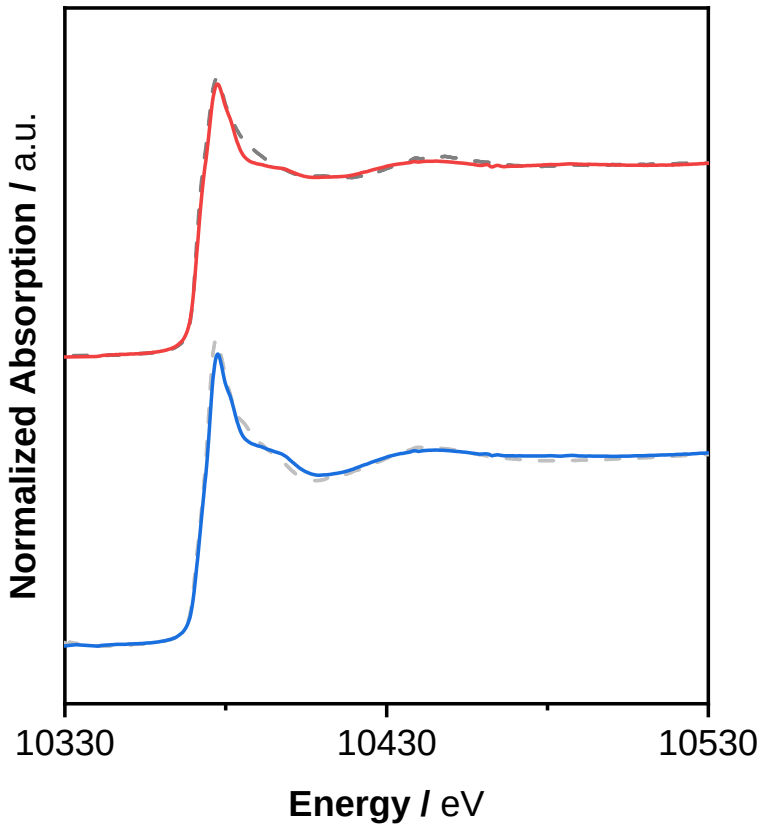

Figure S 25. LCF of Ga K edge XANES for (top) pristine PdGa@SiO_2, red trace – experimental data, dark grey trace – model; and (bottom) PdGa@SiO_2 after reaction, blue trace – experimental data, light grey trace – model. Summary of fits found in Table S 4.

Table S 4. Summary of fitted parameters linear combination fits of PdGa@SiO_2 (Ga K edge) before (PdGa@SiO_2 (pristine)) and after (PdGa@SiO_2 (spent)) reaction.

PdGa@SiO_2 (pristine)			
	LCF composition		
Ga(0)	0.671	+/-	0.011
Ga@SiO_2	0.329	+/-	0.011
***R*-factor**	0.0055		
PdGa@SiO_2 (spent)			
	LCF composition		
Ga(0)	0.457	+/-	0.013
Ga@SiO_2	0.543	+/-	0.013
***R*-factor**	0.0065		

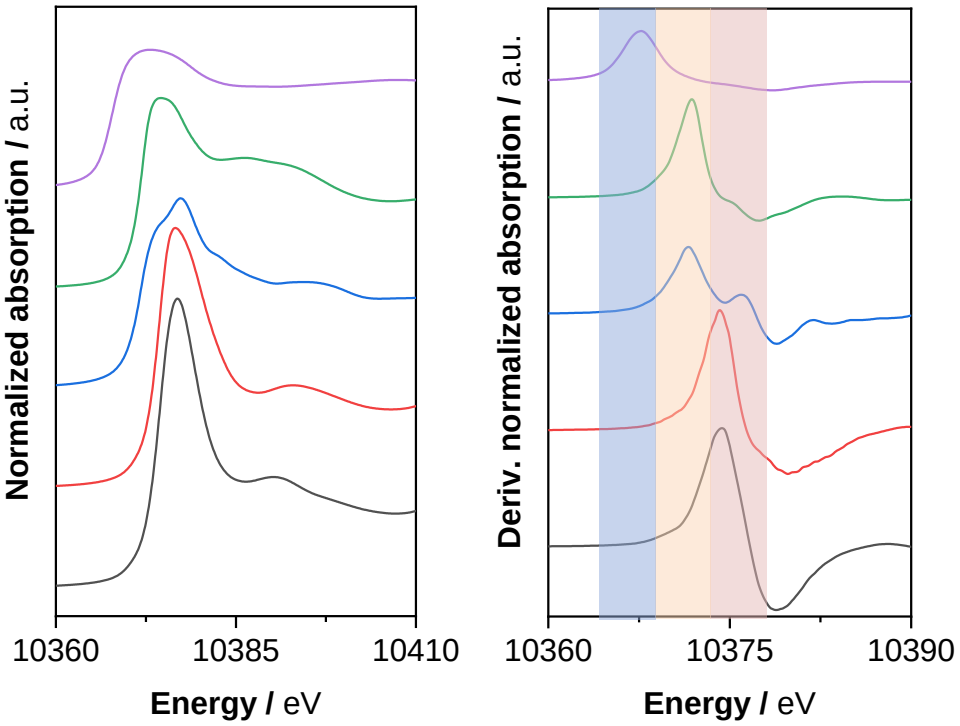

Figure S 26. Ga K edge XANES (left) Normalized absorption, (right) derivative of normalized absorption. Lilac (top) – Ga metal, green (top middle) – Ga@SiO_2, blue (middle) – β-Ga_2O_3, red (lower middle) – $Ga(NO_3)_3(H_2O)_9$, dark grey (bottom) – $Ga(acac)_3$. Coloured bands can be defined as follows: left (blue) – metallic Ga (Ga(0)), centre (peach) – tetrahedral Ga (Ga_{IV}), right (pink) – octahedral Ga (Ga_{VI})

Table S 5. Summary of edge energies for Ga K-edge of various reference (known) and synthesized materials.[1] Assignment of Ga_{IV} and Ga_{VI} energies based on those reported in the literature.[14]

Sample	**Assigned configuration**		
Reference	**Ga^0 / eV**	**Ga_{IV} / eV**	**Ga_{VI} / eV**
Ga metal	10367.7	-	-
Ga@SiO_2	-	10371.8	-
β-Ga_2O_3	-	10371.6	10376.0
$Ga(NO_3)_3(H_2O)_9$	-	-	10374.2
$Ga(acac)_3$	-	-	10374.2
Materials	**Ga^0 / eV**	**Ga_{IV} / eV**	**Ga_{VI} / eV**
Pristine	10367.5	10371.8	-
Spent	10367.2	10371.5	-

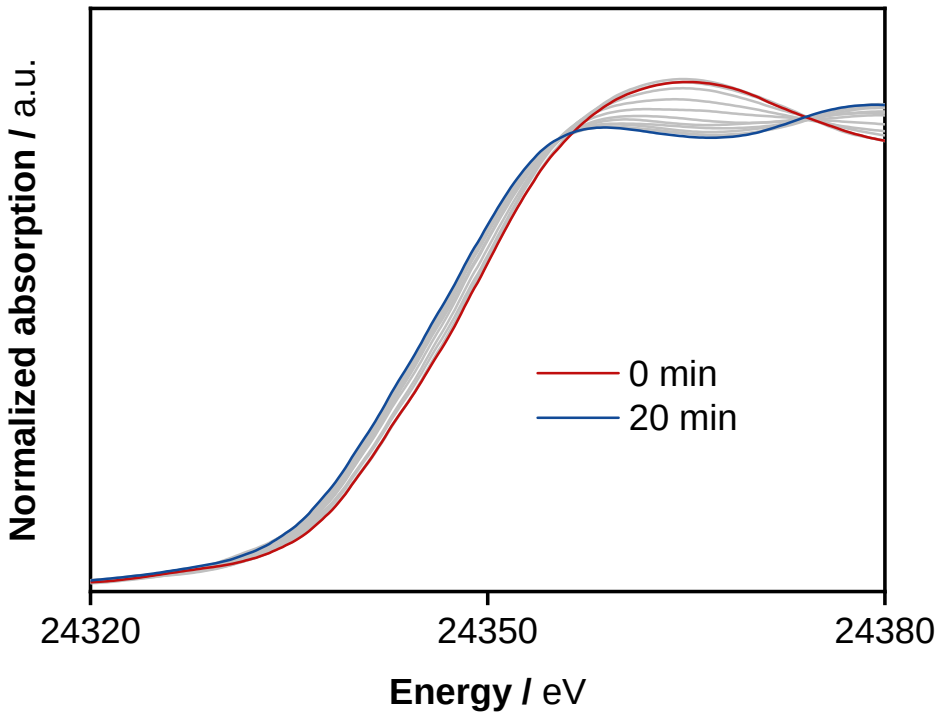

Figure S 27. Pd K edge XANES for Pd(COD)Me@Ga@SiO_2 under a flow of H_2/Ar (1:5, 6 sccm) at 25 ^oC (1 bar (a)). 60 second increments, continuous acquisition. Loss of white line intensity and shift to lower energy consistent with reduction of Pd^{II} to Pd^0. Note that reduction of of Pd^{II} to Pd^0 occurs at room temperature in these conditions.

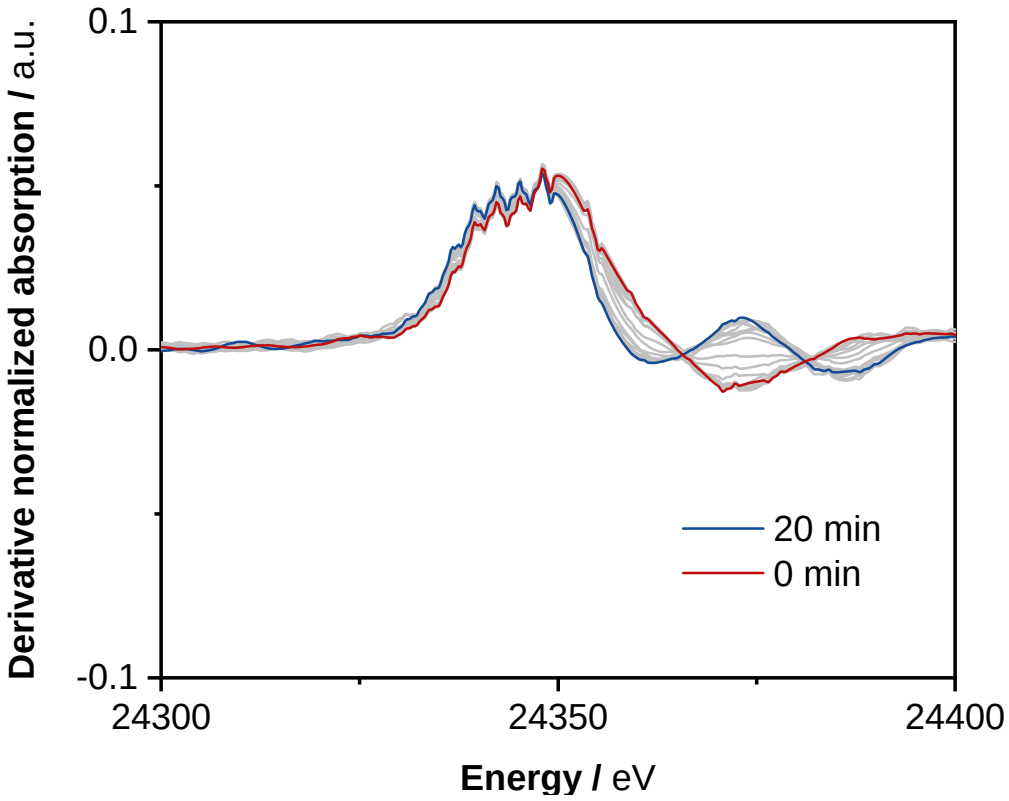

Figure S 28. 1st derivative Pd K edge XANES for Pd(COD)Me@Ga@SiO_2 under a flow of H_2/Ar (10 sccm) at 25 ^oC (1 bar (a)). 60 second increments, continuous

acquisition. Note the continual shift to lower energy for the principle feature at around 24350 eV. Note also the continual evolution of the first derivative, as well as the presence of two isosbestic points at 24366 eV and 24381 eV.

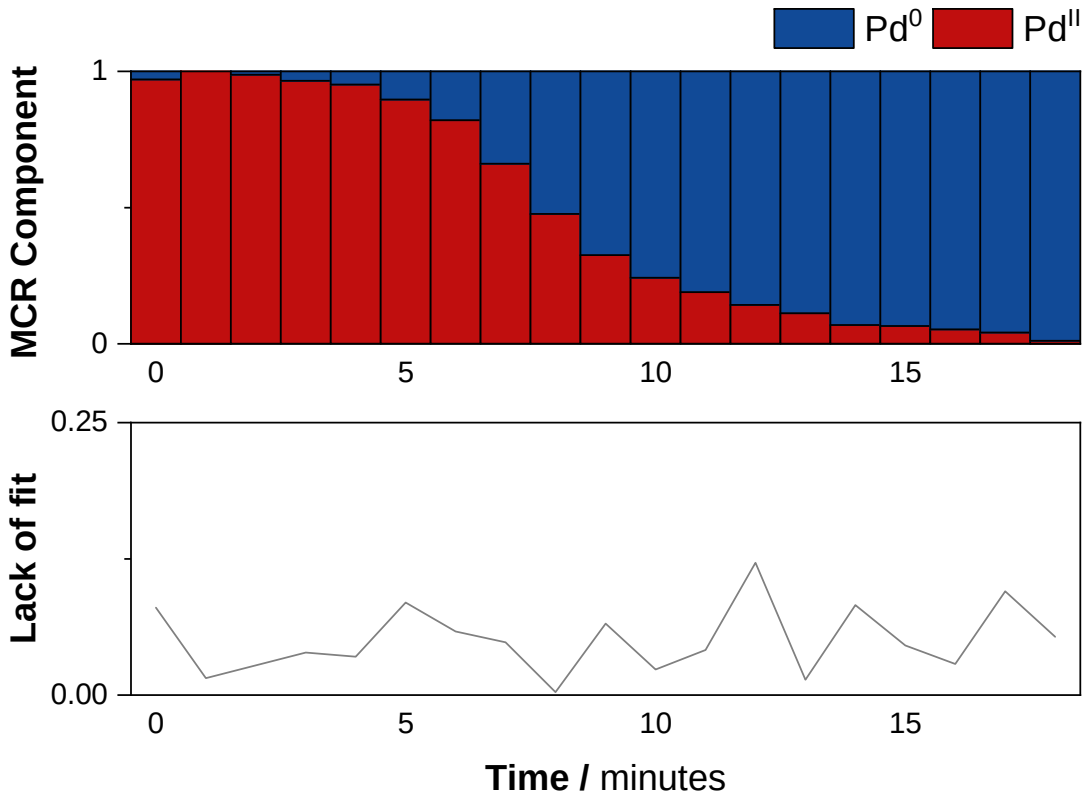

Figure S 29. Pd K edge XANES - MCR component fit for H_2 treatment of Pd(COD)Me@Ga@SiO_2 at room temperature. (top) MCR component (2 component fit), and (bottom) lack of fit.

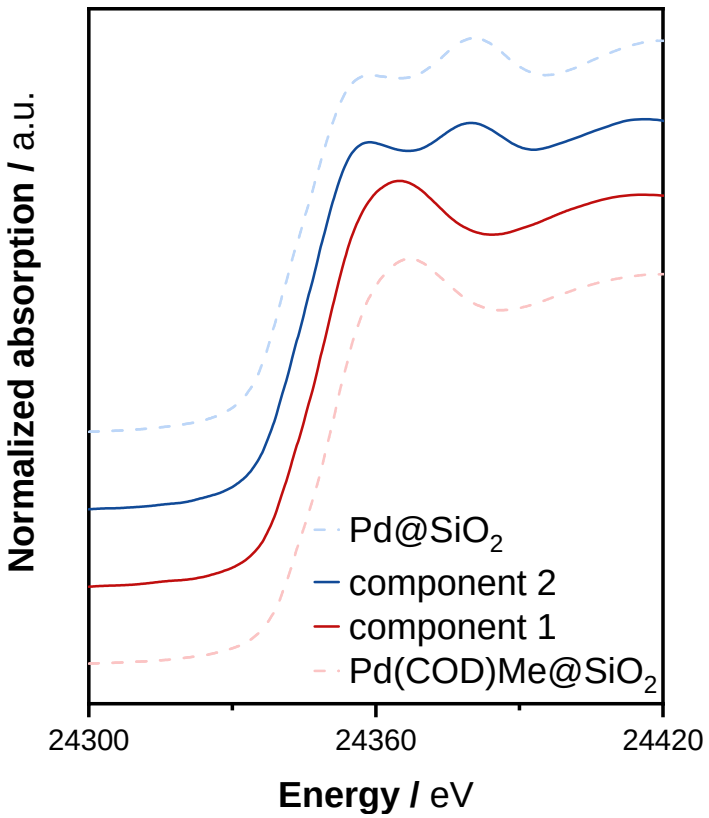

Figure S 30. Pd K edge XANES - MCR-resolved components for H_2 treatment of Pd(COD)Me@Ga@SiO_2 at room temperature.(top, light blue, dashed) Pd@SiO_2 *ex situ*; (top-middle, dark blue, solid) component 2 (MCR)*;* (bottom-middle, dark red, solid) component 1 (MCR); (bottom, light red, dashed) Pd(COD)Me@SiO_2 *ex situ*. Comparison of reference materials (*ex situ*) and components is consistent with reduction at room temperature. Note the increased white line intensity of component 1 and similarity to the grafted species (Pd(COD)Me@SiO_2, *ex situ*), while component 2 has a shifted E_0 and less intense white line feature, and a profile similar to that of Pd@SiO_2. Loss of white line intensity and shift to lower energy consistent with reduction of Pd^{II} to Pd^0. Conditions: H_2 (10 sccm) at 25 °C (1 bar (a))

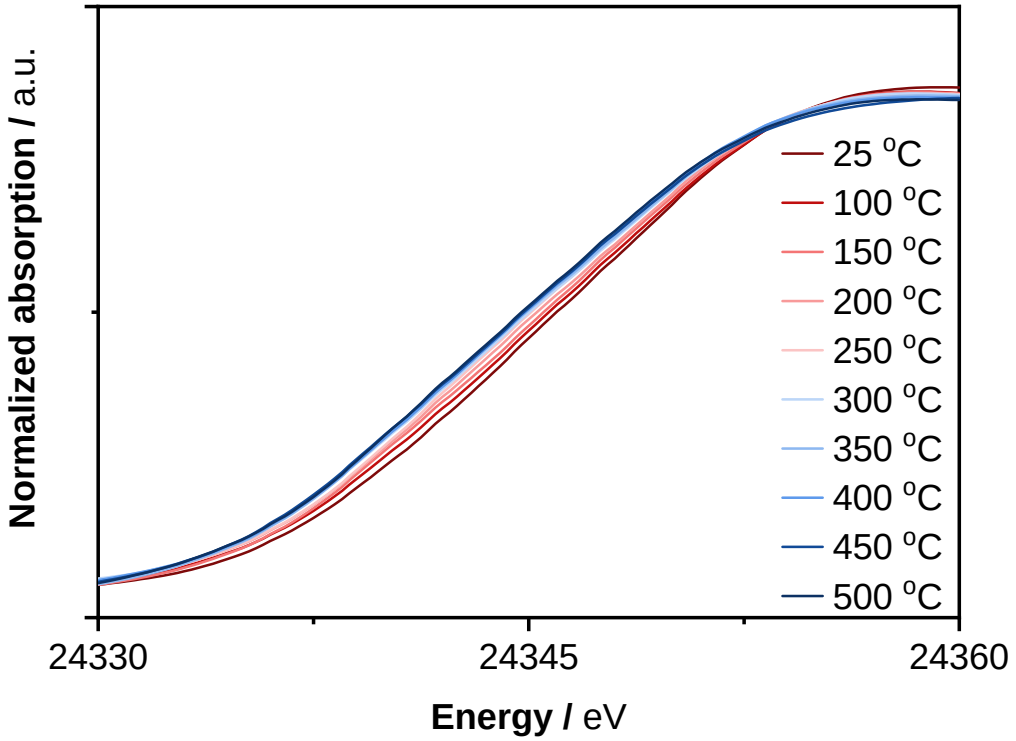

Figure S 31. Pd K edge XANES in range 24330-24345 eV for Pd(COD)Me@Ga@SiO_2 under a flow of H_2 (10 sccm) from 25 °C to 500 °C, , after treatment at room temperature in same gas flow for 20 minutes (ramp: 5 °C min^{-1}, 1 bar (a)). 60 second increments, continuous acquisition. Note continual shift to lower energy

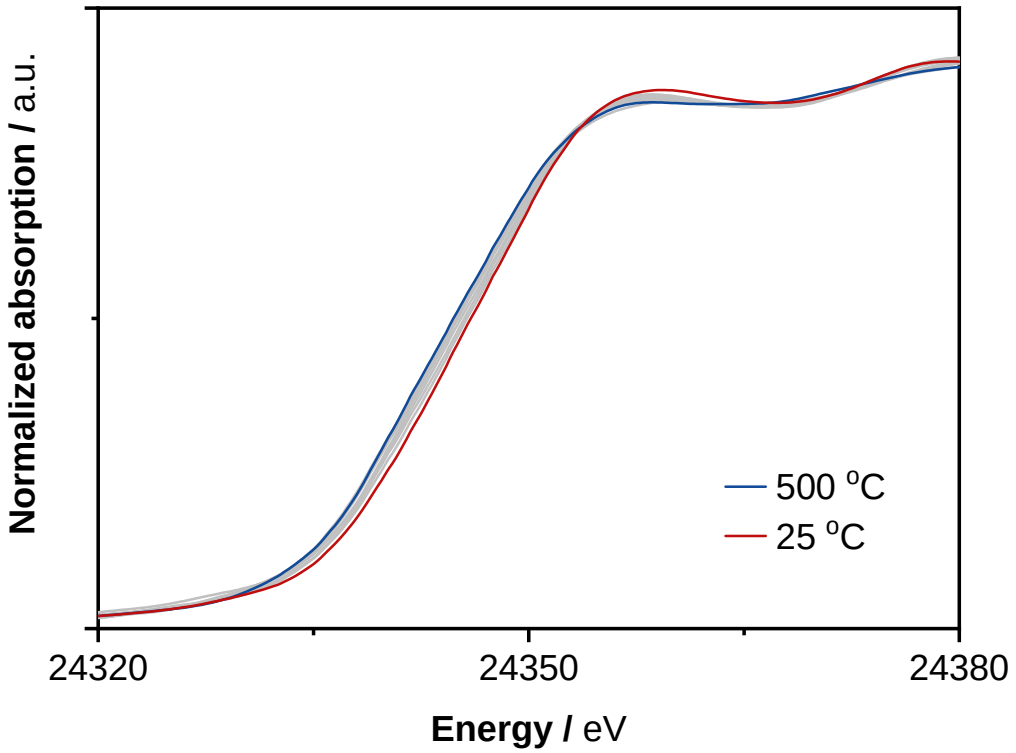

Figure S 32. Pd K edge XANES in range 24320-24380 eV for Pd(COD)Me@Ga@SiO_2 under a flow of H_2 (10 sccm) from 25 °C (red) to 500 °C

(blue), after treatment at room temperature in same gas flow for 20 minutes (ramp: 5 ^{o}C min^{-1}, 1 bar (a)). 60 second increments, continuous acquisition.

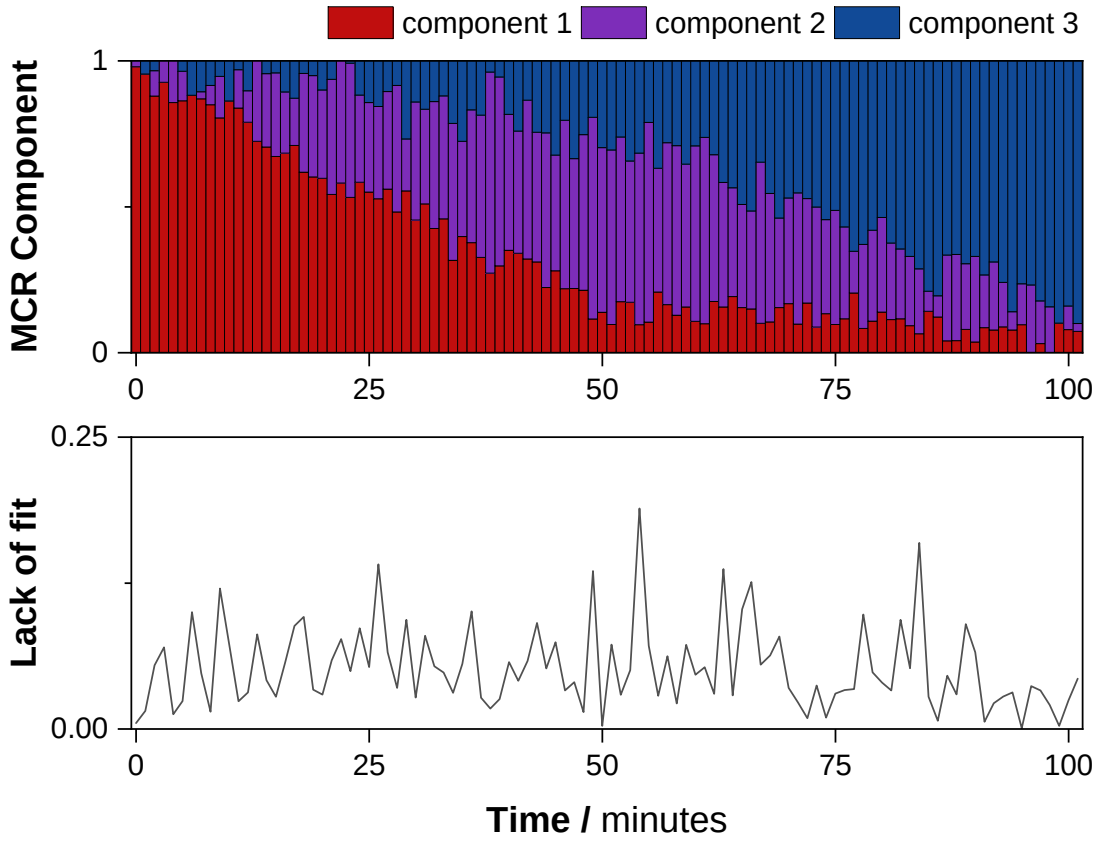

Figure S 33. Pd K edge XANES - MCR component fit for H_2 treatment of Pd(COD)Me@Ga@SiO_2 from 25 ^{o}C to 500 ^{o}C. (top) MCR component (3 component fit), and (bottom) lack of fit. 60 second increments, continuous acquisition. Ramp: 5 ^{o}C min^{-1}, 1 bar (a) (i.e. each bar represents a window of 5 ^{o}C, final 5 data points recorded at terminal temperature (500 ^{o}C))

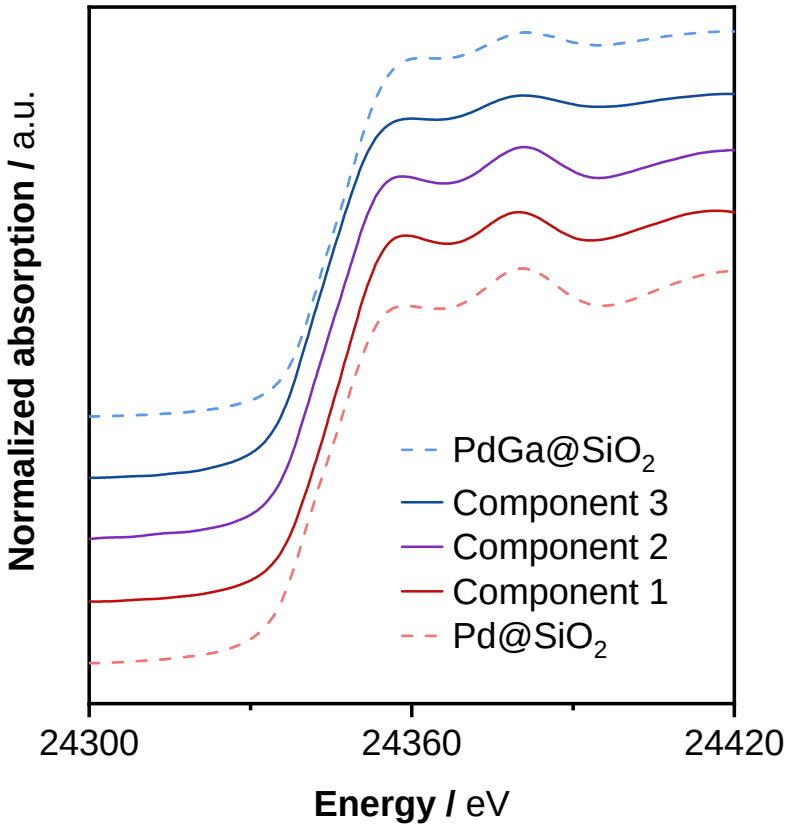

Figure S 34. Pd K edge XANES - MCR-resolved components for H_2 treatment of Pd(COD)Me@Ga@SiO_2 from room temperature to 500 ^oC.(top, light blue, dashed) PdGa@SiO_2 *ex situ*; (top-middle, dark blue, solid) component 3 (MCR)*;* (middle, purple, solid) component 2 (MCR) (bottom-middle, dark red, solid) component 1 (MCR); (bottom, light red, dashed) Pd@SiO_2 *ex situ*. Comparison of reference materials (*ex situ*) and components is consistent with formation of a PdGa alloy at elevated temperatures. Note the slight shift in position of the peak at 24380 eV between component 1 & 2 and the significant damping observed for component 3. While the damping may arise from thermal contributions, it is also consistent with the observed post-edge for the bimetallic PdGa@SiO_2 measured *ex situ* at room temperature. Conditions: H_2 (10 sccm) at 25-500 ^oC, 5 ^oC min^{-1} (1 bar (a))

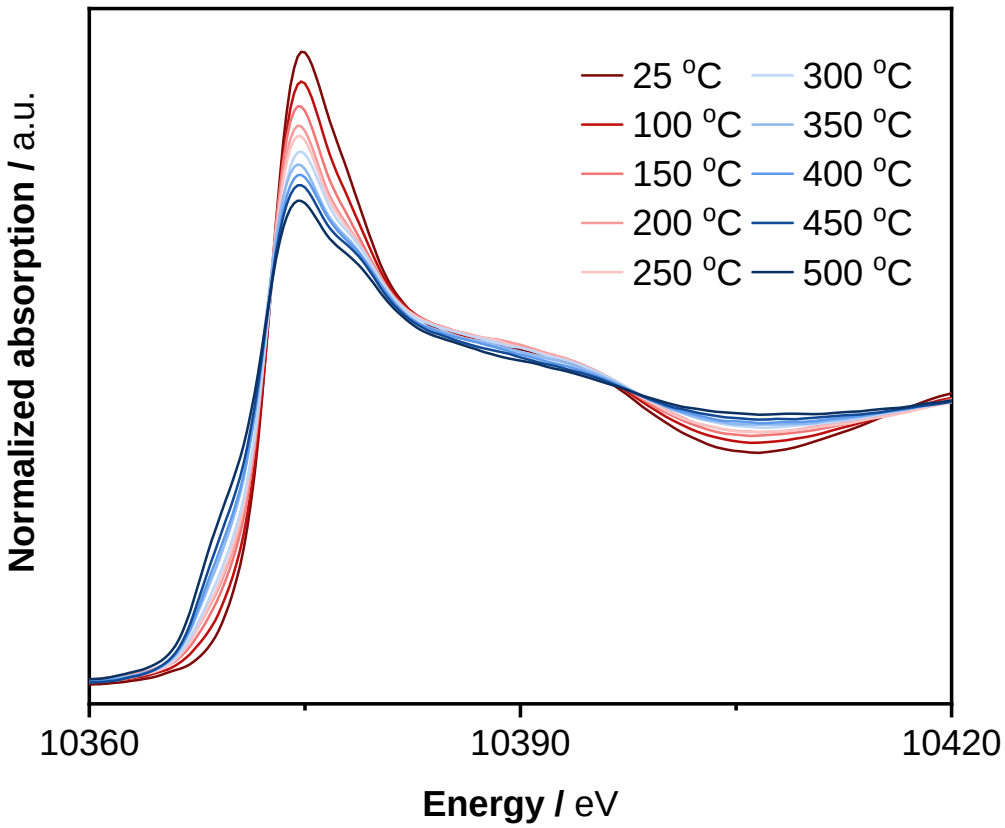

Figure S 35. Ga K edge XANES in range for Pd(COD)Me@Ga@SiO_2 under a flow of H_2 (10 sccm) from 25 °C to 500 °C, , after treatment at room temperature in same gas flow for 20 minutes (ramp: 5 °C min^{-1}, 1 bar (a)). 60 second increments, continuous acquisition. Note emergence of feature in edge as temperature increased, with concomitant loss of white line intensity

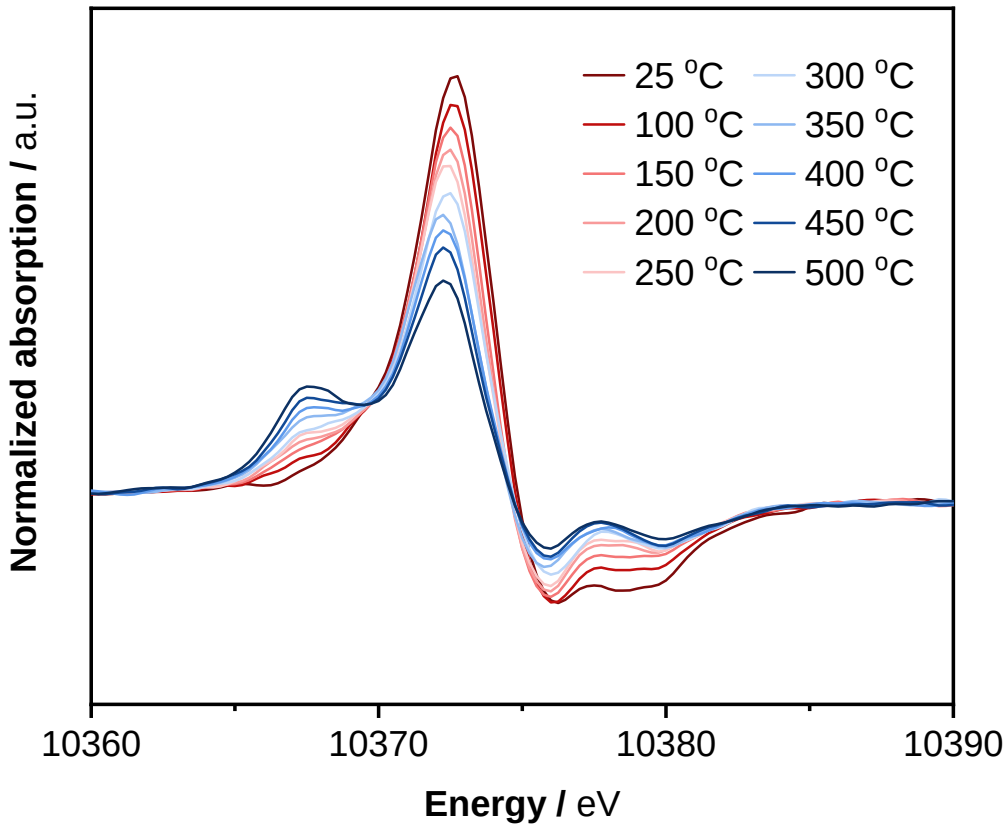

Figure S 36. 1st derivative Ga K edge XANES in range for Pd(COD)Me@Ga@SiO_2 under a flow of H_2 (10 sccm) from 25 °C to 500 °C, , after treatment at room temperature in same gas flow for 20 minutes (ramp: 5 °C min^{-1}, 1 bar (a)). 60 second increments, continuous acquisition. Note emergence of feature at 10367.5 eV as temperature increased, with concomitant loss of intensity for feature at 10372.5 eV. These changes are assigned to the partial reduction of Ga_{IV} to Ga^0, consistent with the edge energies assigned in Table S5

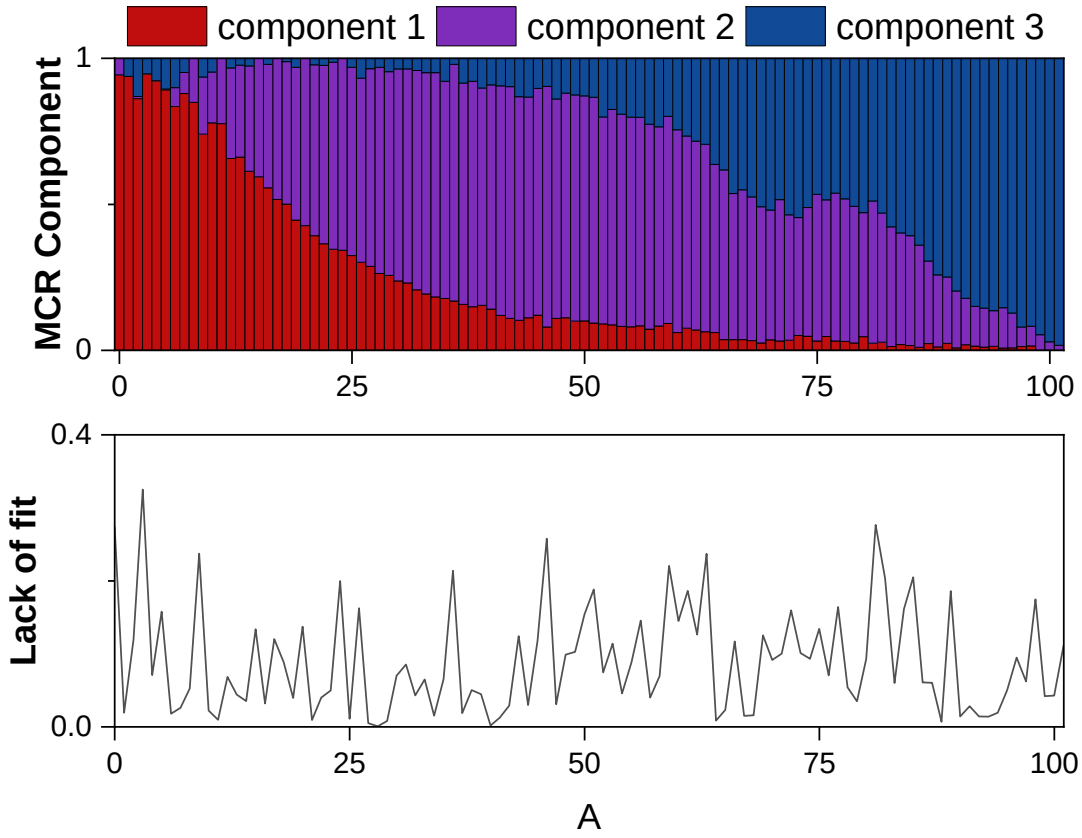

Figure S 37. Ga K edge XANES - MCR component fit for H_2 treatment of Pd(COD)Me@Ga@SiO_2 from 25 ^oC to 500 ^oC. (top) MCR component (3 component fit), and (bottom) lack of fit. 60 second increments, continuous acquisition. Ramp: 5 ^oC min^{-1}, 1 bar (a) (i.e. each bar represents a window of 5 ^oC, final 5 data points recorded at terminal temperature (500 ^oC))

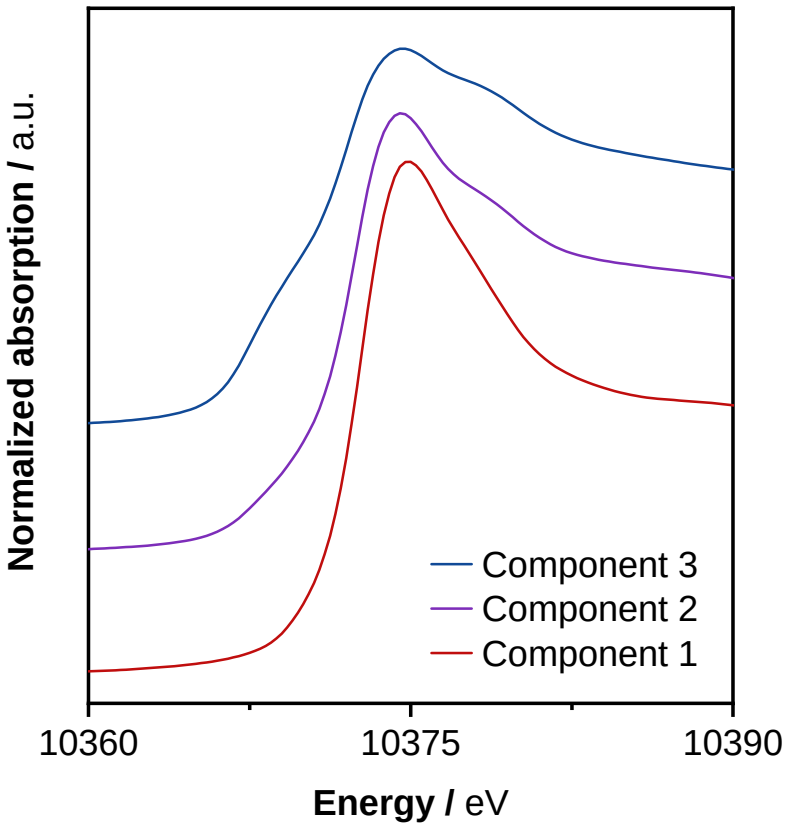

Figure S 38. Ga K edge XANES - MCR-resolved components for H_2 treatment of Pd(COD)Me@Ga@SiO_2 from room temperature to 500 ^oC. (top, dark blue, solid) component 3 (MCR)*;* (middle, purple, solid) component 2 (MCR) (bottom, dark red, solid) component 1 (MCR). Note the emergence of a feature at in the edge between components and the significant loss of White line intensity observed.

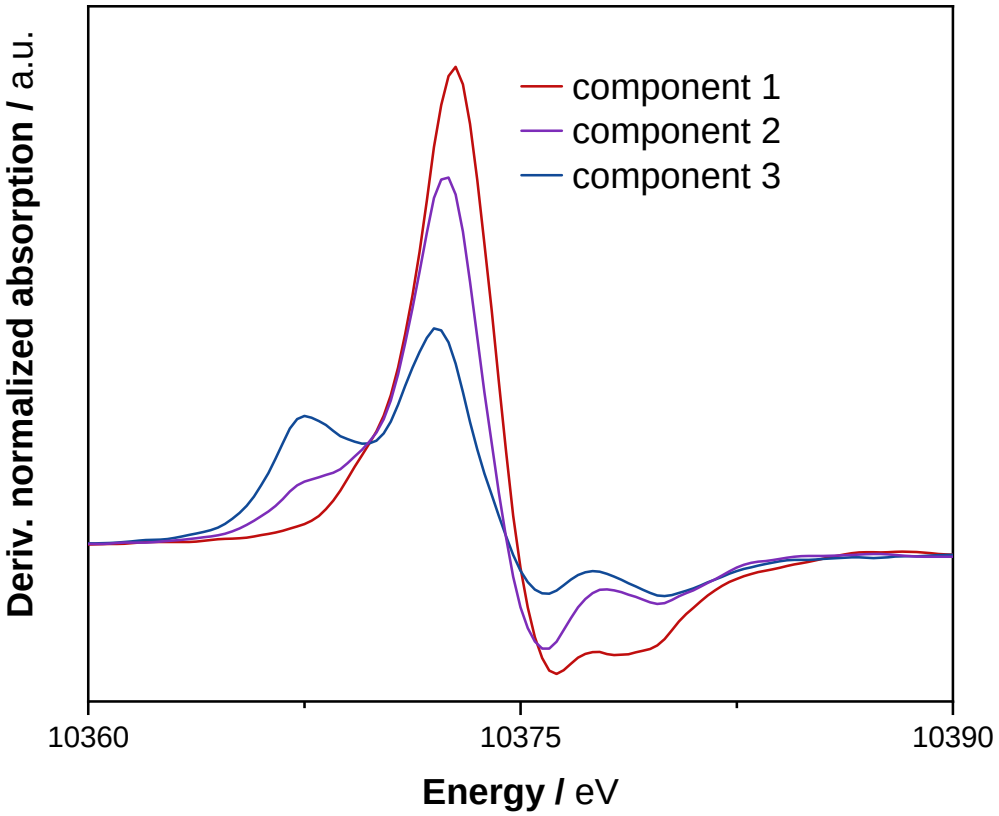

Figure S 39. 1st derivative Ga K edge XANES - MCR-resolved components for H_2 treatment of Pd(COD)Me@Ga@SiO_2 from room temperature to 500 °C. (dark blue, solid) component 3 (MCR); (purple, solid) component 2 (MCR) (dark red, solid) component 1 (MCR); (bottom, light red, dashed). Comparison of reference materials (*ex situ*) and components is consistent with formation of a PdGa alloy at elevated temperatures. Note emergence of feature at 10367.5 eV as temperature increased, with concomitant loss of intensity for feature at 10372.5 eV. These changes are assigned to the partial reduction of Ga_{IV} to Ga^0, consistent with the edge energies assigned in Table S5.

Discussion of room temperature reduction process probed by *in situ* XANES: The room temperature reduction of Pd^{II} to Pd(0) in Pd(COD)Me@Ga@SiO_2 is evidenced by the continuous disappearance of the white line feature at the Pd K edge (24365 eV), in conjunction with the gradual shift of the edge to lower energy (Figure S27 and S28). MCR analysis indicates the presence of 2 spectrally pure components (component 1 & 2, figure 29 and S30), which possess white line intensity and energy that match the grafted species on silica (Pd(COD)Me@SiO_2) and the monometallic particles after H_2 treatment (Pd@SiO_2), respectively. The gradual increase in concentration of the component 2, and the corresponding decrease in concentration of component 1, indicates that reduction is occurring.

Discussion of evolution of material during the temperature programmed reduction of Pd(COD)Me@Ga@SiO_2 probed by *in situ* XANES at the Pd K and Ga K edges:At the Pd K edge, a slight shift in edge position is observed as the temperature is increased to 500 ^oC, alongside a further decrease in white line intensity (Fuigure S31 and S32). Decomposition of the TPR data by MCR reveals the presence of three separate components (components 1, 2 and 3). Component 1, which bears similarity to the monometallic reference (Pd@SiO_2) disappears gradually as temperature is increased, while component 3 is shifted to slightly lower energy and a significant dampening of the post-edge feature at 24380 eV occurs, as observed for PdGa@SiO_2 analyzed *ex situ* (Figure 2c, Figure S34). An intermediate species (component 2) is also observed, with a slight shift in edge energy also apparent, as well as a shift in position of the post-edge feature at 24380 eV from the initial state. At the Ga K edge, as temperature is increased, the emergence of a new feature at 10367.5 eV is observed, with a loss of white-line intensity in parallel. This is consistent with the gradual reduction of Ga^{III} to Ga(0) (SI Table S5). Furthermore, MCR analysis reveals the presence of three separate components (components 1, 2 and 3), which possess a similar temperature dependence to the corresponding Pd K species. Component 1 resembles the monometallic material (Ga@SiO_2, Figure 2 a), while in components 2 and 3 the emergence of a shoulder at 10367.5 eV is apparent. The gradual disappearance of component 1, and the emergence of component 3 indicate that the reduction is a continuous process, while the initial increase in component 2 followed by a gradual decrease in contribution highlight that this component is likely an intermediate phase (Figure S38 and S 39).

S9. Transmission Electron Microscopy

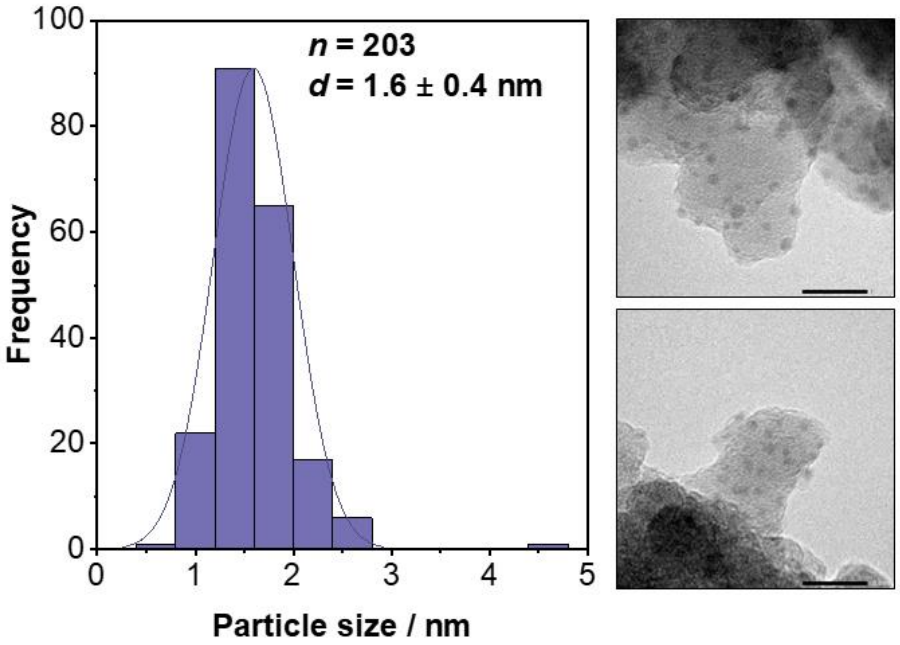

Figure S 40. Particle size distribution for PdGa@SiO_2 with representative TEM images, magnification 8 x 10^5, scale bar (black, 10 nm)

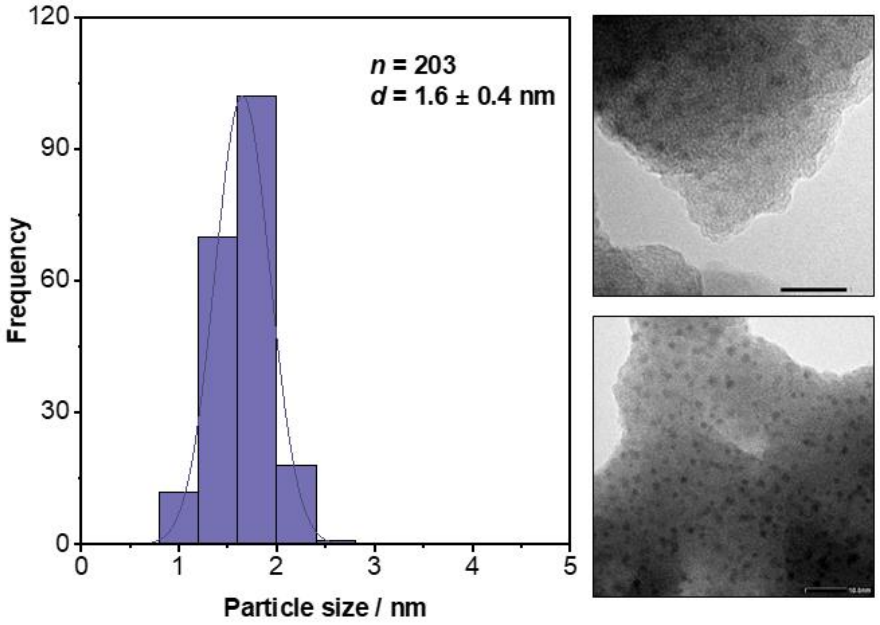

Figure S 41. Particle size distribution for Pd@SiO_2 with representative TEM images, magnification 8 x 10^5, scale bar (black, 10 nm)

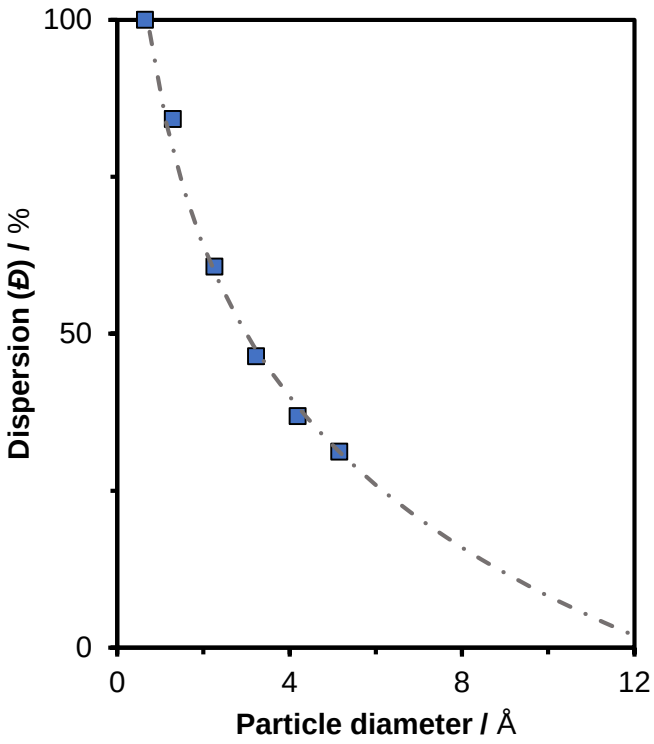

Figure S 42. Expected dispersion using a truncated cube octahedron model. Equation of fit: y = -34.64ln(x) + 88.008, R^2 = 0.9894. Side length 1.6 A, expected dispersion 72%. Assumptions: no lattice contraction (Pd radius 163 nm), zero particle support interface (all surface atoms accessible), all surface atoms counted once (i.e. edge and corner sites equivalent to slabs)

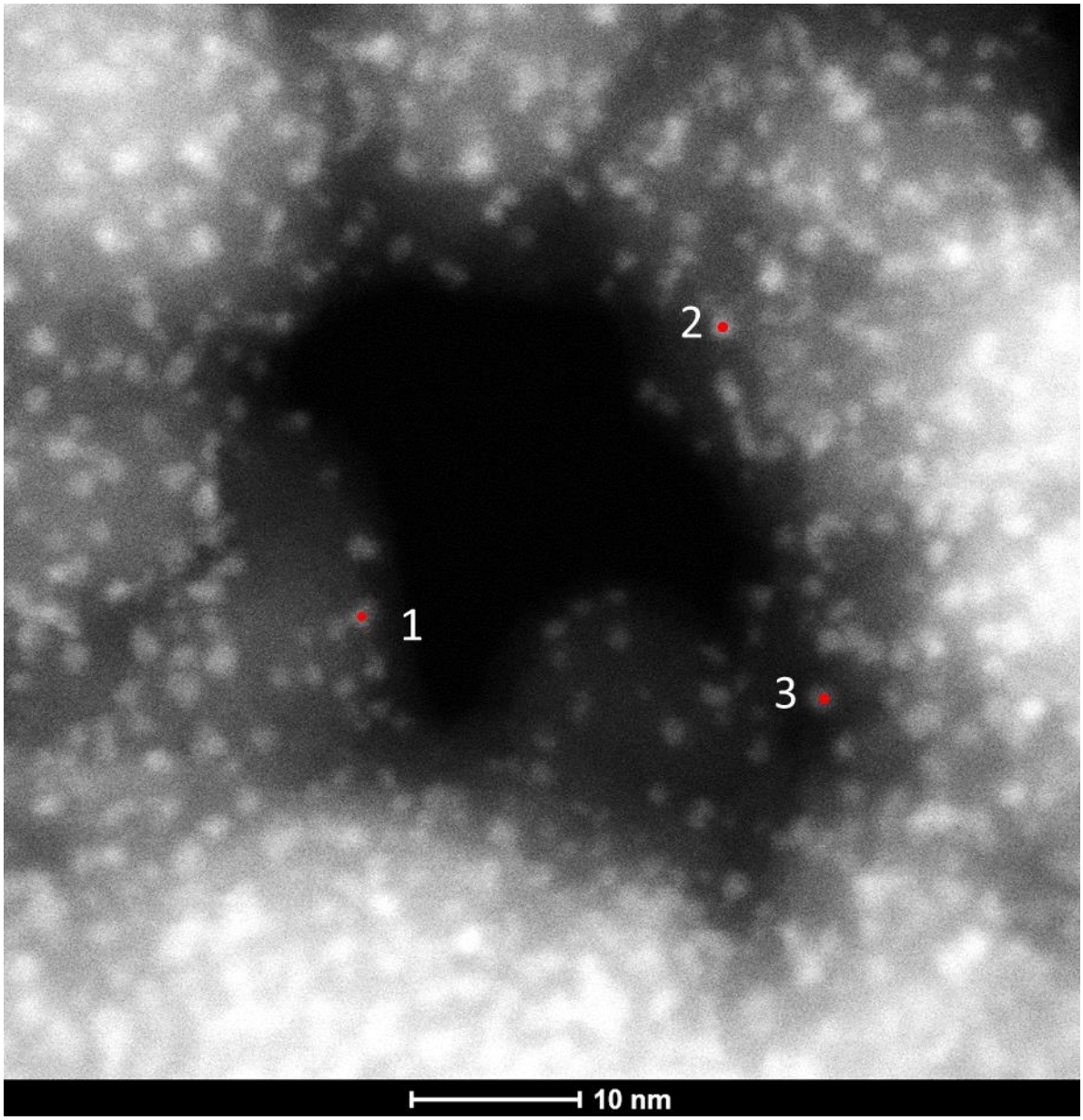

Figure S 43. HAADF-TEM image of PdGa@SiO_2

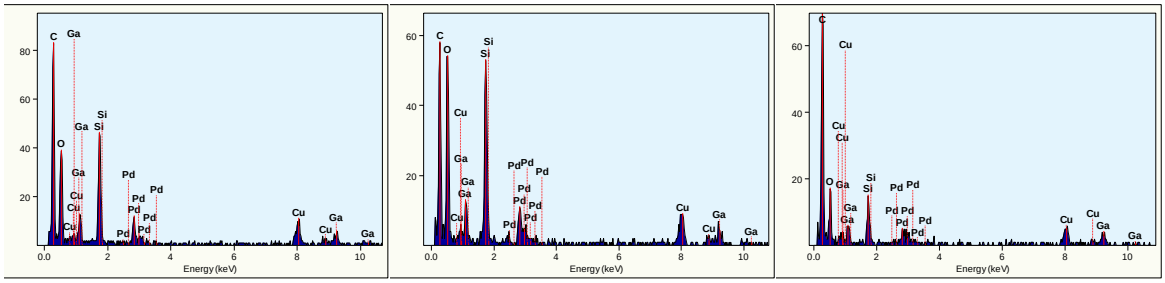

Figure S 44. Point-EDX mapping of (left) point 1, **Figure S 43**, (centre) point 2, **Figure S 43**, (right) point 3, **Figure S 43**. n.b. Carbon and copper signals arise from background scattering of grid.

Table S 6. Elemental distribution at points 1, 2 and 3 in Figure S 43

	Ga / At%	**Pd** / At%
1	0.41	0.61
2	0.31	0.39
3	0.46	1.13

S10. Catalytic Data

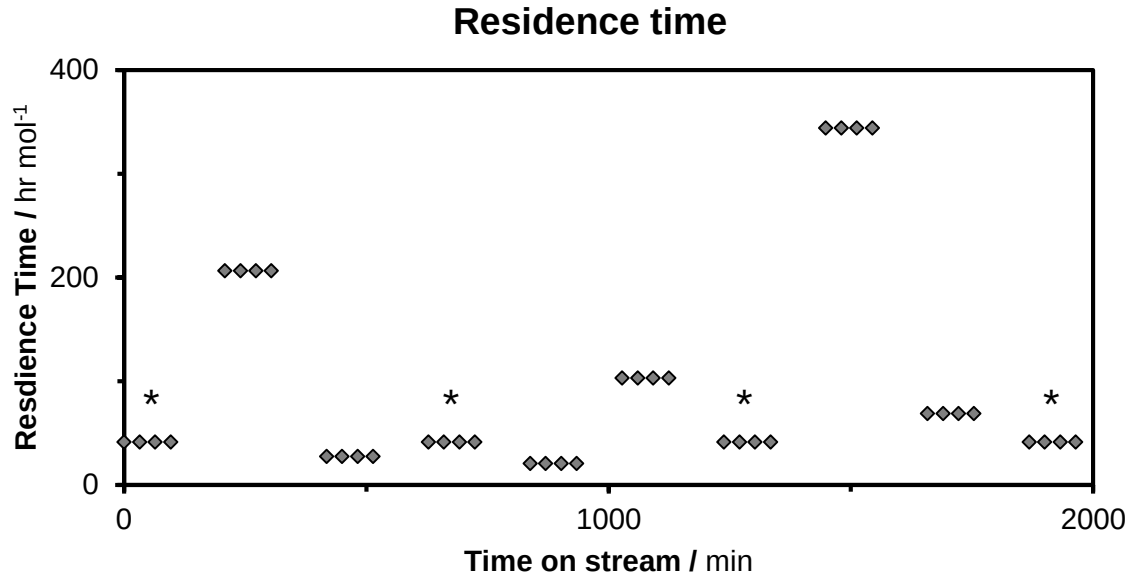

Figure S 45. Residence time vs time on stream. Clusters denoted with an asterisk represent return to a single flowrate

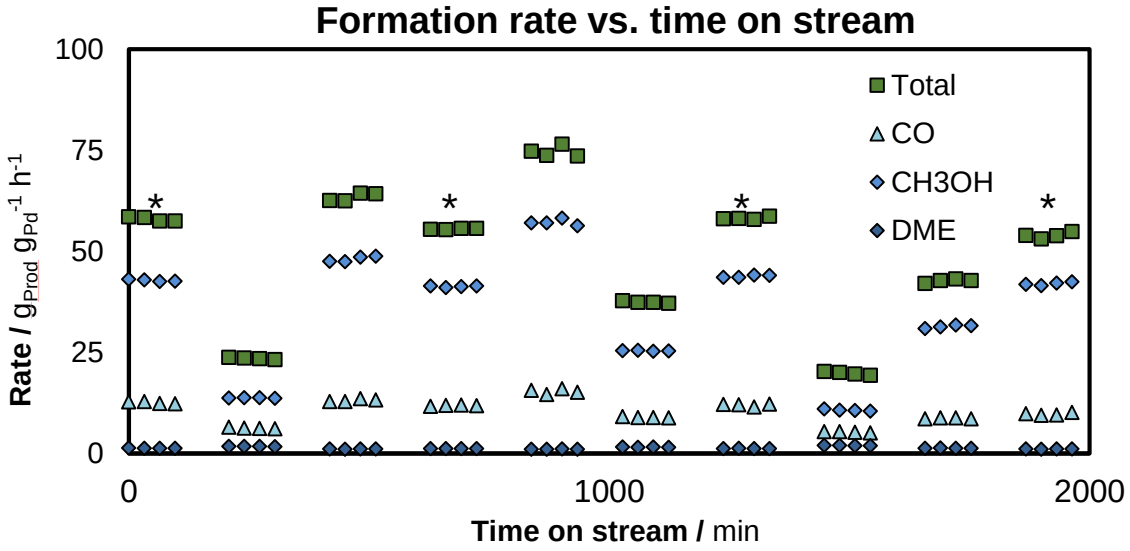

Figure S 46. Formation rate vs time on stream for PdGa@SiO_2, corrected for deactivation. Clusters denoted with an asterisk represent return to a single flowrate

(50 sccm) which are used to quantify deactivation. Flowrates (L-R): 50, 10, 75, 50, 100, 20, 50, 6, 30 and 50 sccm. Total deactivation over course of reaction 25%.

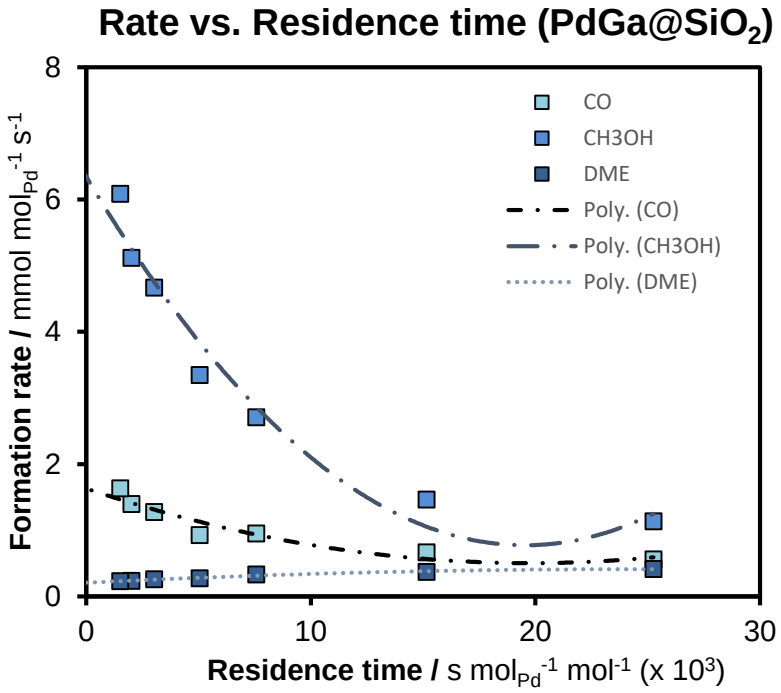

Figure S 47. Formation rate vs residence time for PdGa@SiO_2, corrected for deactivation. 2nd order polynomial fit employed for estimation of intrinsic rates.

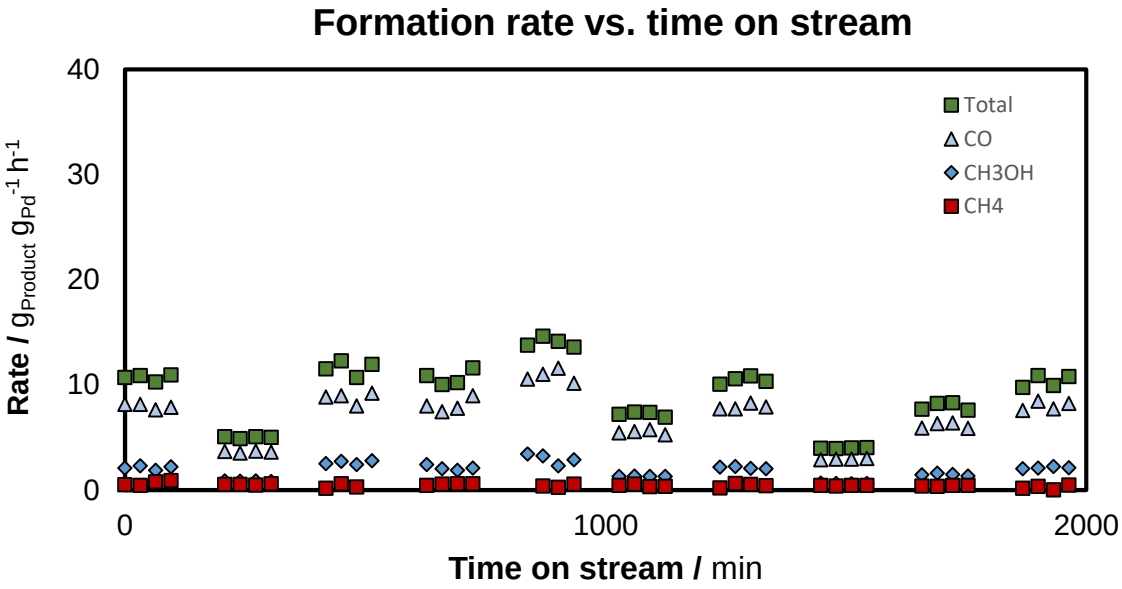

Figure S 48. Formation rate vs time on stream for Pd@SiO_2, corrected for deactivation. Clusters denoted with an asterisk represent return to a single flowrate

(50 sccm) which are used to quantify deactivation. Flowrates (L-R): 50, 10, 75, 50, 100, 20, 50, 6, 30 and 50 sccm. Total deactivation over course of reaction 40%.

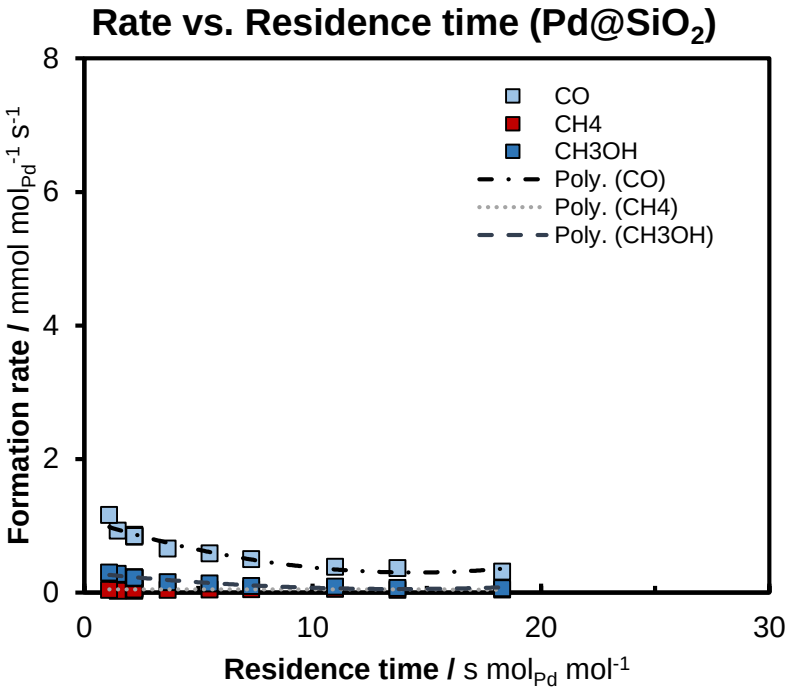

Figure S 49. Formation rate vs residence time for $Pd@SiO_2$, corrected for deactivation. 2nd order polynomial fit employed for estimation of intrinsic rates.

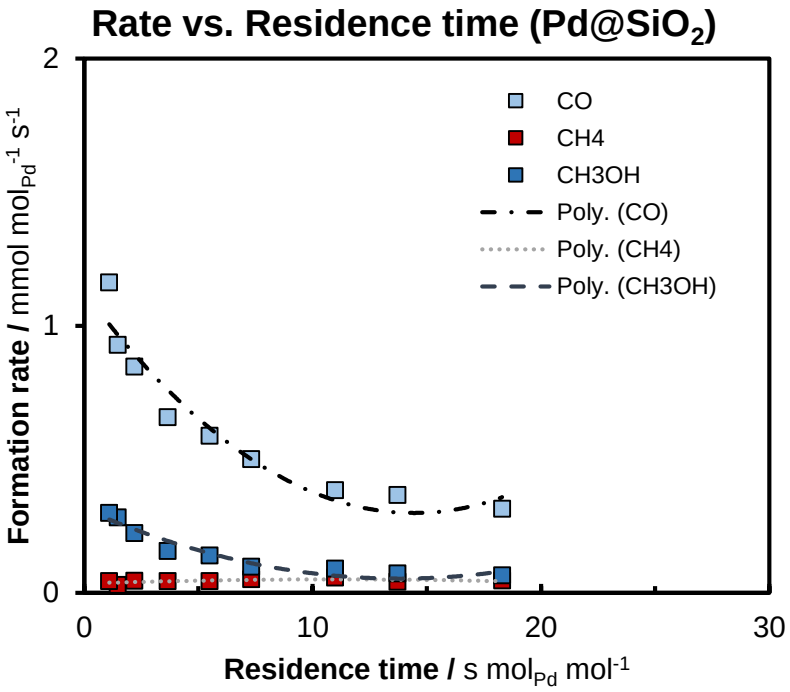

Figure S 50. Formation rate vs residence time for $Pd@SiO_2$, corrected for deactivation. 2nd order polynomial fit employed for estimation of intrinsic rates. Rescaled.

Table S7. Summary of intrinsic formation rates and selectivities for materials investigated, alongside reference data for materials previously tested in the same conditions.

Material / *(wt% Pd/Cu)*	**Formation rate /** mmol s^{-1} mol_{TM}^{-1} *(x10^{-3} g_{prod} g_{cat}^{-1} h^{-1}) with TM = Pd or Cu*				**Selectivity /** *S*(CH_3OH+DME)/*S*(CO)/*S*(CH_4)
	CH_3OH	CO	DME[a]	CH_4	
PdGa@SiO_2 *(1.08)*	6.40 *(72.6)*	1.57 *(16.0)*	0.21 *(1.8)*	<0.01 *(-)*[b]	81/19/-[c]
Pd@SiO_2 *(1.61)*	0.14 *(2.4)*	0.50 *(8.6)*	<0.01 *(-)*[b]	0.03 *(0.5)*	20/75/5
Ga@SiO_2 *(1.6x)*	<0.01 *(-)*[b]	<0.01 *(-)*[b]	<0.01 *(-)*[b]	<0.01 *(-)*[b]	-
Cu@SiO_2[d] *(4.5)*	0.23 *(19.6)*	0.24 *(17.1)*	<0.01 *(-)*[b]	<0.01 *(-)*[b]	49/51/-
Cu@ZrO_2[d] *(2.33)*	0.51 *(22.6)*	0.30 *(8.8)*	-[d]	-[d]	67/33/-
Cu-Ga@SiO_2[c] *(3.88)*	0.72 *(50.7)*	0.06 *(3.7)*	-	-	93/7/-
Cu/ZnO/Al_2O_3 *(n/a)*[d,e]	2.15	0.57			79/21/-[c]

Conditions: 3:1:1 (H_2:CO_2:Ar), 25 bar, 230 °C, 200 mg cat, 5 g SiC, 6-100 sccm. [a] Normalised per mole carbon; [b] below detection limit of TCD/FID; [c] Selectivity PdGa@SiO_2 at 4% conversion: 75%, Selectivity Cu/ZnO/Al_2O_3 at 4% conversion: <60%[15] [d] Previously reported in same conditions[15–17]; [e] 30 mg of catalyst was used, due to the increased Cu content (>50 wt%)

Table S8. Selected Pd, Cu, Pd-Ga and Pd-Cu based catalysts used for hydrogenation of CO_2 to methanol. Comparison of conditions, activities and selectivity to methanol as reported in the literature.

Material	Gas composition	Pressure / bar	Temperature / °C	*S*(CH_3OH) / %	Rate / mmol s^{-1} mol_{TM}^{-1}	Ref.
PdGa@SiO_2	1:3:1 CO_2:H_2:Ar	25	230	81	6.40	This work
Pd@SiO_2				20	0.14	
Pd-Ga/SiO_2	1:3 CO_2:H_2	8	220	13	0.051[a]	18
Pd-Ga/SiO_2 (1:1 Pd:Ga)	1:3 CO_2:H_2	8	220	60	0.46	19
$GaPd_2$/SiO_2	1:3 CO_2:H_2	1	225	<30	n/a	20,21
Pd/Ga_2O_3	1:3 CO_2:H_2	50	250	51	6.01	22
5% Pd/rod-Ga_2O_3	1:3 CO_2:H_2	50	250	41	n/a	23
5% Pd/plate-Ga_2O_3				52	n/a	
Pd/*β*-Ga_2O_3	1:3 CO_2:H_2	30	250	52	75	24
Pd_2Ga/*α*-Ga_2O_3	6:18:1 CO_2:H_2:Ar	30	170-250	50-60	7.98	25
Cu/SiO_2	6:18:1 CO_2:H_2:Ar	40	250	23	0.03	26
Pd/SiO_2				15	0.17	
$Pd_{(0.25)}Cu/SiO_2$				30	0.13[b]	
$Pd_{(0.34)}Cu/SiO_2$				34	0.13[b]	

[a] TOF at 250 °C provided in text was used to calculate rate per Pd. [b] Rate normalized for total number of moles of transition metal (i.e. N(Pd)+(N)Cu)

S11. Analysis of Catalyst after Reaction

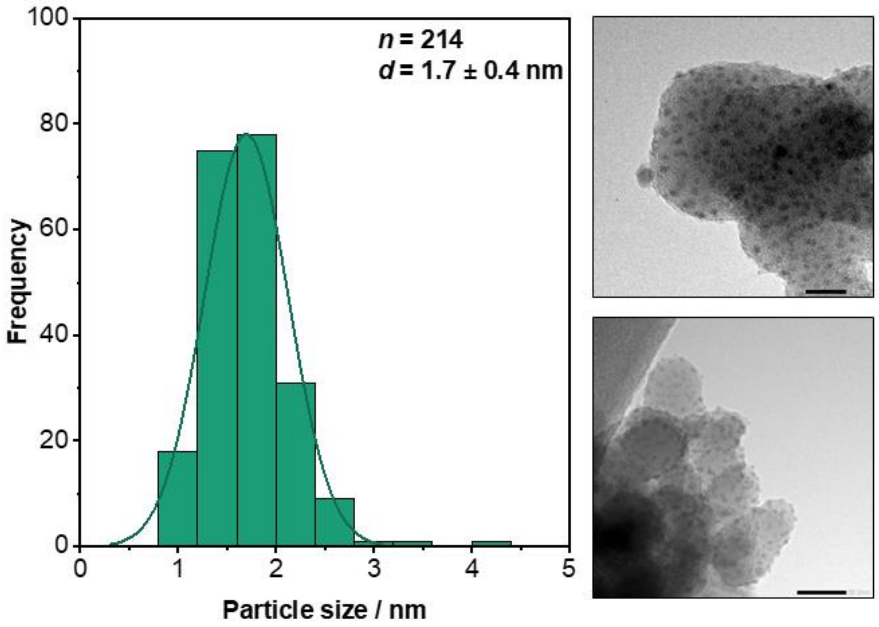

Figure S 51. Particle size distribution for $PdGa@SiO_2$ after reaction with representative TEM images, magnification 5 x 10^5, scale bar (black, 20 nm)

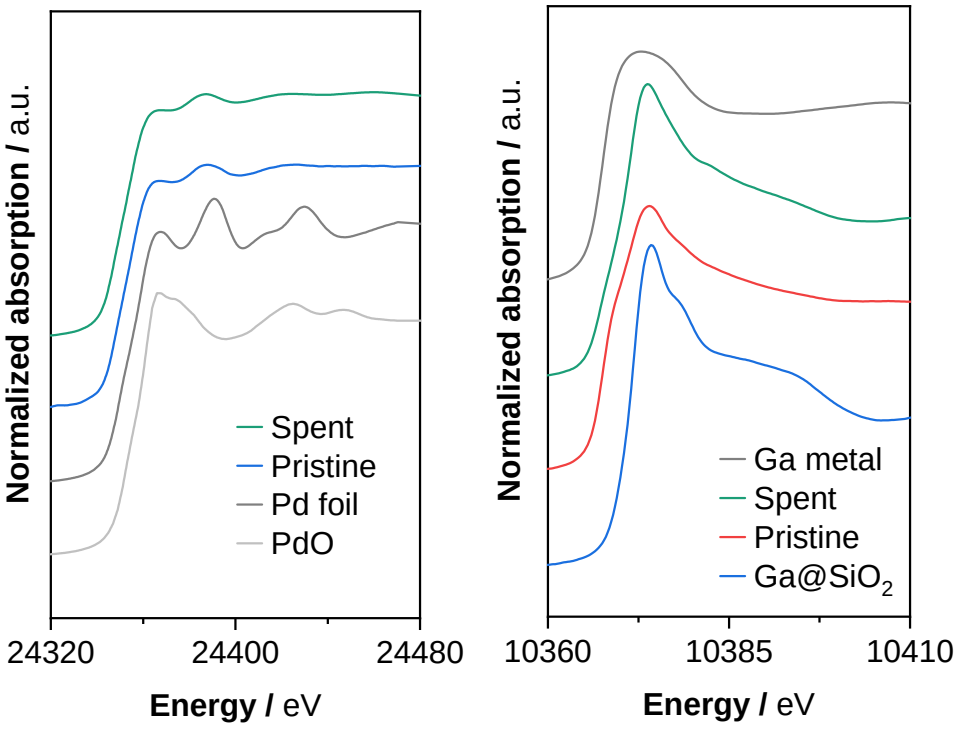

Figure S 52. (left) Pd K edge XANES. Green (top) – $PdGa@SiO_2$ (spent), red (top middle) - $PdGa@SiO_2$ (pristine), blue (bottom middle) – Pd foil, light grey (bottom) - PdO. (right) Ga K edge XANES. Green (top) – $PdGa@SiO_2$ (spent), red (top middle) - $PdGa@SiO_2$ (pristine), blue (bottom middle) - $Ga@SiO_2$, light grey (bottom) - β-Ga_2O_3

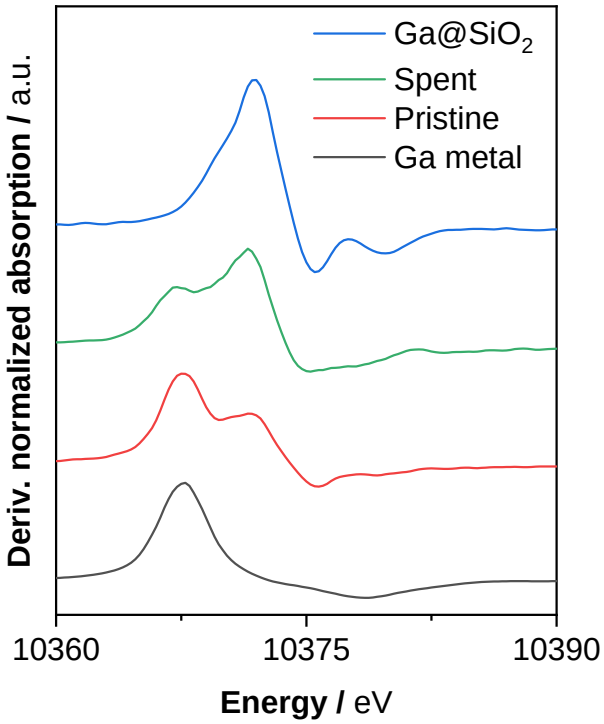

Figure S 53. 1st derivative Ga K edge XANES. blue (top) - $Ga@SiO_2$, green (top middle) – $PdGa@SiO_2$ (spent), red (bottom middle) - $PdGa@SiO_2$ (pristine), dark grey (bottom) - β-Ga_2O_3

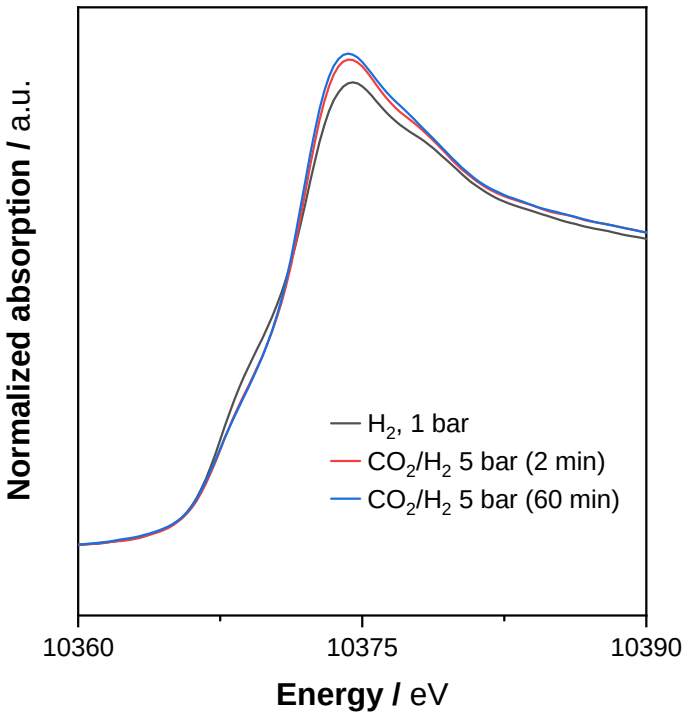

Figure S 54. Ga K edge XANES for $PdGa@SiO_2$ recorded *in situ* at 230 ºC : (black) initial state after reduction at 500 ºC (H_2 1 bar(a) 10 sccm), (red) after 2 minutes recording under reaction gas (H_2/CO_2/Ar (3:1:1), 5 bar, 10 sccm), (blue) after 60 minutes recording under reaction gas (H_2/CO_2/Ar (3:1:1), 5 bar, 10 sccm). Note increase in white line intensity and decrease in intensity for the feature in the edge.

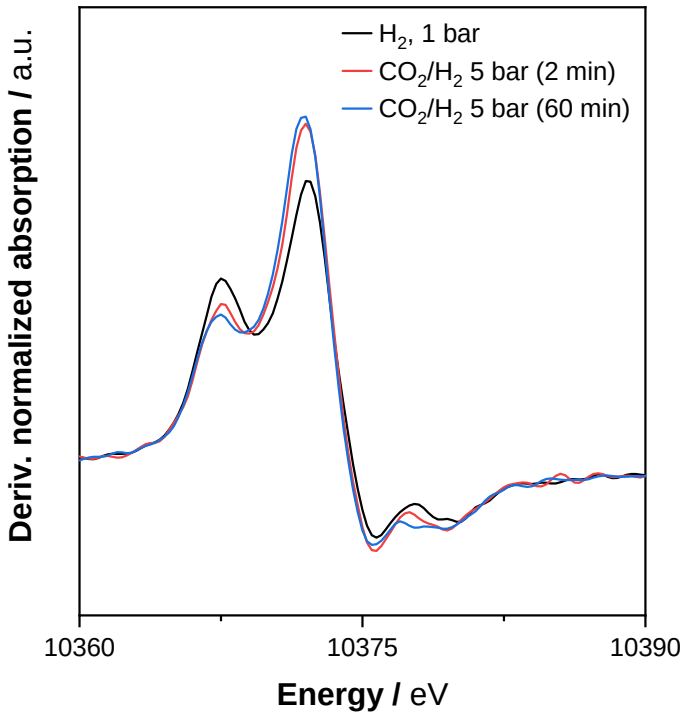

Figure S 55. 1st derivative Ga K edge XANES for PdGa@SiO_2 recorded *in situ* at 230 °C: (black) initial state after reduction at 500 °C (H_2 1 bar(a) 10 sccm), (red) after 2 minutes recording under reaction gas (H_2/CO_2/Ar (3:1:1), 5 bar, 10 sccm), (blue) after 60 minutes recording under reaction gas (H_2/CO_2/Ar (3:1:1), 5 bar, 10 sccm). Note increase in intensity for feature at around 10372 eV and decrease in intensity for the feature at 10367 eV.

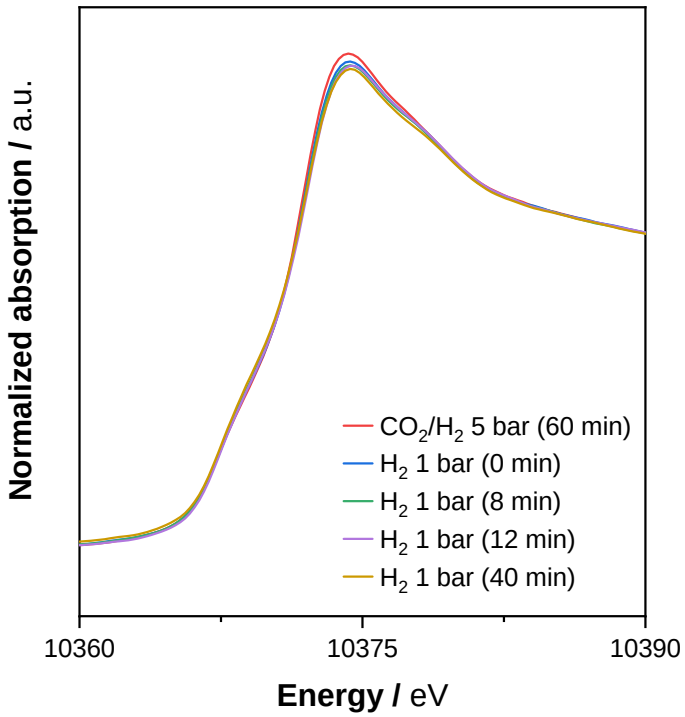

Figure S 56. Ga K edge XANES for PdGa@SiO_2 recorded *in situ* at 230 °C after reaction: (red) after 60 minutes recording under reaction gas (H_2/CO_2/Ar (3:1:1), 5 bar, 10 sccm), (blue) after 0 minutes recording under H_2 post-reaction (H_2 1 bar(a) 10 sccm). (green) after 8 minutes recording under H_2 post-reaction (H_2 1 bar(a) 10 sccm). (purple) after 12 minutes recording under H_2 post-reaction (H_2 1 bar(a) 10 sccm). (gold) after 40 minutes recording under H_2 post-reaction (H_2 1 bar(a) 10 sccm). Note gradual decrease in white line intensity and slight increase in intensity for the feature in the edge – indicative of partial re-reduction of Ga.

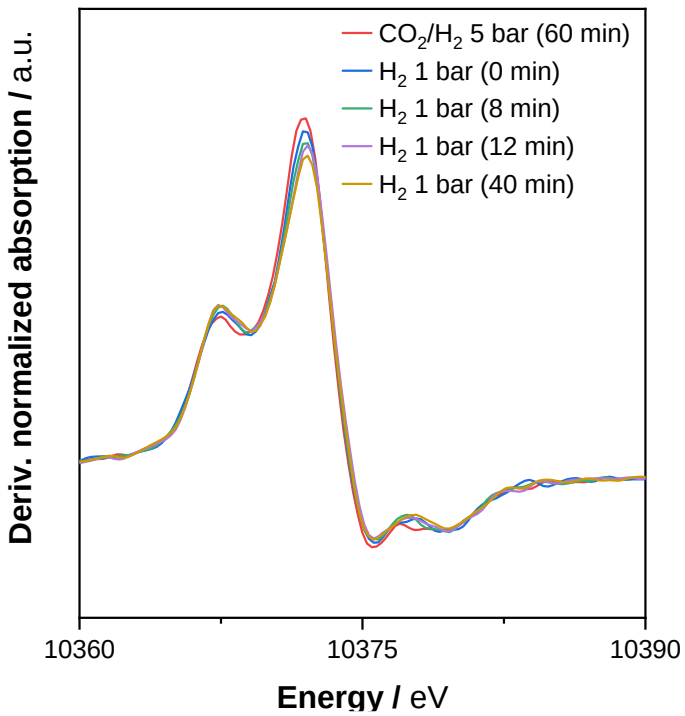

Figure S 57. 1st derivative Ga K edge XANES for PdGa@SiO_2 recorded in situ at 230 °C after reaction: (red) after 60 minutes recording under reaction gas (H_2/CO_2/Ar (3:1:1), 5 bar, 10 sccm), (blue) after 0 minutes recording under H_2 post-reaction (H_2 1 bar(a) 10 sccm). (green) after 8 minutes recording under H_2 post-reaction (H_2 1 bar(a) 10 sccm). (purple) after 12 minutes recording under H_2 post-reaction (H_2 1 bar(a) 10 sccm). (gold) after 40 minutes recording under H_2 post-reaction (H_2 1 bar(a) 10 sccm). Note gradual decrease in intensity for feature at around 10372 eV and increase in intensity for the feature at 10367 eV – indicative of partial re-reduction of Ga.

S12. Reaction Intermediates from Batch Experiments

General procedure: A high pressure glass reactor, charged with 200 mg of solid (Pd@SiO_2 or PdGa@SiO_2), was pressurised with desired reaction gas ($^{13}CO_2$/H_2 (NMR), CO_2/H_2 (Natural abundance) (IR) - 1:3 ratio, calculated pressure at 230 °C: 5 bar (g)), and heated to 230 °C for 12 hours. The reactor was then cooled in liquid N_2 (-196 °C), before evacuating at room temperature (25 °C, 10^{-5} mbar) for 30 minutes. The treated material was transferred to an argon-filled glovebox prior to further

analysis.

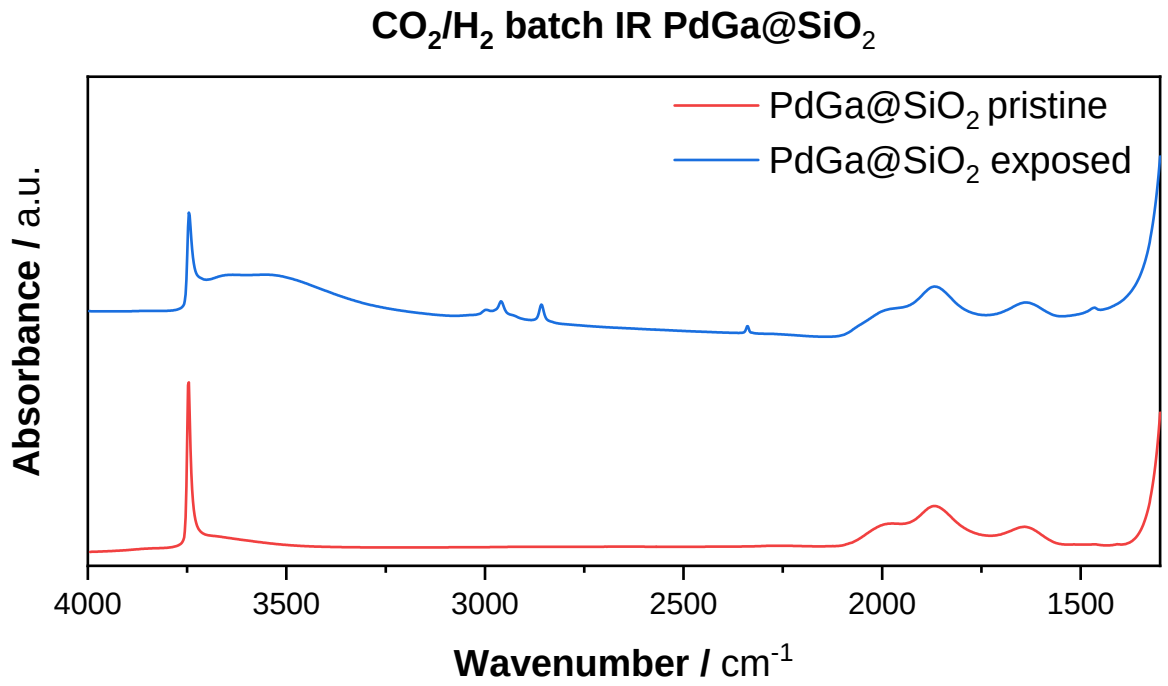

Figure S 58. FTIR spectra of (top) PdGa@SiO_2 after heating in CO_2/H_2 (1:3 CO_2:H_2, 5 bar(g), 230 °C), measured at room temperature, after evacuating, and (bottom) PdGa@SiO_2 (pristine) at room temperature. Spectra are normalized with respect to the Si-O-Si band of silica at 1868 cm^{-1}, peak at 2337 cm^{-1} assigned to adsorbed CO_2

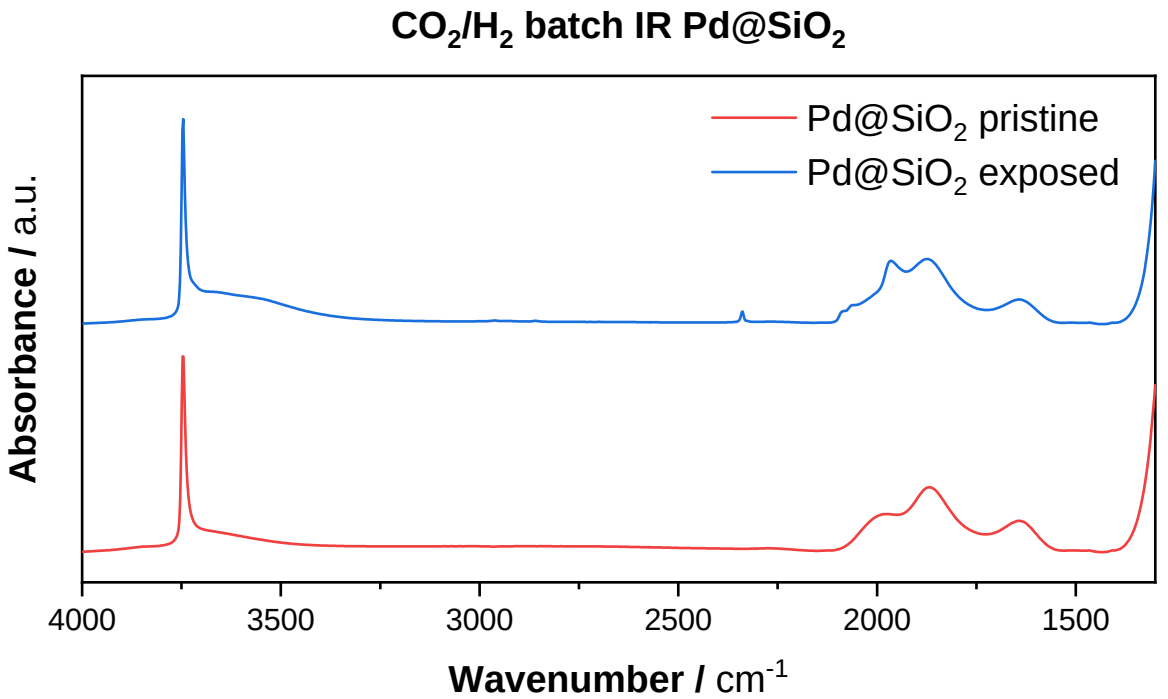

Figure S 59. FTIR spectra of (top) Pd@SiO_2 after heating in CO_2/H_2 (1:3 CO_2:H_2, 5 bar(g), 230 °C), measured at room temperature, after evacuating, and (bottom) Pd@SiO_2 (pristine) at room temperature. Spectra are normalized with respect to the Si-O-Si band of silica at 1868 cm^{-1}, peak at 2337 cm^{-1} assigned to adsorbed CO_2.

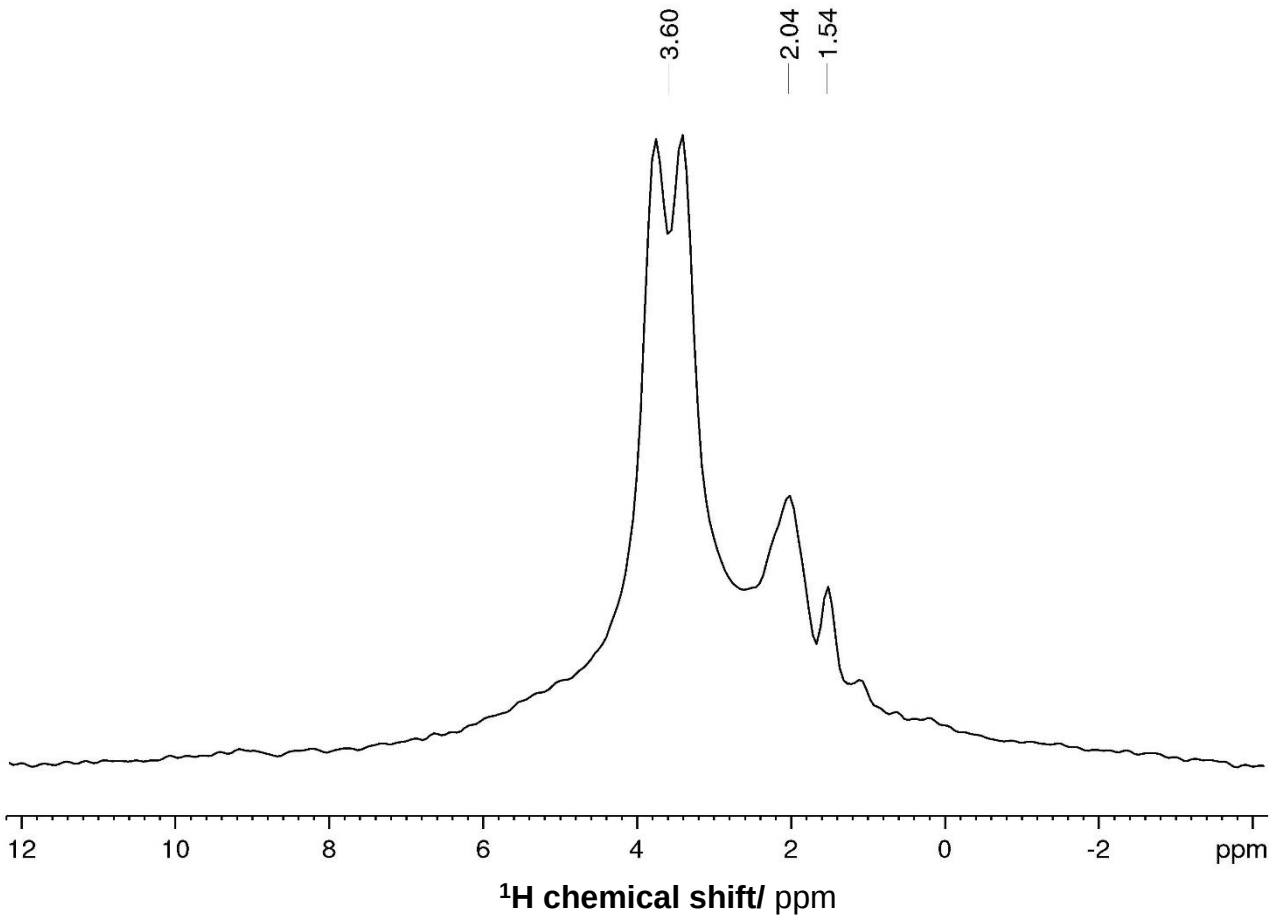

Figure S 60 Solid state MAS ^{1}H NMR spectrum for PdGa@SiO_2 after exposure to $^{13}CO_2$ and H_2 (1:3 CO_2/H_2, 0.5 MPa total pressure; 503 K;12 h), 4.0 mm probe, NS=16, 400 MHz. Well-defined doublet at 3.60 ppm attributed to -O$^{13}CH_3$ ($^{1}J_{C-H}$ = 142 Hz)

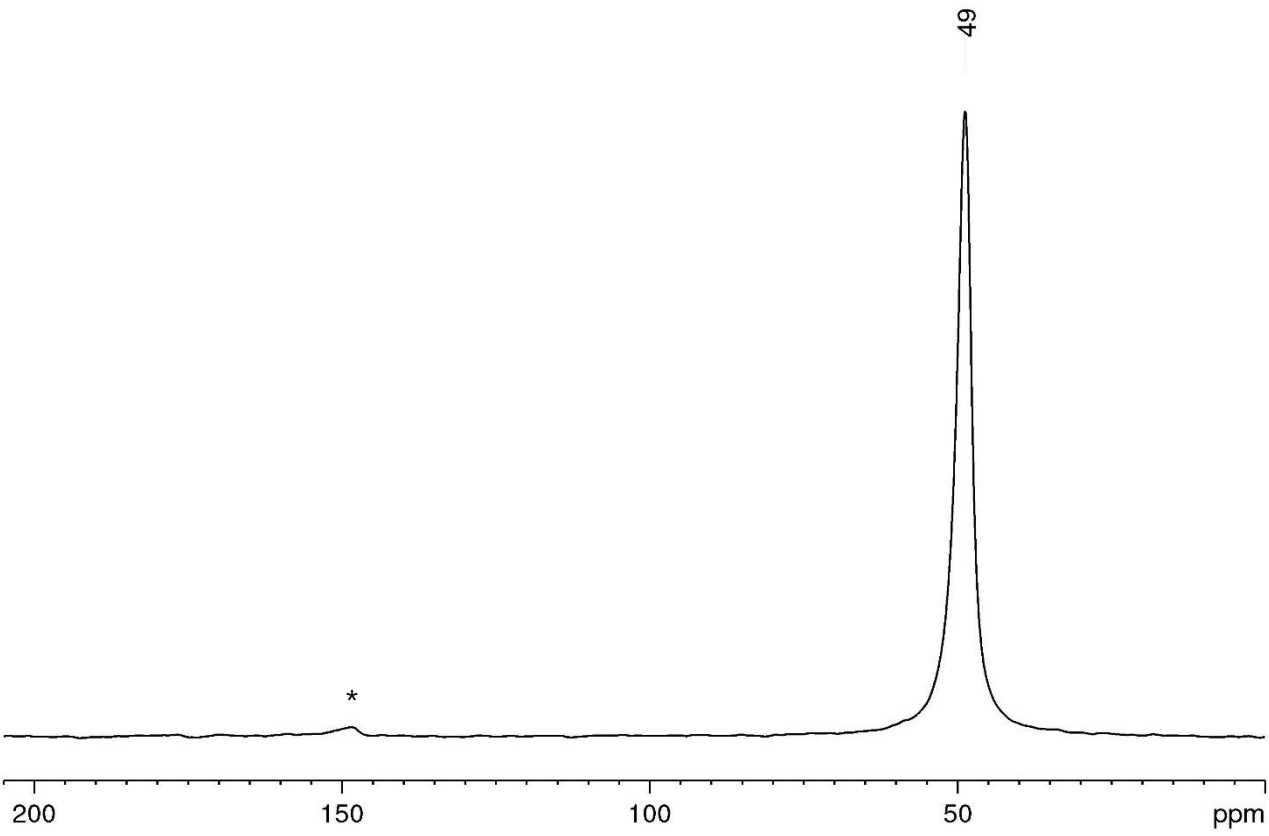

Figure S 61 Solid state CP-MAS ^{13}C NMR spectrum for PdGa@SiO_2 after exposure to $^{13}CO_2$ and H_2 (1:3 CO_2/H_2, 0.5 MPa total pressure; 503 K;12 h), 4.0 mm probe, NS= 17712, 100.6 MHz, asterisk denotes spinning side band

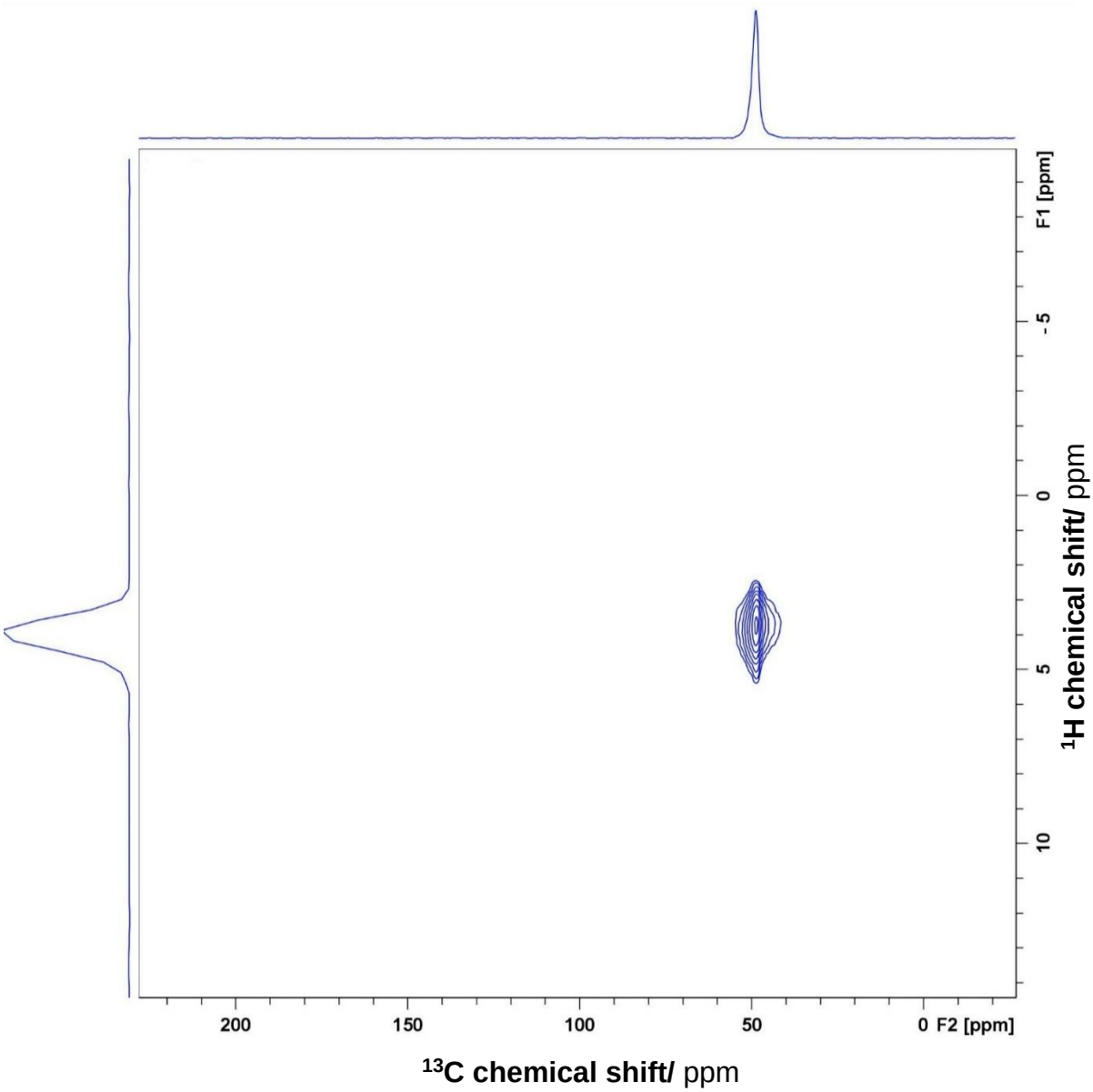

Figure S 62. $^{13}C-^{1}H$ HETCOR spectrum for PdGa@SiO_2 after exposure to CO_2 and H_2 (1:3 CO_2/H_2, 0.5 MPa total pressure; 503 K; 12 h). 4.0 mm probe, NS= 400, 400 MHz, 100.6 MHz.

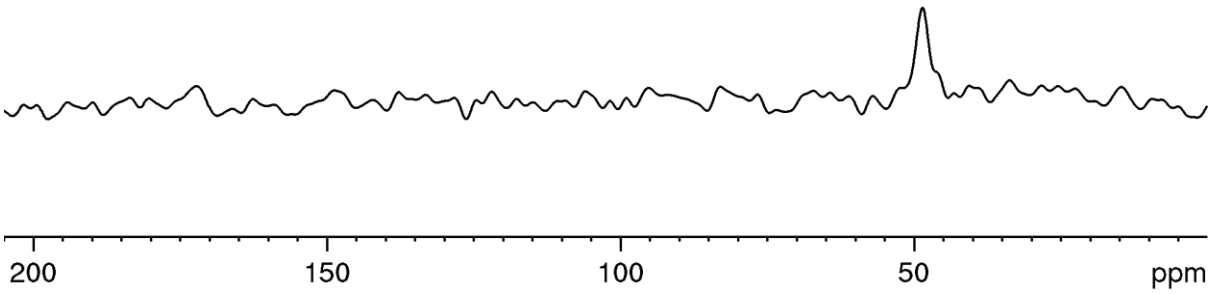

Figure S 63. Solid state CP-MAS ^{13}C NMR spectrum for Pd@SiO_2 after exposure to $^{13}CO_2$ and H_2 (1:3 CO_2/H_2, 5 bar total pressure; 230 °C K;12 h), 4.0 mm probe, NS= 32768, 100.6 MHz

S13. *Operando* transient DRIFTS

Experimental setup: The catalyst powder (10-15 mg) is located in a cylindrical cavity (3 mm in diameter and 3 mm vertical length) of a custom-made high-pressure reaction cell (tested up to 40 bar). The cell is mounted in a Harrick Praying Mantis diffuse reflection (DRIFTS) accessory. The spectra were collected using a Thermo Scientific Nicolet 6700 FT-IR spectrometer equipped with a liquid-nitrogen-cooled MCT detector at 4 cm^{-1} resolution. The flow of gases is controlled by mass flow controllers (Bronkhorst). Switching between two reactant gas streams is done by a 4-way valve. The pressure of the two gas streams (to the cell and vent) is controlled by back-pressure regulators (Bronkhorst). The outlet gas stream is analyzed by a Pfeiffer OmniStar GSD 300C mass spectrometer.

General procedure: Prior to the measurements, the sample is reduced *in situ* at 300 °C in H_2 stream (20 Nml min^{-1} H_2) for 1 h and subsequently cooled to a reaction temperature of 230 °C in the H_2 stream. The cell is pressurized to 20 bar and immediately exposed to the reactant mixture (CO_2:H_2 = 1:3 molar ratio, total flow 20 Nml min^{-1}) at 20 bar by the switching valve. The spectra were acquired every 20

seconds to monitor the reaction, stabilization process of the catalysts as well as the evolution of surface species.

Transient DRIFTS utilizes a periodic perturbation of a system by external parameters (stimulation) to influence the concentration of active species.[27] This experiment is performed in the above-mentioned setup by using a switching valve to change the stream of reactant gases to introduce the periodic concentration perturbation. No baseline correction was applied to the time-resolved spectra due to the baseline movement.

Data processing using multivariate spectral analysis: Multivariate spectral analysis is performed by the Multivariate Curve Resolution-Alternating Least Squares (MCR-ALS) algorithm, as described elsewhere.[28] MCR is a chemometric method used for better data processing and deconvolution of the complex spectra down to individual components based on kinetic resolution. It can deliver the pure response profiles (e.g. spectra, pH profiles, time profiles, elution profiles) of the chemical species of an unresolved mixture when no previous information is available about the nature and composition of these mixtures.

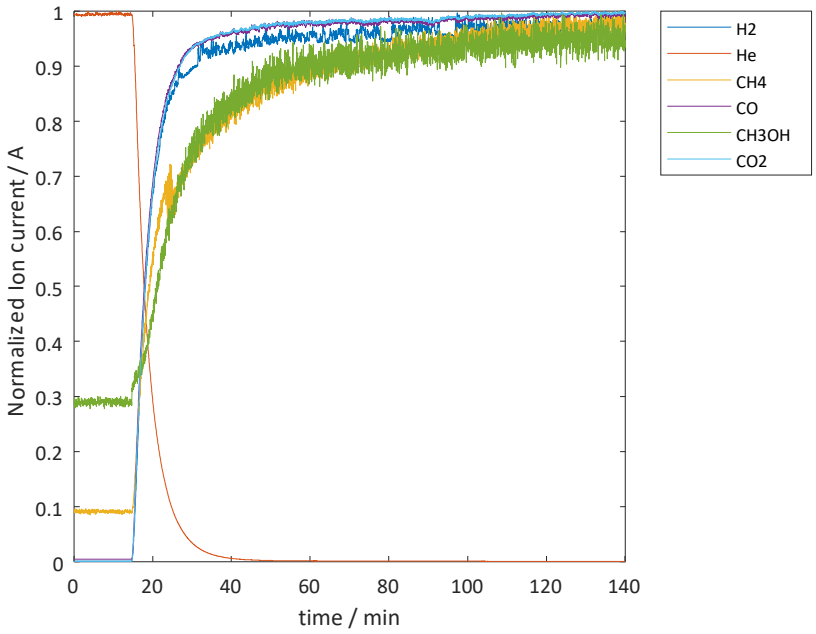

Figure S 64. Normalized ion current for selected relevant mass fragments for steady-state measurements of PdGa@SiO_2 in the hydrogenation of CO_2 to methanol (Conditions: 20 bar, 3:1 H_2:CO_2, 230 ^oC)

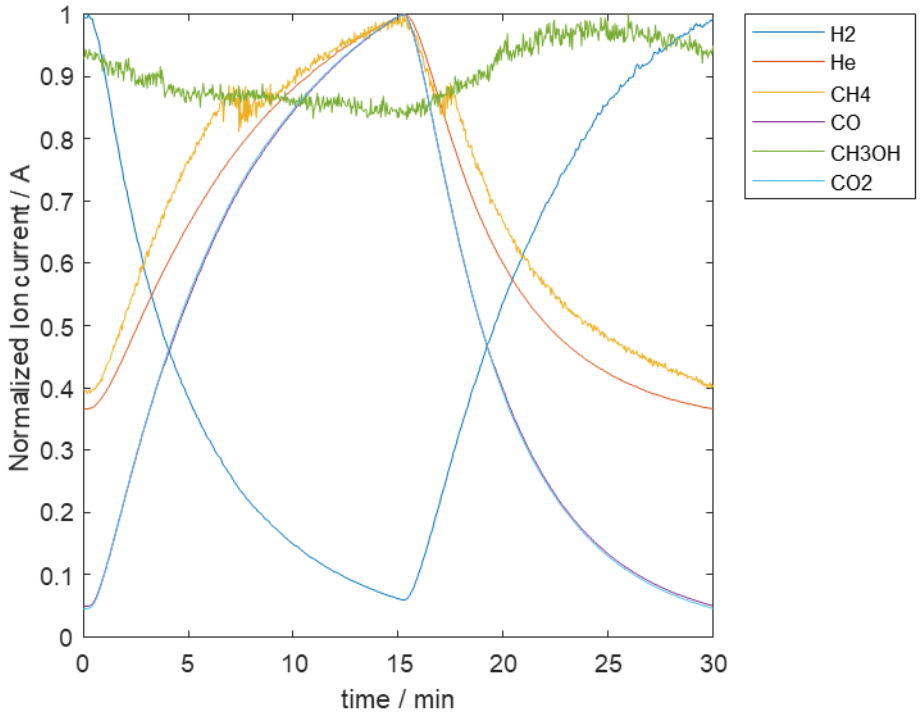

Figure S 65. Normalized ion current for selected relevant mass fragments for modulation-excitation measurements of PdGa@SiO_2 employed in the hydrogenation of CO_2 to methanol (Conditions: 20 bar, 3:1 H_2:He + 1:3 CO_2: He, 15 minute switching interval, 230 ^oC)

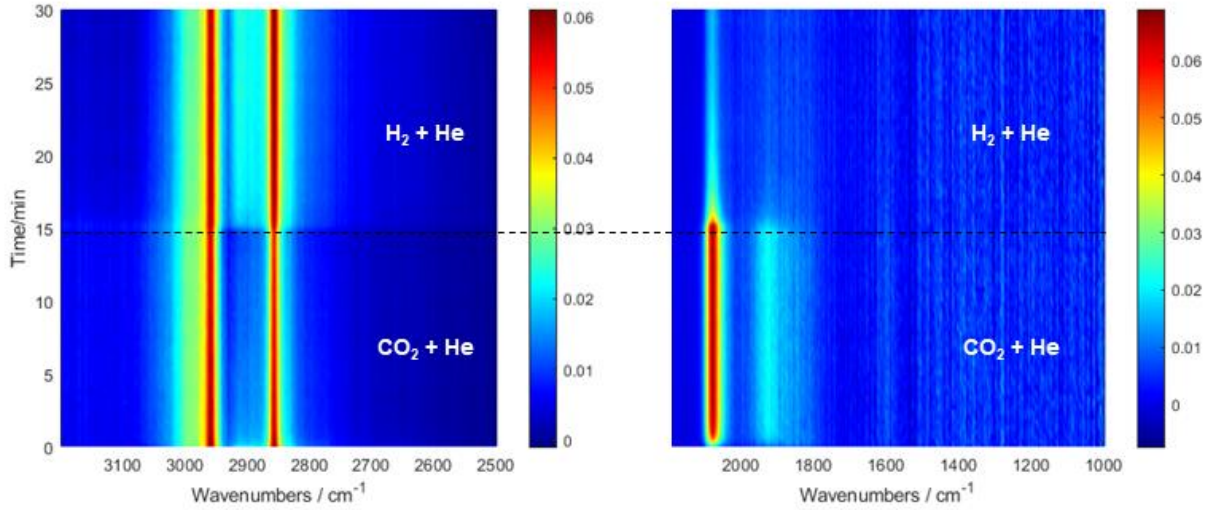

Figure S 66. Evolution of surface species between 3200-2500 cm^{-1} and 2100-1000 cm^{-1} during transient *operando* DRIFTS experiments at 20 bar and 230 ^oC

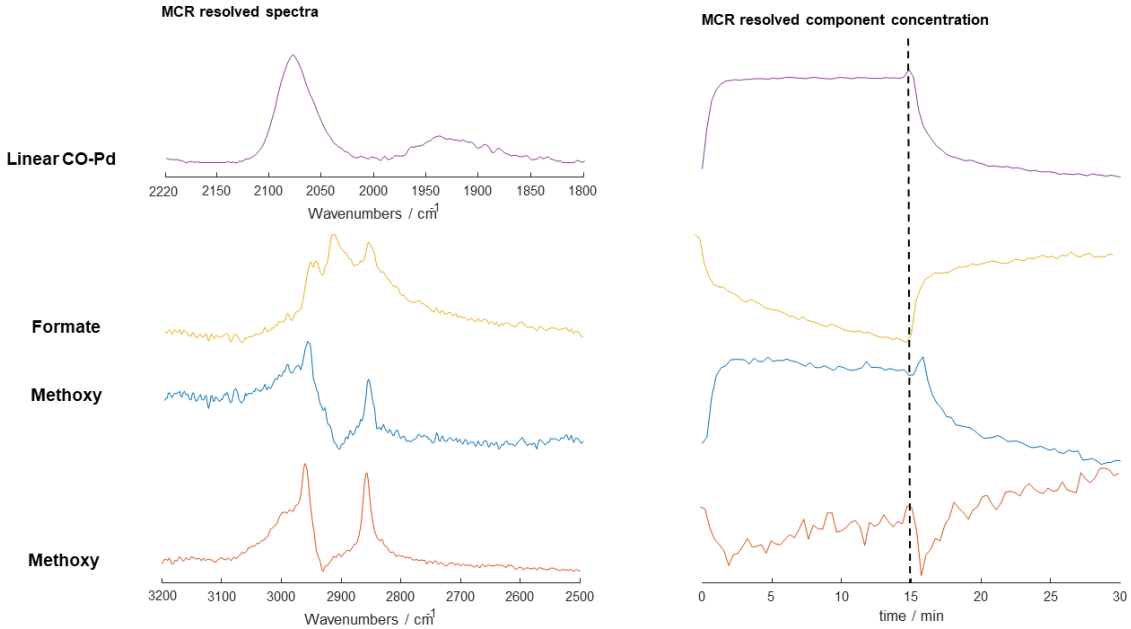

Figure S 67. MCR-resolved spectra and MCR-resolved component concentration from gas switching experiment.

S14. References

(1) Searles, K.; Siddiqi, G.; Safonova, O. V; Copéret, C. Silica-Supported Isolated Gallium Sites as Highly Active, Selective and Stable Propane Dehydrogenation Catalysts. *Chem. Sci.* **2017**, *8* (4), 2661–2666. https://doi.org/10.1039/C6SC05178B.

(2) Drew, D.; Doyle, J. R.; Shaver, A. G. Cyclic Diolefin Complexes of Platinum and Palladium. In *Inorganic Syntheses*; John Wiley & Sons, Ltd, 2007; pp 47–55. https://doi.org/10.1002/9780470132449.ch11.

(3) Sandoval, J. J.; Palma, P.; Álvarez, E.; Cámpora, J.; Rodríguez-Delgado, A. Mechanism of Alkyl Migration in Diorganomagnesium 2,6-Bis(Imino)Pyridine Complexes: Formation of Grignard-Type Complexes with Square-Planar Mg(II) Centers. *Organometallics* **2016**, *35* (18), 3197–3204. https://doi.org/10.1021/acs.organomet.6b00528.

(4) Docherty, S. R.; Estes, D. P.; Copéret, C. Facile Synthesis of Unsymmetrical Trialkoxysilanols: $(RO)_2(R'O)SiOH$. *Helv. Chim. Acta 101* (3), e1700298. https://doi.org/10.1002/hlca.201700298.

(5) Fulmer, G. R.; Miller, A. J. M.; Sherden, N. H.; Gottlieb, H. E.; Nudelman, A.; Stoltz, B. M.; Bercaw, J. E.; Goldberg, K. I. NMR Chemical Shifts of Trace Impurities: Common Laboratory Solvents, Organics, and Gases in Deuterated Solvents Relevant to the Organometallic Chemist. *Organometallics* **2010**, *29* (9), 2176–2179. https://doi.org/10.1021/om100106e.

(6) Tew, M. W.; Miller, J. T.; van Bokhoven, J. A. Particle Size Effect of Hydride Formation and Surface Hydrogen Adsorption of Nanosized Palladium Catalysts: L_3 Edge vs K Edge X-Ray Absorption Spectroscopy. *J. Phys. Chem.*

C **2009**, *113* (34), 15140–15147. https://doi.org/10.1021/jp902542f.

(7) McMullen, A. K.; Tilley, T. D.; Rheingold, A. L.; Geib, S. J. Preparation and Characterization of the Monomeric Copper(II) Siloxide Complex $Cu[OSi(OCMe_3)_3]_2(Py)_2$. *Inorg. Chem.* **1989**, *28* (19), 3772–3774. https://doi.org/10.1021/ic00318a032.

(8) Salo, E. V; Guan, Z. Late-Transition-Metal Complexes with Bisazaferrocene Ligands for Ethylene Oligomerization. *Organometallics* **2003**, *22* (24), 5033–5046. https://doi.org/10.1021/om034051r.

(9) Dolomanov, O. V; Bourhis, L. J.; Gildea, R. J.; Howard, J. A. K.; Puschmann, H. *OLEX2*: A Complete Structure Solution, Refinement and Analysis Program. *J. Appl. Crystallogr.* **2009**, *42* (2), 339–341. https://doi.org/10.1107/S0021889808042726.

(10) Bourhis, L. J.; Dolomanov, O. V; Gildea, R. J.; Howard, J. A. K.; Puschmann, H. The Anatomy of a Comprehensive Constrained, Restrained Refinement Program for the Modern Computing Environment - Olex2 Dissected. *Acta Crystallogr. Sect. A, Found. Adv.* **2015**, *71* (Pt 1), 59–75. https://doi.org/10.1107/S2053273314022207.

(11) Sheldrick, G. M. Crystal Structure Refinement with *SHELXL*. *Acta Crystallogr. Sect. C* **2015**, *71* (1), 3–8. https://doi.org/10.1107/S2053229614024218.

(12) Copéret, C.; Comas-Vives, A.; Conley, M. P.; Estes, D. P.; Fedorov, A.; Mougel, V.; Nagae, H.; Núñez-Zarur, F.; Zhizhko, P. A. Surface Organometallic and Coordination Chemistry toward Single-Site Heterogeneous Catalysts: Strategies, Methods, Structures, and Activities. *Chem. Rev.* **2016**, *116* (2), 323–421. https://doi.org/10.1021/acs.chemrev.5b00373.

(13) Ravel, B.; Newville, M. *ATHENA, ARTEMIS, HEPHAESTUS*: Data Analysis for X-Ray Absorption Spectroscopy Using *IFEFFIT*. *J. Synchrotron Radiat.* **2005**, *12* (4), 537–541. https://doi.org/10.1107/S0909049505012719.

(14) Nishi, K.; Shimizu, K.; Takamatsu, M.; Yoshida, H.; Satsuma, A.; Tanaka, T.; Yoshida, S.; Hattori, T. Deconvolution Analysis of Ga K-Edge XANES for Quantification of Gallium Coordinations in Oxide Environments. *J. Phys. Chem. B* **1998**, *102* (50), 10190–10195. https://doi.org/10.1021/jp982704p.

(15) Lam, E.; Noh, G.; Larmier, K.; Safonova, O. V; Copéret, C. CO2 Hydrogenation on Cu-Catalysts Generated from Zn^{II} Single-Sites: Enhanced CH_3OH Selectivity Compared to $Cu/ZnO/Al_2O_3$. *J. Catal.* **2020**. https://doi.org/10.1016/j.jcat.2020.04.028.

(16) Larmier, K.; Liao, W.-C.; Tada, S.; Lam, E.; Verel, R.; Bansode, A.; Urakawa, A.; Comas-Vives, A.; Copéret, C. CO_2-to-Methanol Hydrogenation on Zirconia-Supported Copper Nanoparticles: Reaction Intermediates and the Role of the Metal–Support Interface. *Angew. Chemie Int. Ed. 56* (9), 2318–2323. https://doi.org/10.1002/anie.201610166.

(17) Lam, E.; Noh, G.; Chan, K. W.; Larmier, K.; Lebedev, D.; Searles, K.; Wolf, P.; Safonova, O. V; Copéret, C. Enhanced CH_3OH Selectivity in CO_2 Hydrogenation Using Cu-Based Catalysts Generated via SOMC from Ga^{III} Single-Sites. *Chem. Sci.* **2020**. https://doi.org/10.1039/D0SC00465K.

(18) Manrique, R.; Jiménez, R.; Rodríguez-Pereira, J.; Baldovino-Medrano, V. G.; Karelovic, A. Insights into the Role of Zn and Ga in the Hydrogenation of CO_2 to Methanol over Pd. *Int. J. Hydrogen Energy* **2019**, *44* (31), 16526–16536. https://doi.org/10.1016/J.IJHYDENE.2019.04.206.

(19) Manrique, R.; Rodríguez-Pereira, J.; Rincón-Ortiz, S. A.; Bravo-Suárez, J. J.; Baldovino-Medrano, V. G.; Jiménez, R.; Karelovic, A. The Nature of the Active Sites of Pd–Ga Catalysts in the Hydrogenation of CO_2 to Methanol. *Catal. Sci. Technol.* **2020**, *10* (19), 6644–6658. https://doi.org/10.1039/D0CY00956C.

(20) Fiordaliso, E. M.; Sharafutdinov, I.; Carvalho, H. W. P.; Grunwaldt, J.-D.; Hansen, T. W.; Chorkendorff, I.; Wagner, J. B.; Damsgaard, C. D. Intermetallic $GaPd_2$ Nanoparticles on SiO2 for Low-Pressure CO_2 Hydrogenation to Methanol: Catalytic Performance and In Situ Characterization. *ACS Catal.* **2015**, *5* (10), 5827–5836. https://doi.org/10.1021/acscatal.5b01271.

(21) Fiordaliso, E. M.; Sharafutdinov, I.; Carvalho, H. W. P.; Grunwaldt, J.-D.; Hansen, T. W.; Chorkendorff, I.; Wagner, J. B.; Damsgaard, C. D. Corrections to “Intermetallic $GaPd_2$ Nanoparticles on SiO_2 for Low-Pressure CO_2 Hydrogenation to Methanol: Catalytic Performance and In Situ Characterization.” *ACS Catal.* **2018**, *8* (2), 938. https://doi.org/10.1021/acscatal.7b04342.

(22) Fujitani, T.; Saito, M.; Kanai, Y.; Watanabe, T.; Nakamura, J.; Uchijima, T. Development of an Active Ga_2O_3 Supported Palladium Catalyst for the Synthesis of Methanol from Carbon Dioxide and Hydrogen. *Appl. Catal. A Gen.* **1995**, *125* (2), L199–L202. https://doi.org/10.1016/0926-860X(95)00049-6.

(23) Zhou, X.; Qu, J.; Xu, F.; Hu, J.; Foord, J. S.; Zeng, Z.; Hong, X.; Edman Tsang, S. C. Shape Selective Plate-Form Ga_2O_3 with Strong Metal–Support Interaction to Overlying Pd for Hydrogenation of CO_2 to CH_3OH. *Chem. Commun.* **2013**, *49* (17), 1747–1749. https://doi.org/10.1039/C3CC38455A.

(24) Collins, S. E.; Baltanás, M. A.; Bonivardi, A. L. An Infrared Study of the Intermediates of Methanol Synthesis from Carbon Dioxide over Pd/β-Ga_2O_3. *J. Catal.* **2004**. https://doi.org/10.1016/j.jcat.2004.06.012.

(25) Studt, F.; Behrens, M.; Kunkes, E. L.; Thomas, N.; Zander, S.; Tarasov, A.; Schumann, J.; Frei, E.; Varley, J. B.; Abild-Pedersen, F.; Nørskov, J. K.; Schlögl, R. The Mechanism of CO and CO_2 Hydrogenation to Methanol over Cu-Based Catalysts. *ChemCatChem* **2015**, *7* (7), 1105–1111. https://doi.org/10.1002/cctc.201500123.

(26) Jiang, X.; Koizumi, N.; Guo, X.; Song, C. Bimetallic Pd–Cu Catalysts for Selective CO_2 Hydrogenation to Methanol. *Appl. Catal. B Environ.* **2015**, *170–171*, 173–185. https://doi.org/10.1016/j.apcatb.2015.01.010.

(27) Urakawa, A.; Bürgi, T.; Baiker, A. Sensitivity Enhancement and Dynamic Behavior Analysis by Modulation Excitation Spectroscopy: Principle and Application in Heterogeneous Catalysis. *Chem. Eng. Sci.* **2008**, *63* (20), 4902–4909. https://doi.org/https://doi.org/10.1016/j.ces.2007.06.009.

(28) de Juan, A.; Jaumot, J.; Tauler, R. Multivariate Curve Resolution (MCR).

Solving the Mixture Analysis Problem. *Anal. Methods* **2014**, *6* (14), 4964–4976. https://doi.org/10.1039/C4AY00571F.